UNIVERSITÄT BERN

Graduate School for Cellular and Biomedical Sciences

University of Bern

Circadian timing of limbic seizures in the epileptic mouse

PhD Thesis submitted by

Kristina Slabeva

for the degree of

PhD in Neuroscience

Supervisor
Prof. Dr. Maxime Baud
Department of Neuroscience
Faculty of Medicine of the University of Bern

Co-advisor
Prof. Dr. Reto Huber
Department of Neuroscience
Faculty of Medicine of the University of Zürich

b
UNIVERSITÄT
BERN

Accepted by the Faculty of Medicine, the Faculty of Science and the Vetsuisse Faculty of the University of Bern at the request of the Graduate School for Cellular and Biomedical Sciences

Bern, Dean of the Faculty of Medicine

Bern, Dean of the Faculty of Science

Bern, Dean of the Vetsuisse Faculty Bern

Abstract

Circadian timing of limbic seizures in the epileptic mouse

by Kristina Slabeva

Background: In epilepsy, seizures often recur with striking regularity at certain hours of the day in the human and mouse epileptic brain. Fundamentally, this observed preferential timing may result from the active-rest history (or sleep-wake, so-called process S) and/or from the circadian rhythm intrinsic to any neuron (so-called process C). The aim of this thesis is to disentangle the individual contributions of process S and C to the timing of seizures in the Kainic Acid (KA) mouse model of temporal lobe epilepsy.

Methods: We recorded spontaneous seizures in epileptic mice (n=24) over months using 16 depth-electrodes implanted in the limbic circuit. These animals were kept in a 12:12 light-dark cycling environment (LD), before subjecting them to different chronobiological paradigms: 1) Gentle sleep deprivation (GSD), 2) constant dim red light (DD), 2) constant light (LL), 3) 10:10 light-dark cycling (T20). We tested the statistical association of seizures with the physiological circadian cycle (measured as determined circadian seizure timing based on the core temperature and locomotor cycle) and with the sleep-wake state and history. Vigilance states were automatically annotated in month-long EEG recordings using non- negative matrix factorization.

Results: We observed a circadian clustering of seizures between the peak and the falling phase of 24-hour activity in LD (PLV= 0.25+/-0.13). While the circadian clustering persisted at the same phase during DD (PLV= 0.33+/-0.11) it was attenuated in LL (PLV= 0.26+/-0.03), when the strength of the underlying physiological circadian cycle was also weakened. Under T20, we observed a periodic uncoupling of the locomotor cycle and Core t° cycle (about every third day). The clustering of seizures was higher during the period when both cycles were aligned (PLV= 0.41+/-0.11) and lower when they were misaligned (PLV= 0.18+/-0.7). Furthermore we observed increased epileptic activity when slow wave activity was high after GSD.

Conclusion: The temporal clustering of seizures depends on the strength and alignment of process S and process C. This finding may help guide chronotherapeutic interventions in the future.

Content

List of figures

Abbreviations

BF	Basis function
BMAL1	Brain and Muscle ARNT-Like 1
CA	Cornu Ammonis of the Hippocampus
CLOCK	Circadian Locomotor Output Cycles Kaput
Core T°	Core abdominal temperature
CRY	Cryptochrome
DD	Constant dim red light environment
deEA	detrended cumulative epileptiform activity
DG	Dentate Gyrus
EA	Epileptiform activity
ECG	Electrocardiogram
EEG	Electroencephalogram
EMG	Electromyogram
GABA	Gamma-aminobutyric acid
GSD	Gentle sleep deprivation
IED	Interictal epileptiform discharge
ipRGC	Intrinsically photosensitive retinal ganglion cell
KA	Kainic acid
LD	Cycling 12h light 12h dark environment
LFP	Local field potential
LL	Constant light environment
MTLE	Mesial temporal lobe epilepsy
mTOR	Mammalian target of rapamycin
NREM	Non-rapid eye movement
PER	Period
PLV	Phase locking value
REM	Rapid eye movement
ROR	Retinoid-related orphan receptors
SCN	Suprachiasmatic nucleus
SUDEP	Sudden unexpected death in epilepsy
SWA	Slow wave activity
T20 LD	Cycling 10h light 10h dark environment

1 Introduction

1.1 Epilepsy

Epilepsy is a chronic neurological disorder and affects approximately 1% of the global population. Individuals with epilepsy experience recurrent, spontaneous (unprovoked) seizures, which can vary in severity from one individual to another. The frequency of seizures varies widely, ranging from several seizures per day to less than one seizure per year.[1]

Clinically manifesting seizures can be seen in the electroencephalogram (EEG) in the form of an ‘ictal’ discharge, but not all ictal discharges have an obvious clinical correlate. Additionally, evanescent ‘interictal’ discharge can occur between seizures. Thus, interictal and ictal epileptiform discharges are the hallmark of an “epileptic brain” and are typical patterns in the EEG of such brains. While interictal epileptiform discharges (IED) do not manifest behaviourally, seizures can induce various neurological and behavioural symptoms dependent on the brain region affected by the seizures. Seizures originate from the so called seizure onset zone or epileptogenic focus. They are termed "focal seizures" when they are limited to a specific brain region and "generalized seizures" when they affect both brain hemispheres and all brain regions. Generalized seizures are either classified as “primary generalized seizures” which simultaneously start in both hemispheres and “secondary generalized seizures”, evolving from focal seizures that have spread across both hemispheres. Symptoms can range from brief muscle jerks or momentary attention lapses to severe tonic-clonic movements. In severe cases generalized seizures can lead to sudden unexpected death in epilepsy (SUDEP)[2]. Periods with “continuous seizure activity” with series of seizures occurring in close succession of one another or prolonged seizures during which the mechanisms of seizure termination fail are referred to as status epilepticus (SE)[3].

The aetiology of epilepsy often remains unidentified, although in some cases it can be linked to genetic[4], structural[5], immune[6] or metabolic factors[7].

1.1.1 Mesio-Temporal lobe epilepsy

Mesio-Temporal lobe epilepsy (MTLE) is the most prevalent form of focal epilepsy and is often resistant to pharmacological interventions[8]. In MTLE seizures originate from hippocampal structures but might also involve other limbic areas like the entorhinal cortex or the amygdala[8,9].

The aetiology of MTLE is mostly unknown or acquired and the development of MTLE can be divided in three phases: (i) An *initial insult* to the limbic structures such as a febrile seizure, a SE, a trauma or an inflammatory reaction (i.e. limbic encephalitis)[10] (ii) A *latent period* accompanied by molecular and structural changes leading to neuronal loss and gliosis in the hippocampus, a histopathological hallmark called hippocampal sclerosis[11] (Fig.1). More specifically neuronal loss can be found in the Cornu Ammonis (CA) region of the hippocampus and adjacent regions[12] together with aberrant mossy fibre sprouting and granule cell dispersion in the dentate gyrus (DG)[13,14], which is believed to increase cortical excitability in this region[15–17]. Additionally, alterations of the interneuron population[18,19] have been observed. At the cellular level, alterations in ion channel and neurotransmitter receptor expression have been reported[20,21]. (iii) *Chronic epilepsy* characterized by recurrent, spontaneous (unprovoked) seizures. Clinically, individuals with MTLE typically experience focal seizures with a variety of symptoms due to the extensive connectivity of the hippocampus with the rest of the brain. Individuals with MTLE may experience an epileptic aura like an epigastric sensation or a psychic sensation (e.g. Fear, Deja-vu or Jamais-vu). As the seizure propagates out of the hippocampus affecting the contralateral temporal lobe or other regions of the brain they may experience, reduced awareness sometimes accompanied by the development of mouth or hand automatisms[22].

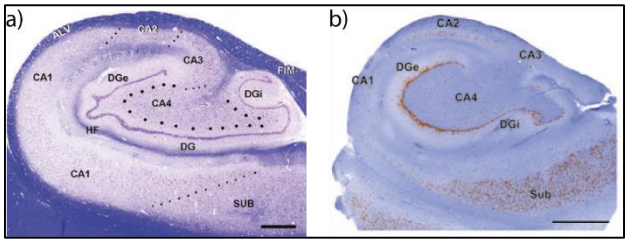

Figure 1 Example of Hippocampal sclerosis in human.

a) *Example of a healthy human hippocampus (post-mortem, cresyl-violet staining). (SUB: subiculum, CA1–CA4: subfields 1-4 of the hippocampal CA; DG: dentate gyrus with external (DGe) and internal limbs (DGi); HF: hippocampal fissure; ALV: alveus; FIM: fimbria).* ***b)*** *Example of hippocampal sclerosis with cell loss in all subfields of the cornu ammonis and granule cell loss in the DG. Adapted from Blümcke et al. 2013.*[11]

1.1.2 Electrophysiological correlates of epilepsy

Electrophysiological recordings are the gold standard for diagnosis and characterization of physiological brain oscillations and pathological epileptiform activity. EEG signals reflect the dipoles generated by changes in ionic current caused by synaptic activity of single neurons and can be recorded at various levels of resolution. While macroelectrodes placed on the scalp can record the activity of many neurons in a broad area of the brain, intracranial microelectrodes are used to record the local activity of a smaller number of neurons, referred to as local field potentials (LFP).

Under physiological conditions brain oscillations appear in the EEG as an ever-changing sea of waves and wavelets. The different brain oscillations visible in the EEG reflect different vigilance states and cognitive processes, e.g. activity in the beta/ gamma range reflect wake, while slow oscillations in the delta range reflect deep sleep[23]. However, in epilepsy these physiological brain oscillations are disrupted by "epileptiform abnormalities" encompassing seizures and IEDs.

Seizures are visible in the EEG as synchronised rhythmic events with temporal evolution in frequency, amplitude and space and can be followed by cortical slowing, reflecting the post-ictal state[24] (Fig. 2). The exact role of different neuronal subtypes during seizure initiation is still a debate and studies have shown either the involvement of gamma-

aminobutyric acid (GABA)ergic or glutamatergic neurons[25]. Overall, it is thought that ictal activity is associated with an increased activity of inhibitory neurons during the seizure onset, while the pyramidal cells remaining silent[26]. Interestingly, during seizures, single neurons in affected regions show diverse behaviours[27]. Some cells synchronize at the onset and later fall silent, while others become entrained as the seizure progresses. Towards the end of the seizure increased synchronisation of excitatory and inhibitory cells results in bursting activity in the EEG sometimes followed by post-bursting depression[28].

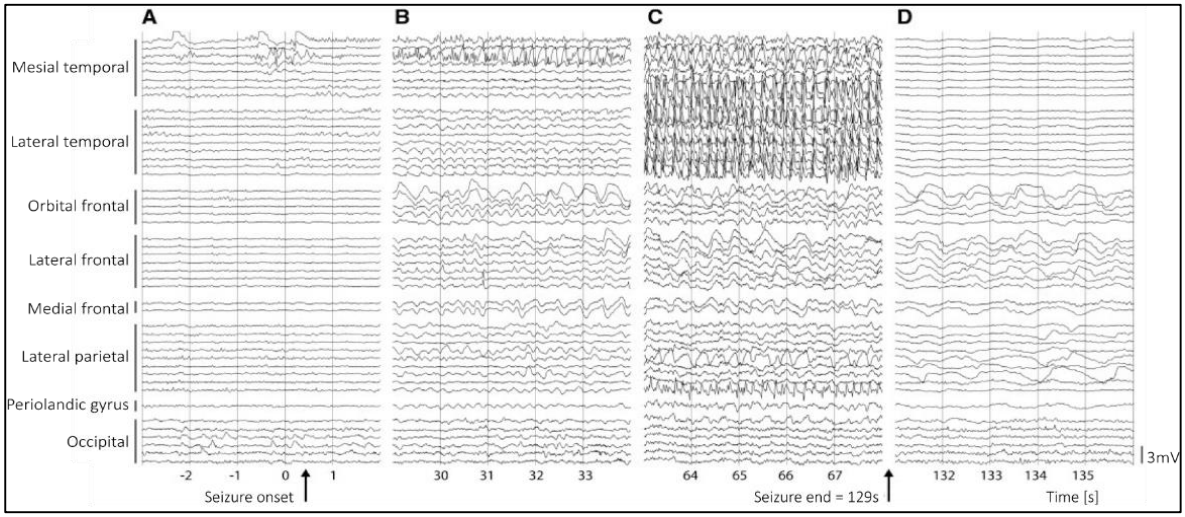

Figure 2 Example of a seizure in patient suffering from MTLE

*Example of a focal seizure originating in the medial temporal lobe with the characteristic temporal evolution in frequency, amplitude and space followed by post- ictal slowing. The seizure shows a low- voltage fast activity onset in the mesial temporal lobe **(A)**, followed by rhythmic poly-spikes and sharp waves in the same contacts **(B)**. As the seizure progresses ictal activity can be observed in the mesial and lateral temporal lobe (**C**) and is followed by post- ictal suppression after termination (**D**). Adapted from Englot et al. 2010[29].*

IEDs correspond to spikes (20-70ms[24]) and sharp waves (70-200ms[24]) which are the result of a synchronised discharge of neuronal groups, involving pyramidal cells and inhibitory neurons[30]. They are characterized by their high amplitude, asymmetric rise and fall, and may be accompanied by an after going slow wave[31].

High frequency oscillations such as such as ripples (80-250Hz) or fast ripples (250-500Hz) have been associated with the epileptogenic focus and have been therefore associated with

an “epileptic EEG”. Since they can also be observed in physiological EEG their association with epilepsy remains debated[32].

1.1.2.1 Cortical excitability

Both, IEDs, and seizures, are caused by transient disruption of physiological brain activity. Under physiological conditions the brain must exhibit sufficient excitability to respond to incoming stimuli, yet it should also possess sufficient resilience to withstand strong external stimuli or stochastic perturbations capable of disrupting physiological equilibrium[33]. While in any mammalian brain strong enough perturbations can overcome this resilience, leading to the development of self-sustained transient seizures[34,35], epileptic brain tissue is particularly susceptible to entering a seizure state presumably due to increased cortical excitability and therefore disturbance of the physiological inhibitory- excitatory balance[36–39]. In this context, cortical excitability refers to the responsiveness of brain tissue to incoming stimuli, and resilience is defined as the recovery rate of brain tissue from perturbations[33,40].

The level of cortical excitability is determined by complex interactions between excitatory and inhibitory mechanisms. While increased glutamate (the primary excitatory neurotransmitter) release or disturbed reuptake can lead to an increased excitatory signalling in epilepsy[41], disturbance of GABA (the primary inhibitory neurotransmitter in the brain) release or alterations in the GABA receptor functions can either lead to decreased inhibitory signalling and in some cases to increased excitatory signaling[42]. Disruption of the GABAergic system has been further associated with decreased seizure threshold[43] and increased seizure likelihood[44], as well as prolonged seizure duration[45] and increased seizure severity[46].

The assessment of cortical excitability involves measuring the brain's response to small perturbations delivered through electrical stimuli[47,48], transcranial magnetic pulses[49–52], or

optogenetic pulses in animal models[33,53]. The amplitude of the evoked response can be directly correlated with cortical excitability[33].

1.2 Epilepsy as a multiscale cyclical disorder

Seizures are commonly considered as unpredictable, random events, affecting everyday life in individuals suffering from epilepsy. However, since ancient times, healers have been struck by the remarkable cyclical regularity of seizure occurrence in some individuals and have associated it with various external cycles, such as the sleep-wake cycle or even the lunar cycle. Today, it is known that epilepsy is a multiscale cyclical disorder with cycles at the circannual, multidian, circadian and ultradian level. It is believed that seizure probability and occurrence are co-modulated by these cycles of different time scales[54], and gaining a deeper understanding of them can be used for seizure forecasting[55]. The following paragraphs will introduce each of these cycles in human epilepsy, along with their putative mechanisms and significance in modulating seizures.

1.2.1 Circannual cycles

Circannual cycles are biological cycles of about 1 year, which are thought to be generated endogenously[56] and lead to behavioural and physiological changes in animals and humans[57] (e.g. breeding[58], mood[59,60], cognition[61,62] or hormones[63]). These circannual cycles can also be observed in seizure timing and analysis of a large dataset with yearlong chronic EEG data together with seizure diaries revealed that 12% of individuals (24 of 194 patients) experience more seizures during a specific season[64]. The individual impact of seasons remains a topic of debate and the underlying mechanisms behind these circannual cycles are still not fully understood. They have been linked to variations in weather[65–67] or daylight changes[68] across different seasons. Overall, circannual cycles are modulating seizure occurrence only in a minority of subjects and the influence of circannual cycles is weaker compared to shorter cycles on the multidian, circadian and ultradian timescale[64].

1.2.2 Multidian cycles

Multidian cycles refer endogenously generated biological cycles that occur with a periodicity of more than two days up to several weeks[56]. Historical studies already hinted at the presence of multidian cycles in seizure periodicity[69], while the recent use of month and yearlong chronic EEG data together with seizure diaries has revealed the existence of these cycles also in IEDs and has shed light at the association between multidian IED and multidian seizure cycles: across all patients, seizures tend to occur during the rising phase of the multidian cycles of the average daily IED[64,70–72]. Overall multidian cycles in epilepsy show non-stationary (e.g. the frequencies and spectral characteristic can vary over time) behaviour with an average periodicity of around 20-35 days which can be accompanied by more rapid cycles of 14-15 days and 7-10 days[54,64,68]. They are found in approximately 60% of epilepsy patients[54,64,68,70,72] . Individual multidian cycles tend to remain constant over several years, while differences in periodicities can be observed across individuals. Intriguingly, this multidian cycles in epilepsy cannot only be observed in catamenial epilepsy, where seizures are influenced by the menstrual cycle[73], but also in men, children and post-menopausal women, all of which do not have obvious physiological hormonal cycles at the multidian scale that could be responsible for modulating seizure occurrence on a multidian scale.

Multidian cycles in ictal activity, as well as the phase relationship between IEDs and seizure, is also present in other species. Gregg et al. [74] reported circaseptan and about monthly seizure periodicity in canines with naturally occurring epilepsy. Baud et al.[75] showed the presence of multidian rhythms of IED with periodicity of about 2-3 and 5-7 days in rats with experimentally induced epilepsy. Baud et al.[75] further suggest that the observed multidian rhythms were endogenously generated, since the multidian cycles observed were not synchronous across rats that were housed together, nor could they be

linked to external human interventions. Furthermore, multidian seizure cycles observed in humans showed no correlation with external cues with similar periodicity, e.g. the lunar cycle or the weekday cycle, further supporting the notion that the multidian cycle is endogenously generated[64,68].

The endogenous mechanisms behind these multidian cycles, which besides epilepsy can also be found in other medical fields like psychiatry[76,77], oncology[78] and cardiology[79] remain largely unknown and two possible mechanism are discussed: the systemic oscillators hypothesis suggesting a hormonal basis and the neural oscillators hypothesis suggesting that these multidian cycles are generated through interaction and changes in the resilience of the epileptic network and other networks in the brain over time[56].

Overall, multidian cycles are present in more than half (60%[64]) of patients with focal epilepsy, including those with MTLE and their impact on seizure timing is thought to be as significant as that of circadian cycles[64].

1.2.3 Circadian cycles

Circadian cycles are endogenously generated biological rhythms that last approximately 24 hours and can be influenced by external factors such as light or behaviour[56]. In the early 20th century three different chronotypes in seizure occurrence were described based on observations made in epilepsy patients living in epilepsy colonies: diurnal (seizures occurring during the day), nocturnal (seizures occurring during the night), and diffuse (no specific timing preference)[80–82]. The recent availability of long-term EEG recordings revealed that approximately 90% of patients with epilepsy show a circadian seizure cycle and lead to the refinement of epilepsy chronotypes into five distinct groups: three diurnal chronotypes where seizures predominantly occur in the morning or early respectively late afternoon and two nocturnal chronotypes where seizures tend to occur either during the

early or late stages of the night[64,83] (Fig. 2). These chronotypes tend to remain stable over time, although some individuals can show a shift in preferred seizure timing[68]. In addition to seizures themselves, seizure networks have also been shown to change on a circadian scale leading to changes in seizure propagation pathways across the brain and changes in symptoms depending on the time of day and regions involved[84–89].

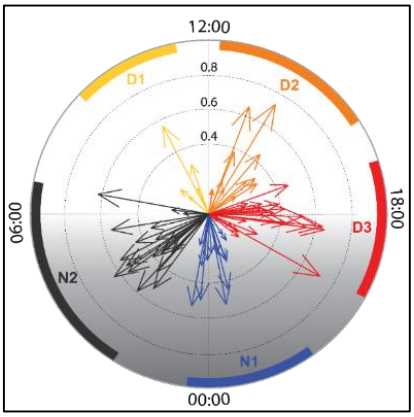

Figure 3 Chronotypes in human epilepsy

Preferred circadian timing of electrographic seizures on a 24-hour clock recorded in 76 patients implanted with long-term EEG devices. The patients are categorized into three diurnal chronotypes (denoted as D1, D2, and D3) and two nocturnal chronotypes (denoted as N1 and N2). The length of the arrow indicates the strength of circadian clustering, while the arrow's angle shows the preferred time at which seizures occurred. Adapted from Leguia et al. 2021. [64]

Contrary to the clear phase relationship between IEDs and seizures on the multidian scale there is no clear relationship between the circadian changes in IED and seizure occurrence. Different studies associated seizure occurrence with different phases of the circadian IED cycle[54,70,90]. Furthermore, the circadian cycle in IED and seizures behave in different ways: while the circadian modulation of IED is similar across days with the highest IED counts occurring during nighttime[91,92], seizures do not occur during each circadian cycle.

Circadian patterns in seizure occurrence are not limited to humans but can be also extend to other species. For example Gregg et al[74]. observed a circadian clustering of seizures in epileptic canines where seizures occurre predominantly in the morning, similar to the morning chronotype observed in epilepsy patients.

Overall, the impact of circadian cycles on seizure occurrence is considered to be highly significant[64].

1.2.4 Ultradian cycles

Ultradian cycles are biological cycles that manifest multiple times within a single circadian cycle and have a periodicity shorter than 24 hours[56]. The sleep cycle is a prominent example for an ultradian cycle. Each sleep cycle consists of transitions between different sleep stages: non-rapid eye movement (NREM) sleep, featuring increased slow wave activity (SWA), and rapid eye movement (REM) sleep, marked by low voltage, faster, and desynchronized EEG patterns similar to the ones observed in wakefullness[23]. Specific epilepsy syndromes like sleep-related hypermotor epilepsy (with seizure occurring during sleep[93]), or juvenile myoclonic epilepsy and grand mal seizures upon awakening (with seizures often occurring within 2h after awakening[94]) suggest a connection between epilepsy and specific sleep stages.

Seizure occurrence is strongly influenced by different sleep stages. Ng et al.[95] reviewed 42 studies with total of 1458 patients in a meta-analysis and characterized the overall occurrence of seizure during different vigilance states. They revealed a notable trend: focal and generalized seizures were most commonly observed during NREM sleep. Conversely, REM sleep appeared to exert a protective influence, with only a limited percentage of focal seizures occurring during REM. Furthermore, seizures seem to be more prone to generalize during NREM sleep. Comparable results have been found in animal models of epilepsy where seizure threshold was higher during REM sleep compared to NREM sleep[96] and enhancing the characteristic oscillations of REM sleep showed a protective effect towards seizures[97–99].

Like seizures, IEDs are most frequent in NREM sleep, while REM sleep seems to have a protective effect[100–102]. More specifically IEDs are more prone to occur during the transitions between "up" and "down" states of the slow (0.5-4Hz) cortical oscillations observable during N3 and N2 NREM sleep, due to increased neuronal synchrony during these vigilance states [103,104]. Interestingly this correlation can also be found in patients with a diurnal chronotype in seizure occurrence[64]. The permissive effect of NREM sleep alone on IED occurrence was confirmed by Pavlova et al.[105]. They recorded five epilepsy patients under a constant dim-light protocol, depriving the study participants from any external timing cues for three days. These patients showed an even distribution of sleep and wake over their circadian cycles which were assessed by melatonin measurements. Intriguingly they observed an increase in IEDs during NREM sleep, independent of the circadian cycle.

Overall, both the circadian and the ultradian cycle, can be seen as strong modulators of epileptic activity, and it is important to distinguish between their respective impacts. On one hand the characteristics of different vigilance states (e.g. increased synchronisation across the thalamocortical network during NREM sleep as a promoting factor for seizures[106,107]) may influence seizure occurrence. On the other hand, sleep and sleep stages are modulated on the circadian scale by an interplay between circadian and homeostatic processes[108,109].

1.3 Animal models in epilepsy research

Different animal models have been developed to replicate MTLE in humans, exhibiting its hallmark features, including spontaneous recurrent seizures and hippocampal sclerosis. In rodent models, MTLE is induced by replicating the initial insult commonly observed in human MTLE, which can involve febrile seizures[110], kindling[111,112], or SE (induced either using chemiconvulsants[111,113,114] or electrical stimulation[115,116]). Rodent post-status epilepsy models, particularly those chemically induced, such as the Pilocarpine or Kainic acid (KA)

model, are extensively utilized and well-established. Both, pilocarpine (a muscarinic acetylcholine receptor agonist) and KA (a cyclic analogue of L-Glutamate binding glutaminergic receptors) can be administered either systemically (intraperitoneal[117,118] or subcutaneous[119]) or localized (intracerebral[120]).

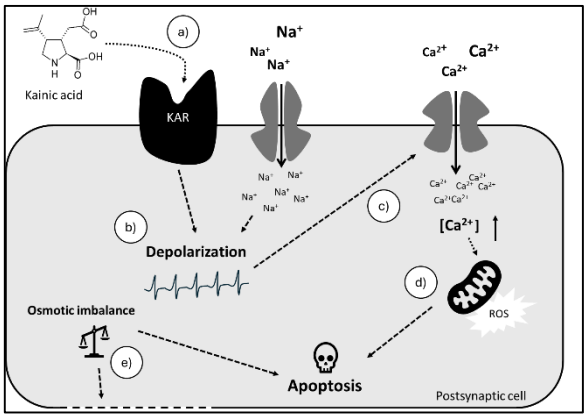

Figure 4 Mechanism of action for KA

Injection of KA causes excessive depolarization of neurons in the targeted area and causes cellular damage and apoptosis through a pathological process called excitotoxicity. ***a)*** *KA binds to Kainic acid receptors (KAR) leading to excessive depolarization of the cell (**b**) and intracellular accumulations of Ca2+ (**c**). Increase in intracellular Ca2+ concentration triggers a cascade of detrimental effects resulting in mitochondrial mediated apoptosis (**d**) characterized by the release of reactive oxygen species (ROS). Additionally, intracellular accumulation of Ca2+ and Na+ due to excessive depolarization leads to disturbance of the tightly controlled osmotic balance within the cell and the extracellular space ultimately causing rupture of the cell membrane(**e**).*

The process of epileptogenesis in post-status epilepsy models closely mirrors that observed in humans with MTLE and can be divided into three distinct periods: (i) the *acute phase* characterized by status epilepticus, (ii) the *latent phase* spanning the period between status epilepticus and the occurrence of the first unprovoked seizure. The latent phase is characterized by histopathological changes[112,115,121–125] and the development of HS and (iii) the *chronic phase* characterized by the occurrence of spontaneous seizures.

The model studied in this thesis, is the post-status intrahippocampal kainic acid model of MTLE in mice. Mice are rendered epileptic by a localized injection of KA into the hippocampal formation. The direct intrahippocampal administration of KA leads to restricted focal damage at the injection site leading to high levels of precision and reproducibility, while mortality is decreased compared to other administration routes, e.g.

intraperitoneal injection of KA[126]. After KA injection mice will rapidly enter into status epilepticus which can last up to several hours[127]. It is common practice to stop the overt part of status epilepticus beforehand using anti-convulsant drugs (e.g. Diazepam) to decrease mortality[128]. The first spontaneous seizures in this model appear as of approximately two weeks after acute induced status epilepticus and the number of seizures shows high variability between and within mice. Studies have documented instances of electrographic seizures happening as frequently as every other minute, while at other times, animals can go for several hours without experiencing seizures[129,130]. The electrographic features (localisation and electrographic patterns) resemble those seen in human MTLE[131]. Seizures typically last longer than 10 seconds with the majority of seizures showing a hypersynchronous onset, visible in the EEG as periodic spikes with a frequency of approximately 2Hz. Rarely seizures shown a low voltage fast activity onset, with high frequency activity above 25Hz[132]. Seizures originate in the hippocampal formation but can also propagate to other (limbic) structures.

1.4 Circadian cycles in animal models

Circadian patterns in seizure occurrence are not limited to humans and canines but can be also observed in rodents.

In epileptic rats, seizures primarily manifest during the late resting phase[75,133–135] and more specifically during periods of inactivity[133]. Consistent with the other studies Matzen et al.[48] observed a preference for seizure occurrence during the resting phase in a rat model with electrically induced epilepsy. Additionally, the authors evaluated cortical excitability in these animals and found increased cortical excitability coupled with reduced inhibition during periods associated with heightened seizure risk.

Epileptic mice show a slightly different circadian seizure cycle, with seizures primarily occurring during the transition from the inactive phase (day) to the active phase (night) in various models with chemically[131,136] induced epilepsy. Increased susceptibility to audiogenic or electrically induced seizures during the resting phase has also been documented[137]. In line with rats, mice genetically predisposed to epilepsy tend to experience seizures during the early[138]or late[139] resting period. Notably, these seizures often manifest during sleep or immediately upon transitioning from sleep to wake[139,140].

Rodent epilepsy models have been used to shed light on the endogenous nature of circadian cycles in epilepsy: Purnell et al. [141] reported an increased risk of SUDEP during the resting phase in a transgenic mouse model with audiogenic seizures. In the same study, they also assessed the risk of SUDEP from electrically induced seizures in wild-type mice exposed to a constant dark environment, where mice exhibit a free-running rhythm. In line with their findings in the transgenic model, the risk of SUDEP was elevated during the individual resting phase, while there was no change in seizure severity at different circadian time points. These results suggest an endogenous modulation of SUDEP risk based on the endogenously generated circadian rhythm in these mice.

More importantly Quigg et al.[135,142] conducted a pivotal study where they recorded both seizures and locomotor activity over several days in a model of MTLE in rats. First, they characterised the circadian timing of seizures and showed that seizures preferentially occurred during the resting phase in a 12-hour light-dark environment. Then they took the experiment one step further where they characterized the occurrence of seizures in a constant environment without external timing cues. The animals developed an free- running circadian rhythm and intriguingly the preferred seizure timing during the individual resting phase was preserved. This is a noteworthy result as it suggests that the circadian seizure

cycle persists without external timing cues and must be therefore endogenously generated. Surprisingly, such experiments have not been replicated since.

1.5 Putative mechanisms responsible for circadian seizure timing

Circadian seizure cycles are present across different species (humans, canines, rodents), daily activity patterns (diurnal and nocturnal) and epilepsy aetiologies (acquired, induced or genetic). This suggests that a common circadian biological process, plays a crucial role in governing seizure risk on a 24-hour scale. In a pivotal study Quigg et al[142]. showed that the circadian timing of seizures is preserved in the absence of any external timing cue, indicating the endogenous nature of the circadian seizure cycle. Both the circadian cycle, whose rhythmicity is governed by core clock genes and is intrinsic to any neuron[143] (so-called process C) and the sleep-wake history and its homeostatic regulation (so-called process S or sleep homeostat) are oscillating at a 24h scale[108,144]. Under physiological circumstances these two processes are tightly coupled and are thought to cumulatively influence the regulation and timing of sleep, as explained by the theoretical framework "Two process model of sleep"[108]. The two process model of sleep explains the interaction of a process S, which is a sleep-wake dependent homeostatic process and process C which corresponds to the circadian cycle and is controlled by the circadian pacemaker. It is important to note that process S is not dependent on the circadian rhythm as sleep homeostasis is maintained also in arrhythmic animals[145] and is influenced by the time previously spend awake, rather than the circadian timing[146]. Recent work on transcriptome studies shed further light on the interaction between process S and process C. While the expression of rhythmic genes is always influenced by both processes, cortical gene expression is more markedly affected by the sleep-wake rhythm, while gene expression in the liver and blood shows a more pronounced circadian influence[147]. This shared influence

of process S and process C on gene expression suggests that both may also exert varying degrees of influence on the timing of seizures.

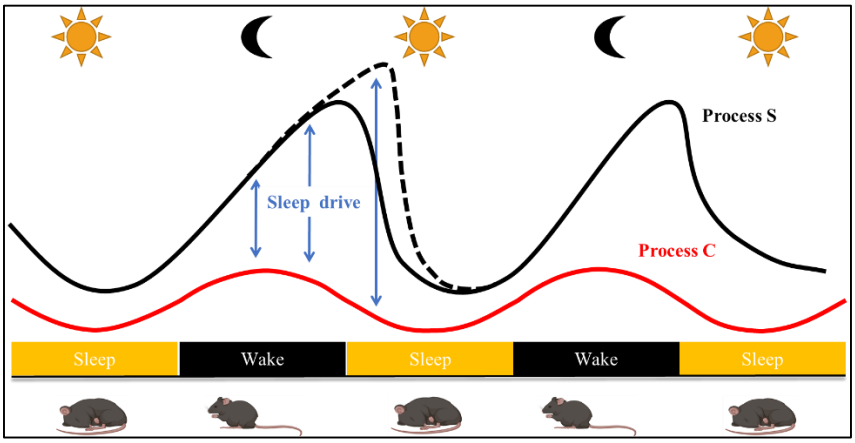

Figure 5 Two process model of sleep adapted to nocturnal animals.

The timing and regulation of sleep can be explained by the interaction between a circadian Process C (red) and a homeostatic Process S (black). Process S reflects sleep pressure and is accumulating during the active phase (night) of the animal and decreasing during sleep in the inactive phase (day). Process C is known as the endogenous circadian rhythm and regulates different processes in the body. In the context of the two process model of sleep process C promotes wakefulness during the dark and sleep during light phase aligning the sleep wake cycle in nocturnal animals like mice with the natural day-night cycle. Sleep drive (blue arrows) corresponds to the distance between both processes and is lowest during the active phase (night) and highest during the resting phase (day). Prolonging wakefulness over the time of the usual active phase (dotted black line) phase leads to a further increase in sleep pressure and further increase in sleep drive.

1.6 Process C: the circadian clock

The circadian clock refers to an intrinsic timekeeping system present across different species leading to daily changes in behavioural and/ or physiological processes with an ~24h periodicity[56]. Process C is generated through an auto regulatory oscillatory feedback loop of different core clock genes on the molecular level and on the systemic level by a hierarchical interplay between the central circadian clock located in the superchiasmatic nucleus (SCN, a bilateral structure in the hypothalamus dorsal to the optic chiasm) and peripheral clocks (present across the whole body) [148].

1.6.1 The molecular circadian clock

The molecular circadian clock oscillator consists of two intertwined transcriptional and translational feedback loops involving the core clock genes: CLOCK (Circadian

Locomotor Output Cycles Kaput), BMAL1 (Brain and Muscle ARNT-Like 1), the Per (Period) gene family (Per1, Per2, and Per3), the Cry (Cryptochrome) gene family (Cry1, Cry2), the REV-ERB gene family, and the ROR gene family(Retinoid-related orphan receptors, RORα, RORβ, RORγ).

The primary autoregulatory feedback loop consists of the activators CLOCK and BMAL1 and repressors PER and CRY. CLOCK and BMAL1 are subunits of the PER-ARNT-SIM[149] transcription factor which induces the transcription of clock-controlled output genes, including their own repressors Per and Cry. After their transcription and translation PER and Cry proteins are translocated in the cytosol where they form heterodimers (a complex of two proteins) which, after phosphorylation, is translocated back to the nucleus, where it inhibits the activity of the CLOCK-BMAl1 complex. This, in turn, indirectly suppresses also further transcription of Per and Cry genes. Over time the phosphorylated PER and Cry proteins are degraded via ubiquitin-dependent pathways, slowly decreasing their inhibitory effect on the Clock-BMAl1 complex, allowing for a re-initiation of the transcriptional cycle. The different kinases (enzymes catalysing the transfer from phosphate groups from a donor molecule to acceptor molecule in a process called phosphorylation) and phosphatases (enzymes catalysing the removal of a phosphate group from a molecule in a process called dephosphorylation) involved in the phosphorylation of the PER-Cry complex play an important role in determining he intrinsic rate of the circadian cycle by controlling the speed at which the Per-Cry complex is translocated to the nucleus or degraded. The time delay between CLOCK-BMAL1 complex activation and PER-Cry heterodimer accumulation, along with the gradual degradation of the PER-Cry heterodimer creates a rhythmic, self-sustained cycle of approximately 24h[150,151]. In addition to the primary autoregulatory loop, a secondary autoregulatory feedback loop involving ROR and REV-ERB fine-tunes the intrinsic circadian cycle. ROR positively regulates the circadian

clock by inducing BMAL1 transcription, while REV-ERB, initiated by the CLOCK-BMAL1 complex, acts as a transcriptional suppressor of BMAL1 and delays Cry transcription[150,151].

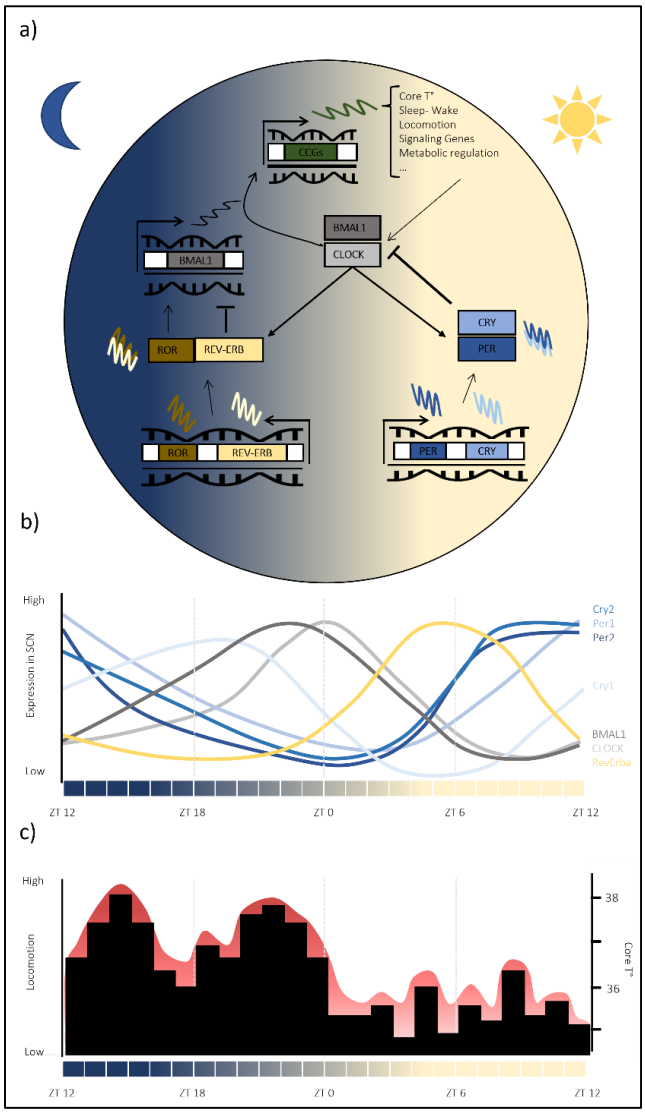

Figure 6 The molecular circadian clock and its output.

a) *The molecular circadian clock oscillator and the involved autoregulatory feedback loops between different core clock genes. CCGs= clock-controlled genes. Adapted from Lee et al. 2021*[152]. ***b)*** *Expression of different core clock genes in the SCN over the course of one circadian cycle. ZT= Zeitgeber time.* ***c)*** *Core body temperature (red shading) and locomotion (black bars) as examples of physiological processes controlled by the circadian machinery in a nocturnal animal.*

1.6.2 Synchronisation of the endogenous circadian clock

The endogenous circadian clock undergoes a daily resetting induced by a so called "Zeitgeber," a German term translating to "time giver"[153]. A Zeitgeber is an external cue

that can entrain the circadian machinery and therefore adjust the endogenous circadian clock to the external 24-hour day-night cycle. The most powerful Zeitgeber is the ambient light[154] and its information is integrated by the central circadian clock in a process called "internal synchronisation". In diurnal (e.g. humans) and nocturnal species (e.g. rodents) intrinsically photosensitive retinal ganglion cells (ipRGCs) send direct information about ambient light to the suprachiasmatic nucleus (SCN) via the retinothalamic tract[155]. The SCN integrates the ambient light information received by the ipRGCs by synchronising the local molecular circadian clock via the rapid induction of mPer1 and mPer2 upon light sensation[156,157]. Vasoactive intestinal polypeptide (VIP) expressing neurons hold a significant role in synchronizing the local molecular circadian clock and are crucial for generating a robust circadian cycle. Disruption of VIP signalling or the absence of VIP neurons can lead to disturbances in the circadian rhythm and arrhythmia in animal models[158,159].

The SCN relays the information about the external time to the peripheral clocks via hormonal and neuronal pathways. Upon light exposure corticotropin-releasing hormone from the SCN stimulates the paraventricular nucleus of the thalamus to release adrenocorticotropic hormone, eventually leading to cortisol release from the adrenal cortex. Simultaneously the SCN sends inhibitory signals to the pineal gland, preventing the secretion of melatonin. Both cortisol and melatonin play pivotal roles in aligning the peripheral clocks with the external 24-hour light-dark cycle with cortisol peaking at the beginning of the active phase and melatonin peaking at the beginning of the resting phase[148]. Additionally, the SCN synchronizes peripheral clocks through neuronal pathways, including the autonomic nervous system, encompassing the sympathetic and parasympathetic branches, which influence the local release of neurotransmitters and hormones[160].

1.6.3 Linking Process C and epilepsy

The molecular clock can be directly linked to cortical excitability. Studies in healthy rodents have shown circadian fluctuations in the majority (70%) of genes regulating synaptic changes in neurotransmission and ionic conductance[161,162]. Molecular studies in epileptogenic tissue resected during epilepsy surgery have shown altered expression of core clock genes: decreased expression CLOCK and downstream targets of the Cock-BMAL1 heterodimer[140] or either decreased[163] or increased[164] expression of REV-ERBα.

In animals models acute seizures, induced either electrically or chemically, lead to transient changes in core clock gene expression, including both increase and decrease, as well as alterations in their rhythmic patterns[163–167]. Similar alterations have been found in animals with chronic epilepsy[163,166–169]. Interestingly some genes which have been found to oscillate in healthy tissue do not show oscillatory behaviour in epileptogenic tissue and vice versa. Also, alterations in the expression of specific core clock gene following acute seizures can differ from those observed in epileptogenic tissue collected from of animals with chronic epilepsy.

The use of transgenic models with knock outs for different core clock genes allowed to shed further light on the link between core clock genes and epilepsy. Li et al[140]. showed that mice lacking the Clock gene in pyramidal neurons, but not in inhibitory interneurons, showed altered electrophysiological properties at the microcircuit level resulting in spontaneous seizures which preferentially occurred during sleep. The intact circadian machinery in the SCN, as well as the preserved sleep-wake rhythm suggests that the observed spontaneous seizures are directly caused by the loss of Clock in the pyramidal neurons. Ablation of BMAL1 abolished the circadianicity observed in seizure threshold for electrically induced seizures in wild type mice and lead to an overall reduction in seizure threshold[170]. Ablation of Rev-erbα[164] resulted in a loss of circadianicity in seizure threshold

for chemically induced seizures while a rodent model with a triple knock out of the PAR bZip transcription factor family (a downstream target of the Clock-BMAL1 complex) show sever seizures which predominantly occurred during slow wave sleep[171]. Both Rev-erbα and the PAR bZIP transcriptor factor family are downstream targets of the Clock- BMAL1 complex, indicating a significant role of BMAL1 and the Clock- BMAL1 complex in the regulation of cortical excitability on a 24 hour scale. A possible mechanism of how core clock genes could directly influence seizure occurrence is via the mammalian target of rapamycin (mTOR) pathway[172–174], a potent regulator of many cellular mechanisms and therefore also cortical excitability. Different neurological disorders including epilepsy have been associated with abnormalities in the mTOR pathway[173].

In summary, process C exerts considerable influence on seizure occurrence through intricate mechanisms operating on the molecular level. The molecular clock emerges as a potential direct modulator of cortical excitability, which has been shown to change on a circadian scale[50], and expression of core clock genes has been shown to be altered in both human epilepsy and animal models of epilepsy.

1.7 Process S: the sleep-wake homeostasis

1.7.1 Sleep and wakefulness

Both sleep and wakefulness are generated through a complex interplay between different subcortical structures and their neurotransmitters. Wakefulness is generated by a wake promoting network including the brainstem, hypothalamus and basal forebrain whose output then eventually converges in the thalamus and cortex inducing wakefulness. Sleep on the contrary is generated by inhibition of the wake promoting systems[175]. Both wakefulness and sleep are associated with specific brain oscillations visible in the EEG. Wakefulness is characterised by low amplitude and mixed high frequency oscillations and

increased muscle tone. Sleep can be subdivided into two states: NREM sleep or slow wave sleep characterized by high-amplitude slow oscillations in the delta range (0.5-4Hz), sleep spindles (7-15Hz bursts) and low muscle tone and REM sleep characterized by oscillations in the theta range (4-8Hz) and muscle atonia[23]. Over the curse of one-night individuals will cycle between NREM and REM sleep with one cycle lasting approximately 90 minutes. While at the beginning of the resting phase cycles of NREM and REM sleep are characterised by long NREM episodes and short REM episodes, the duration of REM episodes will increase towards the end of the resting phase.

In epilepsy patients sleep is disturbed leading to an overall poor quality of sleep[176] and more frequent sleep disorders[177], while the brain oscillations characterizing the different vigilance states are disturbed[178].

1.7.2 Sleep-wake homeostasis

Sleep is regulated via a homeostatic process: Sleep drive or sleep pressure is increasing during the time spend awake and decreases during the time spend asleep. Sleep pressure is believed to be mainly created by accumulation adenosine, a natural by-product of adenosine tri phosphate hydrolyzation. During wakefulness adenosine levels increase in specific regions of the brain leading to the activation of sleep-promoting neuronal pathways. During sleep adenosine levels gradually decrease which in turn reinforces the wake promoting pathways in the brain[175]. Increase and decrease of sleep pressure is reflected by SWA during NREM sleep: high SWA at the onset of the resting phase reflects high sleep pressure, while the transient decrease of SWA during the resting phase reflects the decrease of sleep pressure. Sleep deprivation leads to a continuous increase in sleep pressure until the individual goes to sleep[108].

1.7.3 Linking Process S and epilepsy

The exact connection between Process S and epilepsy remains a subject of debate[179]. It is important in this context to differentiate between sleep stages (NREM and REM), which are cycling on a ultradian scale and process S representing sleep homeostasis and which is cycling on a circadian scale. While the link between sleep stages and seizures is established the link between sleep homeostasis respectively sleep pressure remains a topic of debate.

Overall, in clinics insufficient sleep and poor sleep quality are linked to increased seizure probability and sleep deprivation is often used during pre-surgical evaluation for epilepsy surgery to increase the number of seizures patients experience during their hospital stay and increase the diagnostic yield of IED[180]. Despite its routine clinical use, a definitive causal link between sleep deprivation and increased seizure occurrence is still lacking. Studies in epilepsy patients have reported conflicting results with some studies suggesting a correlation between increased seizure occurrence and sleep pressure[181–183], while others report no such correlation[184–186]. Notably, these studies have several limitations, including a lack of control for confounding factors known to influence seizure occurrence in humans (e.g., stress or alcohol consumption) and, more crucially, a failure to control for the preceding amount of sleep or naps in these patients[179]. Nevertheless, studies in which the cortical excitability was assessed using transcranial magnetic pulses in humans have not only shown circadian variability in cortical excitability, but also an increase in cortical excitability proportional to the time spend awake, e.g. when sleep pressure is increased[49,50]. In a study including year-long recordings of sleep and seizures in patients increased sleep duration was associated with decreased seizure risk[187].

Several studies have opted to examine the relationship between sleep pressure and epilepsy in animal models under controlled laboratory conditions. Cats that have been sleep deprived for 24h showed decreased seizure threshold for kindling and penicillin induced seizures,

independent of whether the seizures were induced during sleep or during wakefulness. Overall NREM sleep showed higher susceptibility to seizures than REM sleep[188]. In a rat model of absence epilepsy, researchers saw an initial increase in seizure rate during the first 4 hours of a 12-hour sleep deprivation period. However, this increase was followed by a rebound effect, where the number of seizures decreased[96]. This reduction coincided with a rebound in both REM sleep and deep NREM sleep after the sleep deprivation period. Similar to total sleep deprivation, isolated REM sleep deprivation has been shown to be sufficient to increase seizure duration[189] and decrease seizure threhold[190,191]

In a mouse model of SUDEP sleep deprivation for 4 hours each day over a 6-day period resulted in a notable increase in seizure frequency during the first 3 days of sleep deprivation. However, this effect diminished in the later days of sleep deprivation. Overall animals subjected to sleep deprivation were more likely to experience status epilepticus or SUDEP compared to animals which were not sleep deprived[192]. In the same model chronic accumulation of rest deficiency over several days was observed prior to SUDEP[193].

Cuddapah et al.[194] have associated sleep loss with increased seizure rate in drosophila. They further suggest that “sleepiness”, which is driven by the need for sleep, plays a more critical role in exacerbating seizures than the total amount of sleep, challenging the common belief that increasing only the duration of sleep is sufficient to prevent seizures. They show that optogenetic silencing of sleep promoting networks, which are hyperactive during sleep deprivation, has protective effect against seizures, while acute activation of these networks, simulating sleep deprivation, worsened seizures, without changing previous sleep amount itself.

In summary, akin to process C, the influence of process S on seizure occurrence remains noteworthy. While human studies have yielded mixed results in this regard, animal models

have consistently showed that sleep deprivation is associated with increased susceptibility to various epileptic outcomes, including epileptogenesis[188], elevated seizure rates[96,194], and the occurrence of SUDEP[192].

2 Aims and Hypothesis

The overall aim of this work is to gain a comprehensive understanding of the combined and individual roles of both process S and process C in shaping the circadian seizure cycle.

The circadian seizure cycle, characterized by the recurrent occurrence of seizures during preferred times of the day, has been observed clinically, as well as in animal models of epilepsy. Although variable as to the specific timing, the circadian seizure cycle is highly prevalent but under-researched. In people with epilepsy, circadian timing of seizures exhibits intra-and inter-individual variations. In animal models of epilepsy, circadian timing shows inter-model variability. Still, the high consistency of any specific circadian seizure cycle across different species, aetiologies and individuals, as well as the persistence of this circadian seizure cycle without external timing cues hints that endogenous physiological cycles with a circadian periodicity are key in governing seizure risk on a 24 hour scale. Although the circadian seizure cycle is known since decades the exact nature of the endogenous circadian cycle governing seizure timing remains unknown.

We hypothesize that one of two mechanisms and/or their interaction is pivotal for the circadian seizure cycle: (i) the circadian clock itself (referred to as process C), which is governed by core clock genes and is intrinsic to every cell (including neurons), and (ii) the sleep-wake cycle along with its homeostatic regulation (referred to as process S or sleep homeostat). These cycles are tightly coupled under physiological circumstances and oscillate with a 24-hour periodicity. Both cycles are known to modulate neuronal activity and have been linked to the circadian seizure cycle through clinical and experimental observations. A causal role has not yet been demonstrated for either cycle.

To test our hypothesis, we conducted long-term multisite recordings in the intrahippocampal KA model of MTLE, while experimentally manipulating the

physiological circadian cycles using established chronobiological paradigms. Our work was divided into three aims:

- Aim 1 aimed at characterizing the circadian seizure cycle in the intrahippocampal KA mouse model of MTLE under physiological conditions. To achieve this goal, we recorded the animals under a light-dark cycling environment.
- Aim 2 aimed at characterizing the endogenous circadian seizure cycle and challenged its robustness. To achieve this, we exposed mice to constant environments known to be more (constant light) or less (constant dim red light) challenging for the maintenance of the physiological circadian cycle over prolonged periods of time.
- Aim 3 aimed at disentangling the contributions of process S and process C to circadian seizure cycle. For this purpose, we subjected mice to a number of interventions that 'decouple' process S and C to some extent: (i) T20 paradigm: we subjected the animals to an artificial light-dark environment with a periodicity of 20 instead of 24 hours, (ii) Jetlag paradigm: we imposed a single time shift in the onset of the dark period, (iii) Gentle sleep deprivation (GSD) paradigm: we selectively manipulated process S by subjecting the animals to GSD at different circadian times.

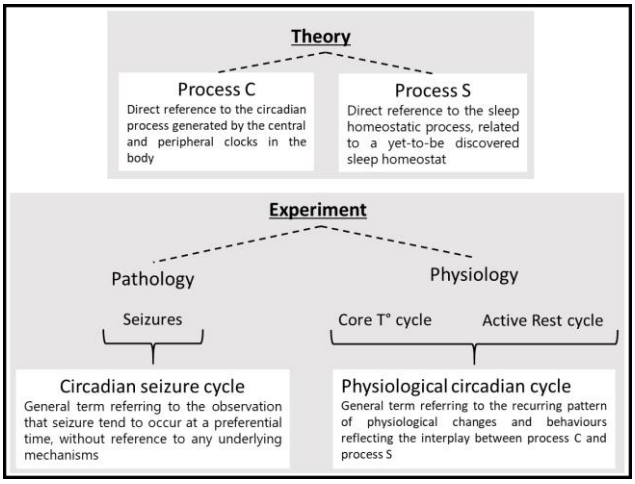

Figure 7 Conceptual and experimental framework

Schematic shows the conceptual framework guiding this thesis and the experimental approach employed. The figure also provides an overview of the nomenclature used throughout the thesis.

Contributions

The following sections of this thesis represent the results obtained achieving the overall goal mentioned in the section above. The experiments were designed by Professor Maxime Baud and myself together with valuable input from Professor Antoine Adamantidis and Professor Markus Schmidt, two principal investigators at the "Zentrum für experimentelle Neuologie" at the Inselspital Bern. The work presented in this thesis will be core of a forthcoming publication of which I will be the first author.

3 Methods

3.1 Mice

A total of 62 adult male C57Bl6 mice (weight [mean±SD]: 29±4g, age: 10 weeks) were implanted with a multi-site EEG and temperature probe for multimodal chronic recording over weeks and months. During surgical preparations, recovery and experimental recordings mice were single housed under controlled conditions (ambient temperature 21±1°C, humidity 50-55%) with food and water ad libitum. If not otherwise specified, the light-dark cycle was 12h-light/12h-dark.

3.2 Surgical procedures

3.2.1 Kainic acid chronic epilepsy model

To render mice epileptic, one unilateral intrahippocampal injection of KA was performed. Mice were anaesthetised (1-1.5h) using isoflurane (flow 600-800ml, induction at 5% and maintenance at 1.5-2%) and their head was fixed in a neurosurgical stereotactic frame with ear-bars. Hair was shaved and the cranium was exposed. The head was aligned, so that Bregma and Lambda were at the same level. KA (5mM dissolved in NaCl, Tocris Bioscience) was injected (280nl, 50nl/min) unilaterally in the right dorsal hippocampus (-2.0AP, +2.0ML, -1.55DV) via a burr hole (Ø 0.59mm). After the scalp was sutured (FST Item No. 18020-50), the mice were removed from the stereotaxic frame. Within minutes, mice developed a status epilepticus which was video-recorded and severity was classified as 0= normal behaviour (no SE), 1= subtly abnormal behaviour like unreactive or uncoordinated movement (subtle SE), 2= forelimb clonus, circling and fast breathing (clear SE) and 3= tonic extension of the tail, stiffness of the mouse during handling and wild jumping (severe SE). A subset of control mice was injected with NaCl (0.9%) intra-hippocampal instead of KA. Diazepam (5mg/kg, Roche) was administered 45 minutes after

removal from the stereotaxic frame for mice injected with KA (to stop the overt signs of SE) and NaCl. Pain management was provided to all mice with Metacam (Boehringer Ingelheim, 5mg/ml, 1ml/kg bodyweight) prior to surgery and the following three days after surgery.

3.2.2 Electrode implantation

Mice were implanted under general anaesthesia (3-4h) one to three weeks after KA/NaCl injection with a custom implant amounting two cranial or 14 intracerebral EEG electrodes as well as electromyography (EMG) electrodes, which served also for the recording of electrocardiogram (ECG). For anaesthesia a reversible mix (10 µl/g) consisting of 10% Midazolam 5mg/ml (Sintetica, Switzerland), 2% Medetomidine 1mg/ml (Graeub AG, Switzerland), 10% Fentanyl 0.05mg/ml (Sintetica, Switzerland) and 78% NaCl (0.9%) was injected i.p. Upon loss of reactivity, mice were placed in a neurosurgical stereotactic frame and the cranium was exposed by re-opening the prior midline incision left after KA respectively NaCl injection. After the skull was aligned as described above, holes were drilled for the placement of the electrodes. EEG screws (Ø1.9mm, Paul Korth GmbH, Switzerland) soldered to a stainless-steel cable (W3 wire, USA) were placed bilaterally on the frontal lobe (+2.0AP, ±2.0 ML from Bregma). EEG screws inserted above the cerebellum (-5.5AP, 0ML) and the olfactory bulb (+4.0AP, 0ML) served as reference and ground, respectively. Custom made intracerebral depth electrodes for the recording of LFP (coated tungsten wires Ø76.2µm, model 796000, A-M System, USA) pinned to an 18-EIB board (Neuralynx, USA) were implanted in different nodes of the limbic circuit (Retrosplenial cortex: -1.2AP, ±0.5ML, -1.5DV, CA1 subfield of the hippocampus: -2.0AP, ±1.3ML, -1.55DV, DG: -2.0AP, ±1.3ML, -2.25DV, CA3 subfield of the hippocampus: -2.0AP, ±2.2ML, -2.25DV, Subiculum: -3.2AP, ±1.6ML, -1.9DV, Entorhinal cortex -4.8AP, ±3.2ML, -2.5DV, Fig 11b). To ensure that the montage was stable during the several weeks

and months of recording the skull's surface was roughened by careful scratching with a needle and cleaned with ethanol to remove any potential connective tissue, debris or blood. It was then covered with Vetbond (3M, No. 1469SB) to provide optimal adherence of the cement (Kulzer Paladur cement, Ivoclar Tetric EvoFlow) placed on and around each electrode. EMG/ECG electrodes were sutured to the trapezius muscle. After implantation anaesthesia was reversed using a mix a (10 µl/g) consisting of 5% Atipamezole 5mg/ml (Graeub AG, Switzerland), 2% Naloxone 4mg/ml (OrPha Swiss GmbH, Switzerland), 50% Flumazenil 0.1mg/ml (Anexate, Roche, Switzerland) and 43% NaCl. Mice were carefully monitored over the following days after surgery and pain management was provided as described above.

3.2.3 Temperature probe

In 20 (n=16x KA, 4x NaCl) out of 32 mice, also core abdominal temperature (core Tº) was recorded using Anipill loggers (BodyCap, Paris, France). One to two weeks after electrode implantation mice were briefly anaesthetized (45 min) using isoflurane, as described above. The abdominal area was shaved, and the skin and muscle were incised separately. The Anipill logger was then placed intraperitoneal, and muscle and skin were sewed back separately. During the same anaesthesia, the EIB board was connected to a RHD headstage with accelerometer (Intan technologies, Part #C3335) and an RHD SPI Interface cable (Intan technologies, Part #C3203).

3.3 Chronobiological paradigms

To characterise the circadian timing of seizures in this model, mice were subjected to different chronobiological paradigms over several months of recording. Five different paradigms have been used:

- *Baseline 12h-light/12h-dark environment,* that is an imposed cycle with a period of 24*hours (LD, ≥ 2 weeks):* At the beginning of the experiment all mice were kept under a light-dark cycle (LD) with 12h white light (22 Lux) and 12h dim red light (wavelength 625nm, 9 Lux), to determine the individual circadian seizure timing under baseline conditions. After at least 10 days in a LD environment different mice underwent a subset of weeks-long blocks of chronobiological manipulations variably ordered.
- *Gentle sleep deprivation* (GSD, 2 weeks): four sessions of GSD every third or fourth day for four hours. GSD was performed either at the beginning or at the end of the light (resting) phase during periods with either high or low endogenous sleep pressure. The mice were kept awake by placing novel objects in the cage, giving condensed milk and gentle poking if mice were falling asleep.
- *Jetlag (one-time time shift). A* subset of mice was subjected to a *jetlag environment (jetlag)* where the light-dark schedule was advanced by four hours resulting in an internal misalignment of the physiological circadian cycle and the external ambient light condition[195]. The Jetlag protocol was performed 6 days after the last session of GSD.
- *Constant dim red light environment (DD, ≥ 2 weeks)* during which mice were exposed to constant dim red light (wavelength 625nm, 9 Lux) over ≥ 2 weeks. This paradigm deprives the mice from any cues about the external time of the day so that they will solely rely on their endogenously generated circadian rhythm. This allows to study the effect of the circadian cycle on seizures in the absence of external cues that may time seizures[196].
- *Constant light environment (LL ≥ 2 weeks)* during which mice were exposed to constant white light (22 Lux) over ≥ 2 weeks. During LL, GSD was performed at

different phases of the underlying circadian cycle using the techniques described above. Like in DD the mice are deprived from external cues and follow their endogenously generated circadian rhythm. Further, constant light is known to impose a constant phase-advancement onto the molecular clock in the SCN, resulting in a longer periodicity than the animal-specific circadian period[197].

- *10h-light/10h-dark environment,* that is an imposed cycle with a period of 20hours (*T20 LD, ≥ 2 weeks)* where mice were exposed to a shortened light-dark cycle with 10h of white light and 10h of darkness imposing an external Zeitgeber with a period of 20 hours, which lies outside the entertainment range of the circadian clock in mice[198], leading to an internal misalignment of the physiological circadian cycle and the external ambient light condition[199].

Each mouse underwent an initial baseline recording session in LD, followed by exposure to a specific subset of the before described chronobiological paradigms. The order of exposure varied among different groups of mice that were recorded together (Fig. 11a, Sup. Fig. 2).

Throughout the experiment mice were minimally disturbed and isolated in a cabinet (Tecniplast, Aria Ventilated cabinet BIO-C36) to eliminate any external cues. Well-being of the mice was checked daily using live video recording of each individual cage. Cages were checked in person every 2nd to 4th day at random intervals and at random time points between 8am and 8pm. Cages were changed every 2 to 3 weeks or at an onset of a new chronobiological paradigm. The light-dark schedule in the cabinet was programmable and the intrinsic white noise (52dB) and vibrations generated by the cabinet isolated the mice from potential external cues.

3.4 Data Acquisition and pre-processing

During the whole experiment EEG, EMG, Core T° as well as video and actimetry were recorded 24/7. Data was stored as one-hour files. Signal processing and analysis were carried out with custom written Python scripts (Python Software Foundation, https://www.python.org/). EEG, LFP, EMG and locomotor activity were amplified and digitised using the RHD recording system (Intan technologies, Los Angeles, USA) and sampled at 2kHz. The data was notch filtered at line-noise frequency and its harmonics (50, 100, 150, 200, 250, 300, 350, 400, 450, 500, 550, 600, 650, 700, 750 and 800Hz). Individual channels were zero-centred (removal of occasional DC component) and band-pass filtered between 0.3 to 800 Hz. Each EEG channel was then normalized by scaling its median absolute voltage to 50 µV.

Locomotor activity was sampled at 250Hz using a 3-axis accelerometer incorporated to the head stage (Intan technologies, Part #C3335). Each accelerometer was calibrated as described by the manufacturer and the overall acceleration in all 3 directions was calculated as follows:

$$|a| = \sqrt{a_x^2 + a_y^2 + a_z^2}$$

With a_x, a_y, and a_z being the acceleration in each direction. In the subset of mice implanted with the Anipill logger the core T° was sampled at a 5 min interval via a telemetry unit (Anilogger monitor, Bodycap France).

3.5 Visual scoring of vigilance states

Vigilance stages were scored visually in a subset of 88 days before and during GSD protocol (onset of the inactive phase) across 12 mice (KA, n= 10 and NaCl, n=2) in three categories: wakefulness, Non-Rapid Eye Movement (NREM) sleep, and Rapid Eye Movement (REM) sleep. Visual scoring was carried out offline based on 4-second epochs

of the bipolar frontal EEG, DG LFP, and the EMG. Channels with high epileptic activity that interfered with visual inspection were excluded. Wakefulness was scored for epochs with high-frequency, low voltage activity in the EEG and high EMG activity. During some periods, high theta activity, typical for locomotion in rodents, along with tonic EMG activity was observed. During quiet wakefulness low activity was observed in the EMG, while the EEG showed the typical characteristics of wakefulness described before. NREM sleep was scored for epochs with low-frequency and high-voltage activity, represented by slow waves (<4Hz) visible primarily in the frontal EEG, along with low EMG activity. REM sleep was scored for epochs with high-frequency, low-voltage activity like that observed during wakefulness, dominated by theta waves in the DG-derived EEG, and very low EMG activity. These scores were used to evaluate the effect of sleep deprivation on the EEG and served as a reference for evaluating the developed algorithm for automated scoring of vigilance states described below.

3.6 Visual scoring of seizures

A subset of seizures was visually evaluated based on an increase in line length. Periods with a pronounced increase in line length were considered potential seizures. For each one-hour file that was reviewed, all potential seizure periods were assessed separately, starting with those displaying the highest line length and then examining events with progressively smaller line length increases until the detected events were not considered as seizure anymore. Seizures were considered as events of increased, uninterrupted ictal activity for more than 10 seconds visible in one or more channels. The seizures detected in this way were used to determine the threshold of 22 spikes/ 10sec in the automated detection of seizures described in a later chapter. Generalized tonic-clonic seizures were manually annotated throughout the entire recording of a single animal. Over the course of 24 hours all recorded one-hour files were concatenated and the total standard deviation across the

line length of all channels was calculated for each one-hour file. Files were reviewed manually starting with those displaying the highest standard deviation and then files with progressively smaller standard deviation until in three subsequent files no generalized seizure was detected (n=5900/ 50553 files reviewed). A subset of convulsive seizures was also cross-referenced with simultaneously recorded videos to confirm their convulsive nature.

3.7 Automated annotation of vigilance states and seizure detection

We employed an automated approach using non-negative matrix factorization (NNMF) to annotate vigilance states and seizures in our dataset. NNMF is a dimensionality reduction algorithm which effectively extracts recurring patterns from large input matrices. We chose NNMF over other clustering algorithms for its flexibility and its non-negativity constraints which allows for a more intuitive interpretation of the results[200].

NNMF was originally introduced by Paatero and Tapper in 1994[201] as positive matrix factorization and the popularized by Lee and Seung in 1999[202]. It operates by decomposing a non-negative matrix V (with dimension m x n) into two lower-dimensionality non-negative matrices W (m x r, referred to as "basis functions", BF) and H (r x n, referred to as "coefficients" or “activation matrix”) so that $V \approx WH$. The extracted BFs in W represent common recurring patterns of features present in the original input matrix V. Intuitively for EEG data, these recurring patterns represent recording channels that share specific features[200]. The associated coefficients in H can be seen as the weight of each BF at a given time point in the input matrix V and provides information of how much the feature pattern (represented by the corresponding BF) is present for a given time point. Therefore, each original data point over time can be approximated by the linear combination of the BFs in W and their coefficients given in H at that time (Fig. 7). NNMF was computed using the following formula:

$$V \sim R = WH = \sum_{i=1}^{r} W_{mi}\, H_{in}$$

Where r corresponds to the rank of the decomposition, m corresponds to the number of features in V and n corresponds to the number of data points in V. For each iteration the fit with the original input matrix V is evaluated by computing the L2 norm, that is the Euclidean distance between the original and the reconstructed data. H and W are updated over several iterations such that their multiplication gradually provides a better approximation of V.

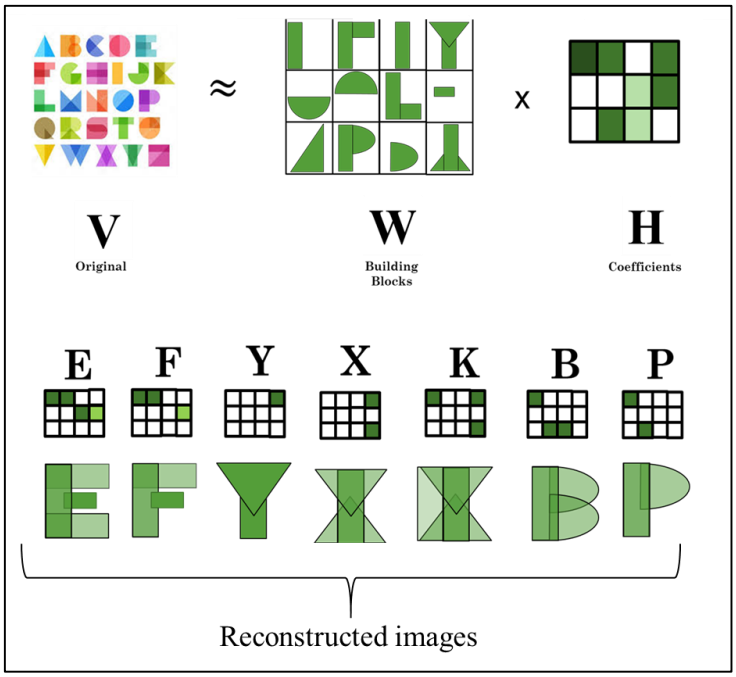

Figure 8 NNMF's working principle, illustrated through printing letters

In this analogy, NNMF operates like a printing machine. It first breaks down the original image of letters (V) into common patterns or building blocks (W) shared across letters. Then, it recreates each letter by combining the shared patterns (W) using the coefficient matrix (H). This process unveils the essence of each letter, resulting in the reconstructed image.

3.7.1 Feature extraction

A feature is a signal or measurement which shows characteristic behaviour for a certain pattern that is present in the original image (e.g. increase in SWA for NREM sleep). Feature extraction refers to the process in which the raw EEG signal is transformed in a feature

vector, which contains the desired features. For feature extraction the raw EEG data was first pre-processed and then down sampled to 100Hz to obtain file sizes which were manageable from a computational standpoint. As the NNMF algorithm requires a non-negative matrix as input, we extracted several non-negative features from the down sampled EEG.

First, we applied the line length transform over a 100ms (10dp) sliding window on all recorded EEG channels, as well as the bipolar EMG. Line length uses the first derivative and cumulates it over a window of time, therefore intuitively line length can be seen as an approximation of the overall power in the EEG and reflects the amplitude-frequency characteristics of the EEG.

$$Line\ length = \frac{1}{n-1}\sum_{i=1}^{n-1} abs(x_{i+1} - x_{i)}$$

Where *n* represents the total number of samples in the sliding window and *x* represents the voltage value of the EEG at a given time. The line length is expressed per unit of time and fulfils the non-negativity constrain for NNMF.

Second, we applied a frequency transform on all EEG channels and bipolar EMG by fitting a frequency-resolved Morlet wavelet (20 cycles per central period). We emphasized the frequency-resolution by using a 20-cycle wavelet to minimize the impact of transient epileptiform discharges, and because we aimed at capturing established oscillations characteristic of different sleep stages and wakefulness. We computed the total power for different frequency bands of interest: delta (δ) 1-4Hz, theta (θ) 4-10Hz, sigma (σ) 10-16Hz, beta (β) 16-30Hz, gamma (γ) 30-50Hz as well as the broad-band total power (1-50Hz). The scales used for the wavelet transform were chosen so that each frequency band of interest

contained five linearly-spaced frequencies (1.18Hz, 1.43Hz, 1.82Hz, 2.5Hz, 3.98 Hz, 4Hz, 4.53Hz, 5.25Hz, 6.23Hz, 7.68 Hz, 10.82 Hz, 11.79 Hz, 12.95 Hz, 14.37 Hz, 15.87 Hz, 16.13 Hz, 17.54 Hz, 19.61 Hz, 22.22 Hz, 25.64Hz, 32.89Hz, 35.97Hz, 39.68Hz, 44.25Hz, 50Hz).

Third, locomotor activity was extracted from the head-mounted accelerometer following the instructions of the manufacturer.

Subsequently, all the extracted features (line length, power, and locomotor activity) were subsampled to 10Hz and combined into a single 24-hour file, representing the data for one single mouse over one calendar day.

3.7.1.1 Feature engineering

To enhance the performance and accuracy of our automated vigilance state annotation algorithm, we introduced various ratios between frequency bands of interest that exhibit characteristic behaviour for different vigilance states. Employing ratios also helped mitigate the impact of epileptiform discharges, as they typically affect a broad range of frequencies, whereas changes between vigilance states primarily affect specific frequency bands of interest. A comprehensive summary of all features used, along with their behaviour during a given vigilance state, is provided in Table 1.

Used for	Feature	Formula	Characteristic behaviour during…		
			…Wake	…NREM	…REM
Automated annotation of vigilance states & Automated seizure detection	Line length (10ms window)	$Line\ length = \frac{1}{n-1}\sum_{i=1}^{n-1} abs(x_{i+1} - x_{i)}$	↑↑	↓	↑
Automated annotation of vigilance states	Total Power EEG	-	↑	↑	↓
	Delta (1-4Hz)	-	↓	↑↑	↓
	Theta (4-10Hz)	-	↑	↓	↑↑
	Sigma (10-16Hz)	-	↓	↑	↓
	Beta (16-30Hz)	-	↑	↓	↓
	Gamma (30-50Hz)	-	↑↑	↓	↑
	Power EMG (30-50Hz)	-	↑	↓	↓↓
	Locomotor activity	-	↑/↓	↓↓	↓↓
	Bipolar EMG	-	↑	↓	↓↓
	Line length Ratio	$\frac{Line\ length\ EEG}{Line\ length\ EMG}$	↓	↑	↑
	EMG Product (EMG_P)	$Line\ length_{EMG} \times Power_{EMG}$	↑↑	↓	↓
	Power Ratio Wake	$\frac{\gamma + \beta}{total\ Power}$	↑	↓	↓
	Power Ratio Sleep	$\frac{\delta + \theta + \sigma}{total\ Power}$	↓	↑	↑
	NREM Ratio	$\frac{\delta * \sigma}{\gamma * \beta * \theta * EMG\_P}$	↓	↑↑	↓
	REM Ratio	$\frac{\theta}{\gamma * \beta * \delta * \sigma * EMG\_P}$	↓	↓	↑
	Wake Ratio	$\frac{\gamma * \beta * EMG\_P}{\delta * \sigma * \theta}$	↑↑	↓	↓
	Sleep-Wake Ratio	$\frac{\delta * \sigma * \theta}{\gamma * \beta * EMG\_P}$	↓↓	↑	↑

***Table 1:** Extracted and engineered features used for the automated annotation of vigilance states.*

3.7.1.2 Choosing the rank of NNMF

A pivotal aspect of employing NNMF is the selection of the rank *r*, which dictates the number of BFs and coefficients used to approximate the original data and depends on the

specific goal of the analysis and the dataset at hand. The overall goal is to choose an optimal number of *r* which simplifies the dataset while still yielding meaningful results[203].

Opting for a small number of *r* usually yields more interpretable BFs since each BF represents more general feature patterns present in the original data. It also comes with the advantage of reduced computational costs, particularly for larger datasets. However, it is important to keep in mind that choosing a small number of *r* can potentially lead to an under fitting of the data, meaning that not all important features of the original data are captured in separate BFs. This leads to an oversimplified representation of the original data[204].

Conversely opting for a higher number of *r* allows for a more complex and detailed representation of the data since more BFs can naturally capture more of the subtler and finer patterns in the dataset. Yet in our experience the interpretation of these BFs can become more complicated with increasing number of *r*. In the worst -case scenario, a high *r* can result in an overfitting of the data where the BFs are either capturing noise or start separating feature patterns, that would belong together, into different BFs. The computational demands also rise with an increase in *r*[204].

While some problems (e.g. detection of sleep stages) come with a naturally clear number of underlying components (e.g. for wakefulness, NREM and REM) other problems might require experimentation to find the right *r*. To determine the optimal rank *r* that yields the best result, it is necessary to explore various ranks. The outcome of different *r* can be evaluated by conducting multiple NNMF transformations on the same dataset using the same rank but employing random initializations. The stability of the obtained solutions (i.e. one global minima versus several local minima) can be visualized in the form of a consensus matrix among the cluster attribution of the samples (or the features) and can be quantified using the cophenic correlation[205,206].

3.7.2 Semi-supervised automated annotation of vigilance states

We employed a semi-supervised approach to NNMF to annotate vigilance states in our extensive dataset. To address the challenge of deciding the ideal rank in NNMF, we leveraged NNMF's inherent capability to capture dominant feature patterns using following steps:

- First, we engineered input matrices containing only state-specific data, e.g., pure Wake, NREM, or REM. Data for these matrices was sampled from six different epileptic mice, with each mouse represented by three days of undisturbed sleep and three days of 4 hours of gentle sleep deprivation at the onset of the resting phase. State-specific data (purely wake, NREM, or REM) was extracted and randomly sampled across mice and days, treating state bouts as distinct entities and excluding micro arousals shorter than 4 seconds. Randomly sampled data was concatenated until the final input matrix V held a reasonable amount of data (25920 data points ≙ 3 days of recording). To avoid overfitting, additional data (5184 data points ≙ 20% of the state specific matrix) from alternative states was introduced to the final input matrix V. Each alterative state was represented equally (Fig. 9 a, b).
- Second, NNMF on each of these state specific input matrices with a rank of 1 was initialized. Employing a rank of 1 in NNMF will capture the most dominant feature pattern of the input matrix which in our case yielded us a universal BF representing the most predominant feature pattern for wake, NREM and REM across mice (Fig. 9c).
- Third, we combined the obtained universal BF for wake, NREM and REM and subsequently used them across all mice and recording days to initialize NNMF on a real data 24h recording file. We labelled the 24h file into potential wake, NREM

and REM periods. Each data point was labelled according to the state, whose BF possessed the highest coefficient value at that time point (Fig. 10a-c).

- Finally, we used these time points labelled as potential wake, NREM, or REM and initialized NNMF with a rank of 1 on data labelled previously as potential NREM respectively wake and a rank of 2 for data labelled as potential wake. This resulted in BF representing the most prominent feature patterns for a given vigilance state in an individual mouse during the 24 hours of interest. Using a rank of 2 for wakefulness data separated wakefulness into periods with high and low locomotor activity. The individual BFs were then combined and used to re-initialize NNMF with a rank of 4 for the entire 24-hour data file. Once again, each data point was labelled based on the state associated with the highest coefficient value. This labelling was then considered as the final annotation of vigilance states for that day (Fig. 10d-f).

A detailed flowchart illustrating these steps is provided in Figure 9 and 10. An assessment of the performance of our semi- supervised automated vigilance state annotation is provided in the supplementary materials. (Sup. Fig. 2)

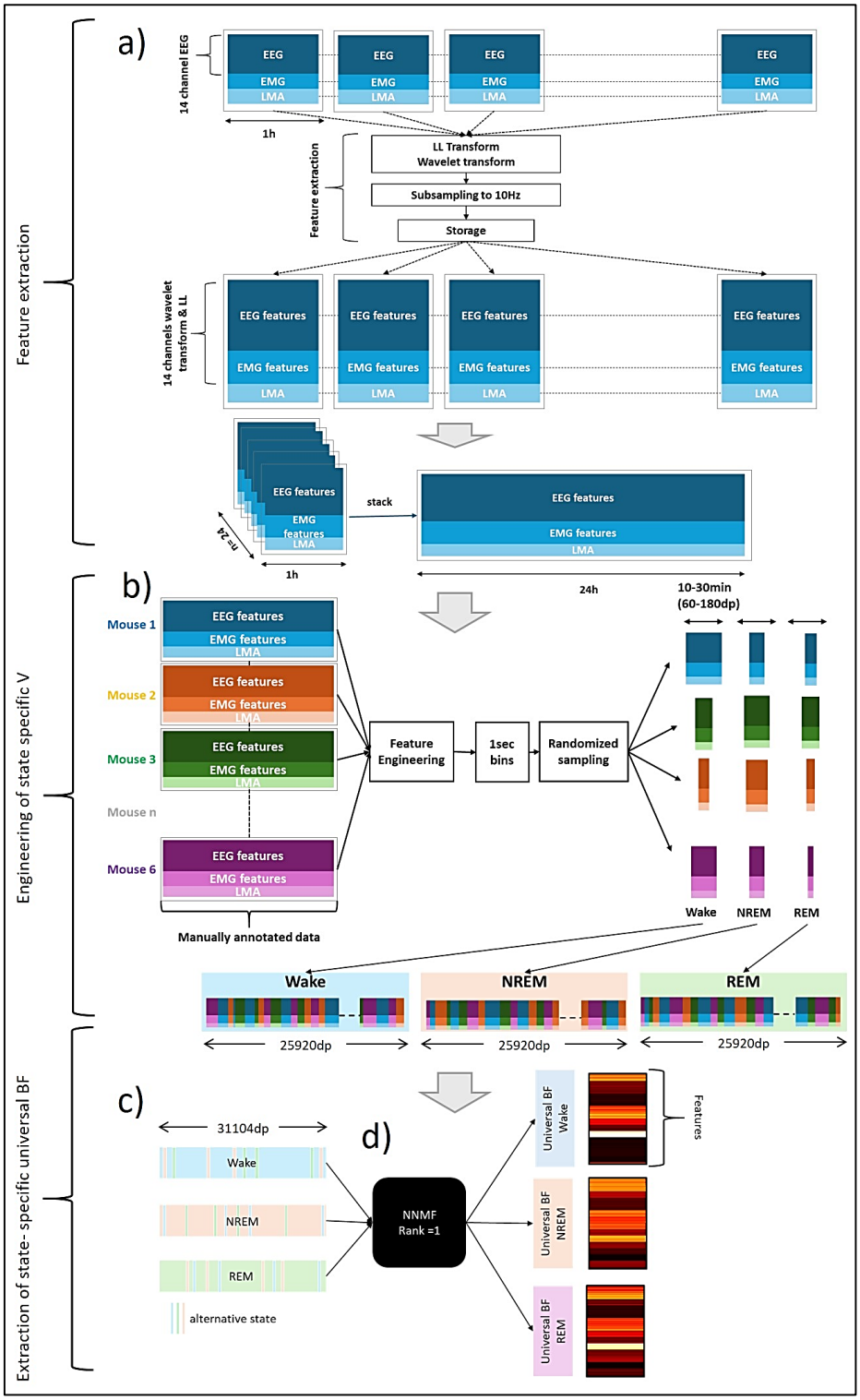

Figure 9 Pipeline for feature extraction and extraction of state-specific universal BF

*Raw EEG data underwent pre-processing and down-sampling. Several non-negative features were extracted, including line length, wavelet-based spectral transform of single EEG channels and locomotor activity. Extracted features (line length, power, and locomotor activity) for each recorded one-hour files of one calendar day way concatenated into a single 24-hour file. (**a**). Input matrices containing only state-specific data (e.g., Wake, NREM, or REM) were engineered by randomly sampling data from six epileptic mice. The data for each mouse was previously annotated manually and contained features extracted directly from the EEG and engineered features (**b**). To avoid overfitting data for alternative states was added to the state- specific input matrices(**c**). NNMF was initialized on these input matrices with a rank of 1, generating universal BFs capturing the predominant feature patterns for each state (**d**).*

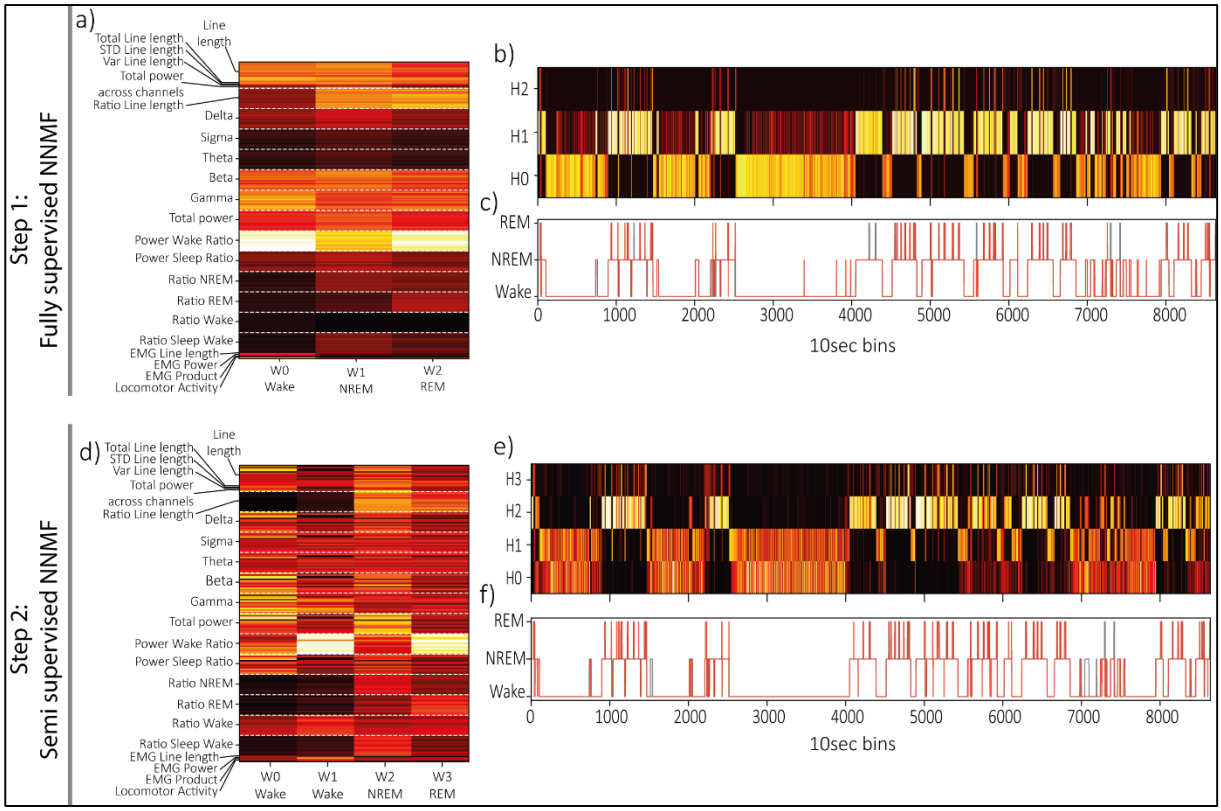

Figure 10 Automated annotation of vigilance states in an extracted 24h file

a) - c) *In a fully supervised approach universal BFs extracted for Wake (W0), NREM (W1), and REM (W2) were used to initiate NNMF on a 24h file containing the data of one calendar day for one mouse (a). Mouse-specific coefficients are derived (b) across the entire 24-hour file and the 24-hour file is annotated into approximate wake, NREM, and REM states, with each time point labelled according to the BF with the highest coefficient (c, with red representing hypnogram of the 24-hour file obtained by the automated annotation algorithm grey being manually scored label)* ***d) - f)*** *In a semi-supervised approach, mouse specific BFs for each state are re-derived using the annotations obtained by the fully supervised NNMF approach. Wake data is decomposed with NNMF using a rank of 2 (W0 and W1), while NREM and REM data are decomposed with NNMF using a rank of 1 (W2 and W3) (d). These mouse-specific BFs are then utilized to re-initialize NNMF on the same 24-hour file deriving mouse-specific coefficients over the entire 24-hour period (e). The final state label is assigned based on the BF with the highest coefficient at each time point, and the hypnogram for the 24-hour file is generated (f, with red= automated annotation, grey= manually labelled annotation)*

3.7.3 Automated seizure detection

As line length can be seen as an approximation of the overall power in the EEG and reflects the amplitude-frequency characteristics of the EEG it can be leveraged to detect epileptiform activity in the EEG[200,207]. IEDs and seizures were automatically detected using custom written python scripts. The signal was band pass filtered between 0.7 and 40Hz and then down sampled to 100Hz. For automated IED detection the maximal line length across all channels was calculated at all time points over a 100ms (10 data points) sliding window.

Line length was calculated as described above A threshold corresponding to the 95th percentile of the maximal line length across channels obtained for one hour of recording was applied. Time points at which the threshold was crossed were identified as IED. The total number of IEDs was calculated within 10 seconds sliding window. Seizures were defined as uninterrupted trains of IED for ≥ 10 seconds and frequency >22Hz in any EEG trace obtained. Detected seizures were classified either as seizures without behavioural correlates or convulsive seizures which had a behavioural correlate, in the form of tonic-clonic convulsions in the corresponding video recording. For further analysis, electrographic seizures were subdivided into seizures with increasing duration (10-20 seconds, 20-30 seconds, 30+ seconds).

3.8 Extraction of slow wave activity

We used the "delta" feature already extracted for the automated detection of vigilance states for the assessment of SWA. SWA corresponded to the average total power in the delta (1-4Hz) frequency band for the left and right frontal EEG channel. Power was extracted using a frequency-resolved Morlet wavelet (20 cycles per central period). The power in the delta frequency band was represented by 5 linearly spaced frequencies (1.18Hz, 1.43Hz, 1.82Hz, 2.5Hz, 3.98 Hz). Only consolidated NREM bouts longer than 1 minute were considered for SWA analysis. For epileptic mice periods with a detected seizure were excluded for SWA analysis.

3.9 Time-frequency analysis of underlying cycles

To characterize the individual physiological circadian cycle and the circadian seizure cycle, we calculated the total locomotor activity, epileptiform activity (EA), and the mean core T° over non-overlapping 5-minute bins. The cyclicity present in the locomotor activity was used as a proxy for process S and is referred to as the active rest cycle. The cyclicity present in the core T° cycle was used as a proxy for process C. The active rest cycle- together

conjointly with the core T° cycle constitute the physiological circadian cycle (Fig. 7). EA is defined as the percentage of time epileptiform activity of any duration >10 seconds was detected and served as a proxy for the circadian seizure cycle (Fig.7). Given their relative stationarity over days, these cycles were characterised by fitting a frequency-resolved Morlet wavelet (20 cycles per central period) with periods ranging from 0.8 to 34 hours The artificially generated multidian cycle in the T20 environment was calculated in an alike way but with periods ranging from 12.5 to 166.6 hours.

For each wavelet-extracted cycle the period and strength were characterised. The period corresponds to the peak in the average power spectrum across days for a given environment, and the strength corresponds to the total average power within a narrow bandwidth around that peak (± two hours). We used instantaneous phase synchrony[208] to measure the phase angle relationship between the active rest and core T° cycle at each time point. The instantaneous phase synchrony ranges from 1 (both cycles have same phase at time point t) to 0 (both cycles have opposing phases at time point t). In the T20 paradigm we considered time points with a phase synchrony >0.6 as periods in which both cycles are aligned and time points with phase synchrony <0.3 were considered as periods where both cycles were misaligned. The instantaneous phase synchrony was calculated as follows:

$$Phase\ synchrony = 1 - \sin(\frac{|\psi_t - \phi_t|}{2})$$

Where ψ and ϕ represents the phase information of the active rest and core T° cycle at different time points *t*. Phase information was extracted using wavelet transform as described above.

To assess the strength of circadian seizure timing we determined the tendency of seizures to cluster at different phases of the underlying circadian cycle. The strength of this “phase clustering” was quantified using the phase locking value (PLV) which corresponds to the

sum of unitary complex numbers, each representing the phase on the underlying cycle for an individual seizure. The PLV was calculated as follows:

$$PLV = Z = R^{-i\varphi} = \frac{1}{S}\sum_{s=1}^{S} e^{-i\varphi s}$$

where φ_s represents the phase of a given cycle at which a single event *s* has been observed. *i* corresponds to the imaginary unit and *S* represents the number of events. The complex number *e* has an angle φ which corresponds to the average phase and a modulus R which corresponds to the resultant strength of the phase-clustering, which we refer to as phase locking value (PLV)[64]. The PLV ranges from 0 to 1 with 0 corresponding to a uniform random distribution of events and 1 corresponding to a non-uniform distribution with all events occurring at the same phase of the underlying cycle[64,209,210]. The PLV was calculated on a minimum of 10 events.

3.10 Statistics

The strength of circadian seizure locking was assessed using the PLV. Statistical significance for individual mice was assessed by comparing the observed data to surrogate data generated through the random shuffling of seizure time points within a given environment. This shuffling process was repeated 200 times to create surrogate datasets for statistical comparison. This approach tested the null hypothesis that seizures are randomly distributed without relationship with the underlying circadian cycle[210]. A PLV exceeding the 95th percentile of that of surrogates was considered significant. Mice that did not show a statistically significant circadian seizure cycle in LD were not considered for further analysis. Correlation between different measurements was measured using Pearson correlation, statistical difference between groups was assessed using Wilcoxon rank test, respectively ANOVA.

3.11 Histology

At the end of the experiment the mice were anaesthetised with Pentobarbital (250mg/kg, Esconarkon 1:20, Streuli Pharma AG, Switzerland) and transcardially perfused with NaCl (0.9%) and 4% formaldehyde (Grogg Chemie, Switzerland). The brain was then extracted and post-fixed in 4% formaldehyde for a minimum 24h and then transferred to a 30% sucrose solution for 48h before being flash-freezed with -80° Methylbutane. The brains were sliced sagittal (30µm), and triplicates were collected in phosphate buffered saline.

To assess the extent of hippocampal sclerosis, the obtained sections were stained with Cresyl violet. Before staining sections were mounted on Superfrost Plus slides (Epredia) and de-and rehydrated in osmotic water, ethanol with increasing concentration (70%, 90%, 95%, 100%) and Xylol for 1min each before covering them in formaldehyde for 7min and osmotic water for 5min. The slides were then immersed in Cresyl Violet staining for 10-20min. Afterwards the slides were rinsed using osmotic water and dehydrated again with ethanol with increasing concentration (70%, 90%, 95%, 100%) and Xylol. Brightfield images were obtained using a microscope at different magnifications (4-10x).

4 Results

We analysed continuous locomotor activity (proxy for process S), core T° (proxy for process C) and seizure data from a total of 32 mice (n= 24xKA, 8xNaCl) with an average recording duration of 85±55 days (Sup. Table 1) amounting approximately 10 years of EEG recording. A total of 28 mice (n= 20xKA, 8xNaCl) were eligible for analysis across different environments. Four KA mice died without sufficient data in baseline light-dark environment and were therefore only included for the analysis of SUDEP timing. Overall, we detected 36'385 bursts of epileptic activity longer than 30sec without convulsions (thereafter 'electrographic seizure'). 'Convulsive seizures', with tonic-clonic movements on video contemporaneous to a burst of epileptic activity, amounted to 1601 events (4.2% of all seizures) among 20 epileptic mice (four without, Sup. Table 1).

To assess the roles of process S and process C in seizure timing we subjected the mice to several chronobiological paradigms. The first paradigms (LD, DD and LL) aimed at characterizing the shared influence of process S and process C, i.e. the physiological circadian cycle, on the circadian seizure cycle, while the second set of chronobiological paradigms (T20, Jetlag, GSD) aimed at decoupling process S and process C and assessing their individual impact on the circadian seizure cycle.

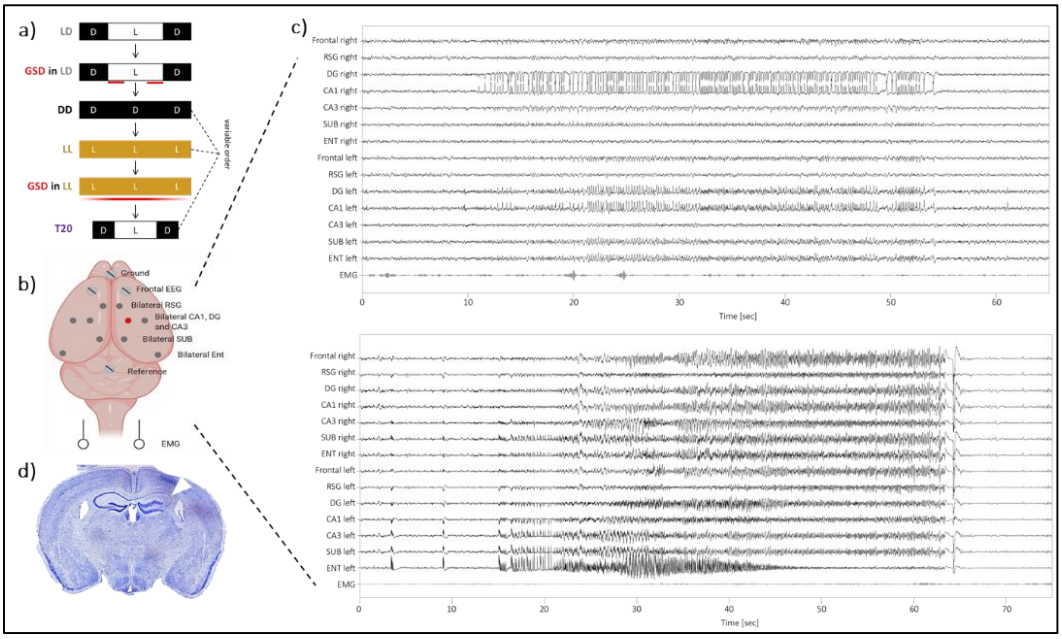

Figure 11 Methods.

a) *Experimental timeline: All mice were first recorded in a baseline 12h-light/12h-dark environment (LD), followed by four sessions of gentle sleep deprivation (GSD) lasting 4 hours each, either at the onset (7 am - 11 am) or offset (3 pm - 7 pm) of the light phase (red underlying line). Recovery after GSD session lasted 2-3 days. Mice were subsequently exposed to constant dim red light (DD), constant light (LL), which included GSD at various time points of the underlying cycle, and a 10h-light/10h-dark environment (T20) in a variable order.* ***b)*** *Electrode montage: Depth electrodes are represented by black dots, and the KA/NaCl injection site is denoted by a red circle. Brain regions implanted bilaterally with depth electrodes include RSG (Retrosplenial cortex), CA1 and CA3 subfields of the hippocampus (CA1& CA3), dentate gyrus (DG), SUB (Subiculum), and Ent (Entorhinal cortex). Surface EEG was recorded from the frontal lobe and EMG/ ECG was sutured to the trapezoid muscle.* ***c)*** *Example of an electrographic seizure (top) and a convulsive seizure (bottom) recorded with the electrode montage described in b).* ***d)*** *Brain section showing hippocampal sclerosis at the site of intrahippocampal KA injection (white arrow).*

4.1 Seizure timing in a 12h light/12h dark cycling environment

Under the real-world like conditions of a 12h light-dark cycle with minimal external intervention, we observed a preferential timing of electrographic seizures during the late dark period, corresponding to the active phase in our epileptic mice (Fig 12f, here ~03:00 AM, PLV: 0.25±0.15, N=20). To relate the circadian seizure cycle to the physiological circadian cycle in in these mice we recorded locomotor activity (3D-accelerometer on headstage, n=20) and core T° (abdominal probe, n=13) and extracted periodicity and phase using a frequency-resolved (20 cycles) wavelet transform. The resulting extracted active-rest and core T° cycle were oscillating in synchrony (phase synchrony$_{LD}$: 0.86±0.1) with proportional strength (Pearson r=0.62) and periodicity (Pearson r=0.45) (Sup. Fig. 4). Based on the circadian synchrony between the active rest cycle and core T° cycle we

consider them as equivalent for this paradigm, and refer to them conjointly as the "physiological circadian cycle".

After characterizing the physiological circadian cycle, we evaluated the circadian seizure cycle using two variables: EA cycle and discrete seizure events of varying duration. As in previous human studies, we sought periodicity in the occurrence of epileptiform activity (EA) defined, as the percentage of time EA of any duration >10sec was detected. We further sought to determine the phase of occurrence of discrete seizure events in relation to the physiological circadian cycle. In any individual mouse (Fig. 12a-e), we found that the EA cycle had a strong oscillatory component at about 24 hours (i.e., circadian) and a clustering of seizures during the active phase (seizure counts in Fig. 12e).

Across mice, the circadian clustering of events was tested against surrogate data and was significant for 18 out of 20 mice (90%). Among these 18 mice, the extracted circadian component of the EA c oscillated with a period of 23.8h±0.6h and its strength was proportional to the strength of the physiological circadian cycle across mice (Fig 12g, Pearson r= 0.71). This suggests a circadian co-modulation of behaviour and epileptic brain activity. In a next step we assessed the preferred phase of seizure occurrence. We could consistently observe an increase in circadian clustering with increasing event duration and which was inversely proportional to the sparsity of events. This suggests a circadian modulation of seizure duration and/or the time of occurrence of longer events. While IEDs showed a uniform distribution over 24h (PLV = 0.02 ±0.02) the PLV increased for seizures with increasing duration ($PLV_{10\text{-}20s}$= 0.11 ±0.08, $PLV_{20\text{-}30s}$= 0.15 ±0.08, PLV_{30+s}= 0.25 ±0.13, Fig. 12h). Prolonged seizures longer than 30sec tended to cluster between the peak and the falling phase of the physiological circadian cycle with on average a weak to moderate PLV for electrographic and convulsive seizures ($PLV_{convulsive\ seizures}$= 0.4±0.2, Fig 12i).

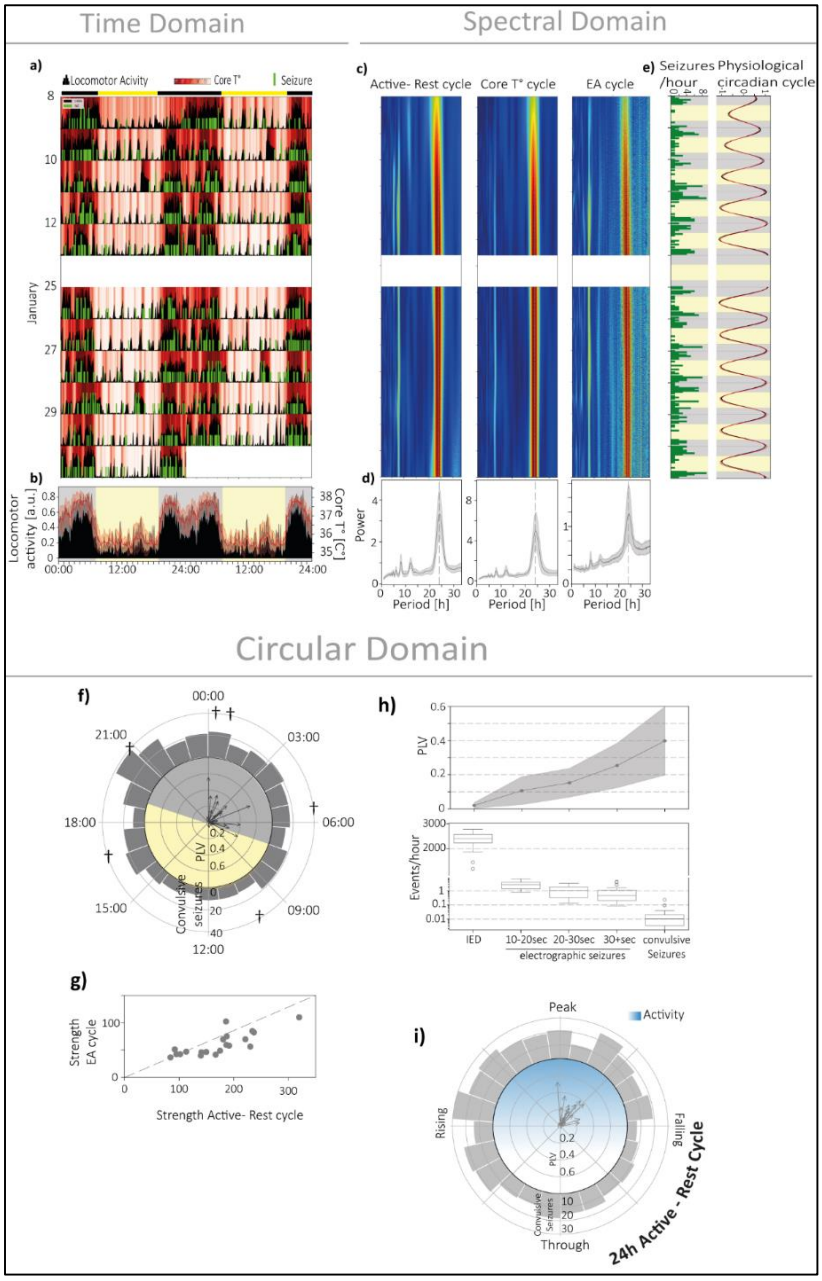

Figure 12 Seizure timing in a 12h light/12h dark cycling environment

a) *Rasterplot showing locomotor activity (black trace), core abdominal temperature (white to red shading) and electrographic seizures longer than 30sec (green ticks) in one epileptic mouse in LD over several days. Data is double plotted such that succeeding days are plotted next to and beneath each other. Yellow and black bars on top indicate lighting conditions at given real-world times (x-axis at the bottom).* ***b)*** *Mean locomotor activity (black trace) and mean core T° (red trace, shading ±SD) over the days shown in a).* ***c)*** *Corresponding wavelet spectrograms for the active-rest cycle (left), core T° cycle (middle) and EA cycle (right).* ***d)*** *Periodogram showing the presence of a dominant circadian period of the active-rest cycle (left), core T° cycle (middle) and EA cycle (right), respectively across all mice.* ***e)*** *Hourly seizure rate with extracted active-rest (black) and core T° (red) cycle for the example shown in a). The cycles are bandpass-filtered at peak circadian period (24h). Shading indicates lighting conditions at given real-world times.* ***f)*** *Circadian timing of seizures longer than 30sec in the late dark phase on a real-world 24h clock shown as individual mean resultant vectors for each mouse recorded in LD. The angle of the vector corresponds to the preferential hour of seizure timing, and the length corresponds to the strength of seizure clustering (PLV). Outer bars represent convulsive seizure counts pooled across mice. Crosses indicated time points of SUDEP.* ***g)*** *Strength of the circadian seizure cycle as a function of strength of the physiological circadian cycle.* ***h)*** *Strength of seizure clustering (top) and counts of discharges (bottom) as a function of the duration of the epileptiform discharge.* ***i)*** *Circadian clustering of seizures longer than 30sec within peak and falling phase of the underlying 24h active rest cycle shown as individual mean resultant vectors as described in f).*

4.2 Seizure timing in a constant environment

In a first step we have confirmed the existence of a circadian seizure cycle in a LD. To characterize the endogenous nature of the circadian seizure cycle and challenge its robustness, we studied the circadian seizure cycle in two constant environments, in which any potential Zeitgeber was removed (light-dark cycle, animal care, etc.). Only mice that had a significant circadian seizure cycle in LD were included for this analysis. Mice were kept in either in DD or LL (n_{DD}= 7xKA, 4x NaCl, n_{LL}= 10xKA, 6xNaCl) with minimal external intervention (Fig. 13 a-h). First, we characterised the physiological circadian cycle. All mice developed a free running cycle (i.e. lack of alignment to real-world time) with maintained ~24h periodicity in DD (24.1±0.1h) and prolonged periodicity in LL (24.8±0.4h). Overall, the strength of the cycles was preserved in DD and weakened in LL (Cycle strength LD: 175±58, DD: 152±46, LL: 79±37, Sup. Fig. 4). Similarly, to observations in the 12h light-dark cycling paradigm the active-rest and core T° cycle had similar periodicity and were oscillating in phase (Phase $synchrony_{DD}$= 0.85±0.15, Phase $synchrony_{LL}$= 0.77±0.18) with proportional strength (Pearson r= 0.67). We therefore consider them as equivalently reflecting the physiological circadian cycle for these paradigms.

We asked how these changes in the underlying physiological circadian cycle may affect the timing of seizures. In any given mouse, we observed a weak and strong drift in the physiological and the seizure circadian cycle in DD and LL compared to the real-world time, respectively (Fig. 13a-h). The wavelet transform of the EA cycle revealed a ~24h periodicity in DD (24.5±0.8h) and a longer periodicity in LL (24.8±0.6h) confirming that the circadian seizure cycle in these mice was endogenously generated (i.e. persisted in the absence of a Zeitgeber). When analysing the preferred phase of seizure clustering, we could observe a circadian modulation of seizure duration with increasing strength of the seizure

clustering inversely proportional to the sparsity of the events similar to what was observed in LD (Fig 13i, PLV_{DD} spikes: 0.02±0.01, 10-20s: 0.17 ±0.07, 20-30s: 0.23 ±0.09, 30+s: 0.33 ±0.11 and PLV_{LL} spikes: 0.01±0.01, 10-20s: 0.12 ±0.04, 20-30s: 0.20 ±0.09, 30+s: 0.26 ±0.03). On an individual level the number of events for epileptic activity was decreased in DD and LL (Fig. 13j). Among the mice which had a statistically significant circadian seizure cycle in LD four out of six (66%) were able to maintain their circadian seizure timing in DD and 6 out of 10 (60%) were able to maintain the circadian seizure timing in LL. One mouse did not show a sufficient number of seizures (<10 electrographic seizures) in DD for the calculation of a PLV value. Both in DD and LL seizures longer than 30sec showed a weak to moderate clustering (PLV_{DD}=0.33 ±0.11, PLV_{LL}= 0.26 ±0.03) and a preserved preferred phase for seizure occurrence between the peak and the falling phase of the physiological circadian cycle (Fig. 13k). Two mice showed a preferred seizure clustering during the rising phase of the active rest cycle in LL. In DD, the strength of the active rest cycle was preserved and weakened in LL. Correspondingly, we observed that the strength of the EA cycle was also preserved in DD but decreased in LL. Importantly, this decrease in the strength of the EA seizure cycle in LL was proportionate to the weakening observed in the physiological circadian cycle (Pearson r= 0.49, Fig. 13l). Thus, the circadian seizure cycle tightly follows the physiological circadian cycle, both in terms of period-length and in terms of strength, suggesting that the latter modulates the former.

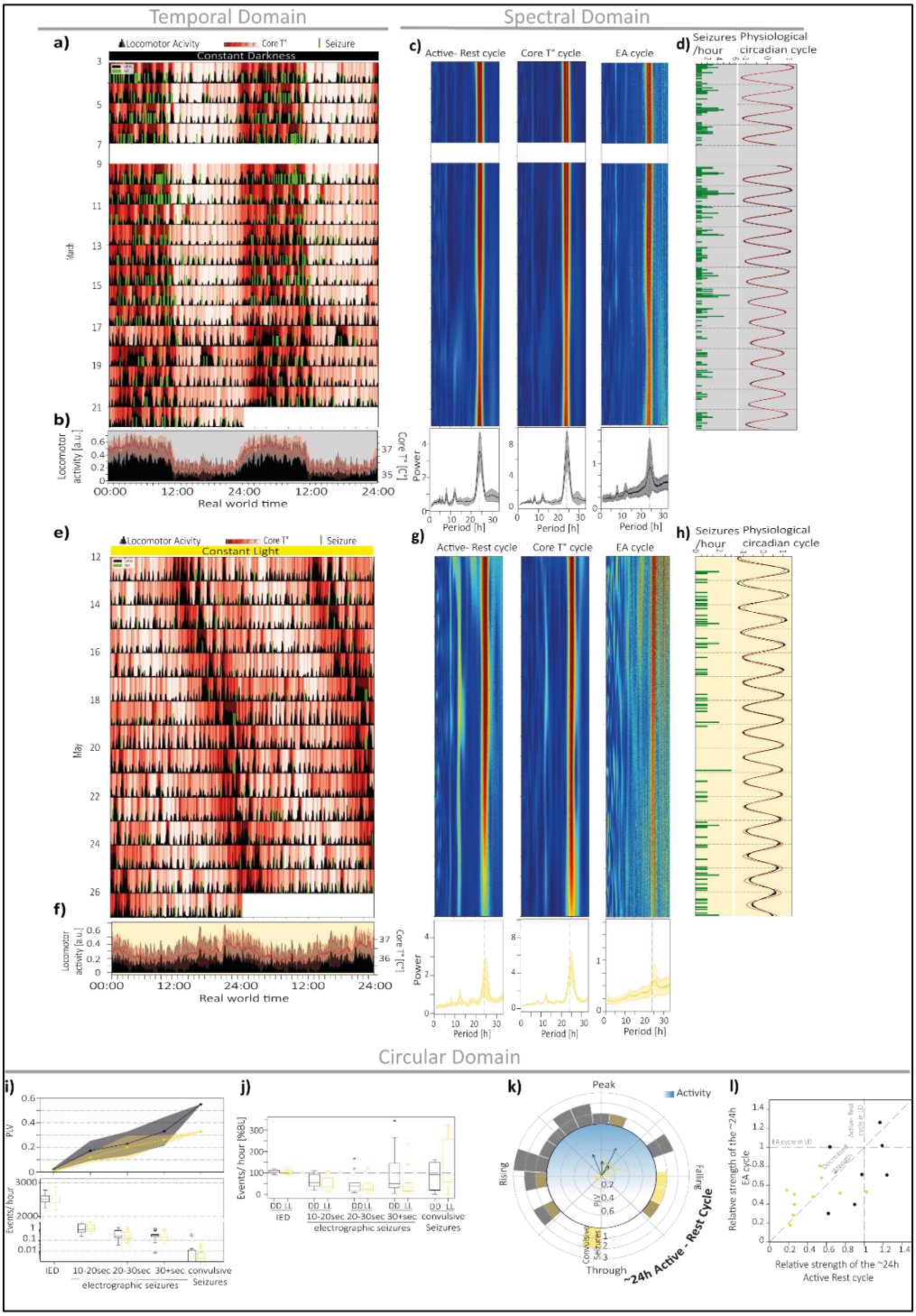

Figure 13 Seizure timing in a constant environment.

a-h) *Double-plotted actimetry, core T°, and seizures longer than 30sec in one epileptic mouse over weeks, with corresponding spectrograms, average periodograms and extracted active-rest and core T° cycles together with the hourly seizure count as in Fig. 12. The mouse was kept in either in DD (a-d) or LL (e-h).* ***i)*** *Strength of seizure clustering (top) and rates of discharges per hour (bottom) as a function of the duration of the epileptiform discharges in in DD (black) and LL (yellow).* ***j)*** *Relative hourly rate for events with increasing duration for mice with significant circadian clustering of seizures in DD and LL. Rate is normalized to the average individual rate in LD for each category.* ***k)*** *Circadian clustering of seizures in DD (black) and LL (yellow) on a ~24h the rest-active cycle. Each mean resultant vector represents a single mouse which had a significant circadian clustering of seizures in LD, which was maintained in DD, respectively LL. Outer bars represent convulsive seizure counts pooled across mice.* ***l)*** *Relative strength of the ~24h EA cycle expressed as a function of the relative strength of the ~24h active rest cycle. Note that the strength of the active-rest and EA cycle is maintained in DD, but decreases in LL.*

4.3 Seizure timing in a 10h light/10h dark cycling environment

After confirming the endogenous nature of the circadian seizure cycle we exposed a subset of mice to a set of chronobiological paradigms (T20, Jetlag, GSD) aimed at decoupling process S and process C. A subset of mice (n=9 KA, 4xNaCl) was submitted to a T20 protocol with an artificial 10h:10h light-dark cycle, which imposes a periodicity outside the natural entrainment range of the circadian clock machinery (Fig. 14a-e). Under these conditions the active rest cycle and core T° cycle exhibited two distinct but interacting periodicities: a 19.98h± 0.08h periodicity imposed by the T20 light-dark schedule and a 24.1±1.0h periodicity due to the endogenously generated circadian cycle. Out of nine mice recorded in the T20 environment, seven mice showed dual periodicity in their active rest cycle, of which five showed also dual periodicity in their core T° cycle and in their EA cycle. The remaining mice showed only a peak at ~24h in their core T° cycle and seizure cycle. Thus, for a majority of mice, two components of the physiological circadian cycle were effectively decoupled, core T° following mostly a circadian rhythm (white diagonal in Fig. 14a), while the active-rest cycle was influenced by both the circadian cycle and the externally imposed schedule (days with increased activity in Fig. 14a).

To further characterize the co-existence of these two rhythms, we studied them at different phases of their interaction (Sup. Fig. 5, Sup. Table 2). We first confirmed that the observed ~24-hour peak in core T° corresponds to a genuine circadian modulation of core T°, unaffected by the changes in locomotion entrained by 10h light/10h dark light schedule (i.e. increased activity during the dark phase and decreased activity during the light phase). We observed an activity independent consistent increase in core T° during the peak of a ~24h core T° cycle, independent of locomotor activity, confirming a true circadian modulation of the core T° cycle. Additionally, locomotor activity displayed a more pronounced influence from the imposed 10h light/10h dark light schedule with a weak additional

circadian modulation indicating entrainment of the active- rest cycle by the imposed light schedule[211] (Sup. Fig. 5 d-g). We therefore characterised the circadian seizure cycle based on an active rest cycle with 20 and a core T° cycle with ~24 hour periodicity. Due to the difference in period length in the active rest cycle and core T° cycle we observed periods when both cycles were oscillating in phase and some periods when they were oscillating out of phase. We termed periods when both cycles are in phase as "aligned periods" and when they are out of phase, we termed it "misaligned periods". All mice spent more time in the misaligned period (Sup. Fig. 5c).

During aligned periods we could observe a strong circadian modulation of seizure duration with an increase of PLV for electrographic seizures with increasing duration (Fig 13f, $PLV_{aligned}$ IED: 0.06±0.03, 10-20s: 0.26 ±0.09, 20-30s: 0.41 ±0.11, 30+s: 0.5 ±0.1). There were not enough convulsive seizures within one mouse to calculate the PLV on convulsive seizures. During misaligned periods, the trend to stronger circadian clustering remained for longer electrographic seizures ($PLV_{misaligned}$ IED: 0.03±0.01, 10-20s: 0.09 ±0.08, 20-30s: 0.16 ±0.08, 30+s: 0.18 ±0.07, convulsive seizures: 0.42 ±0), but was overall weaker than for aligned periods.

The interaction between the imposed ~20h and the endogenous ~24h cycle resulted further in the emergence of an artificial multidian cycle lasting four to six days visible in the active rest cycle and core T°. A weak multidian component can be observed in the EA cycle characterized by individual periodicities (Sup. Fig. 6).

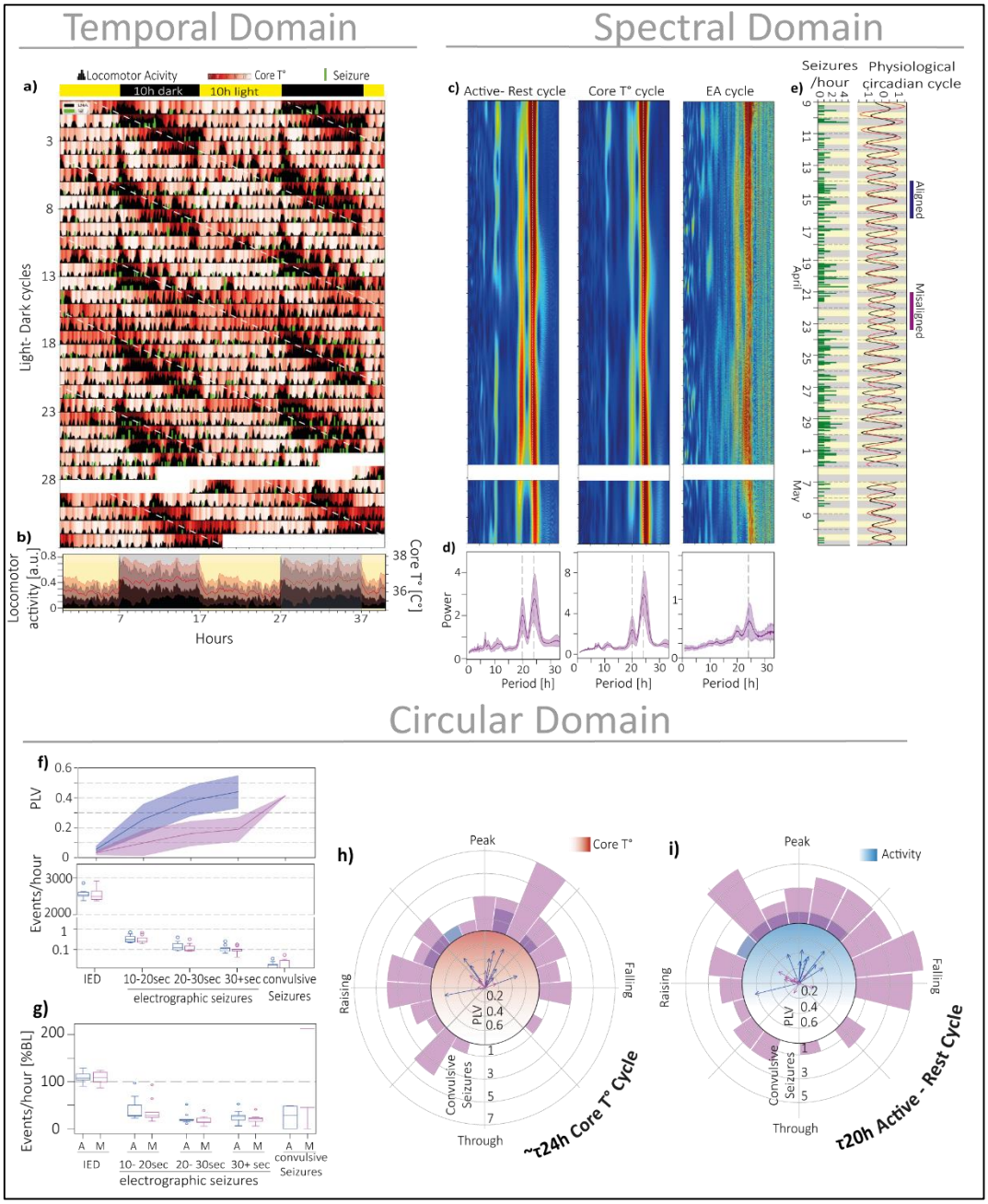

Figure 14 Seizure timing in a 10h light/10h dark cycling environment

a-e) *Double-plotted actimetry, core T°, and seizures in one epileptic mouse recorded in T20 LD over weeks, with corresponding spectrograms, average periodograms and extracted active-rest and Core T° cycle together with the hourly seizure count as in Fig. 12. The mouse was kept in a 10h light/10h dark cycling environment, which induced periods of alignment and misalignment between the active rest and the core T° cycle alternating about every 4-6 days. Note the dual periodicity (20h and ~24h) visible in the Periodogram of the active rest cycle, core T° cycle and EA cycle.* ***f)*** *Strength of seizure clustering (top) and rates of discharges per hour (bottom) as a function of the duration of the epileptiform discharges during periods when both cycles are aligned (blue) and misaligned (magenta).* ***g)*** *Relative hourly rate for events with increasing duration during aligned (A, blue) and misaligned (M, magenta) periods. Rate is normalized to the average individual rate in LD for each category.* ***i)-j)*** *Circadian clustering of seizures in accordance to the extracted ~24h core T° cycle (left) and 20h active rest cycle (right) for periods when both cycles are aligned (blue) and misaligned (magenta). Outer bars represent convulsive seizure counts pooled across mice.*

In another chronobiological paradigm designed to disentangle process S and process C, we implemented a jetlag protocol involving a one-time 4-hour forward shift in the 12-hour light/12-hour dark schedule. The goal was to understand how an abrupt shift in the light-dark cycle would influence the physiological and circadian seizure cycles (Sup. Fig. 7a, n=7xKA). We categorized the days preceding and following the time shift into three phases: “Before”, representing the four days immediately before the time shift; “Adaptation”, which included the day of the induced time shift and the following three consecutive days; and “after”, encompassing the four days following the “adaptation” period.

Before the time shift, both the active-rest cycle and core T° cycle were synchronized with the imposed 12-hour light/12-hour dark schedule. During the adaptation period following the 4-hour time shift, we observed a nearly immediate re-alignment of the active-rest cycle with the new lighting conditions. In contrast, the core T° cycle showed a stepwise adaptation of approximately 1 hour per day. After the adaptation period, both the active-rest cycle and core T° cycle followed the newly shifted 12-hour light/12-hour dark schedule.

To characterize the effect of this abrupt shift in the light-dark cycle on the circadian seizure cycle, we calculated the total EA at each circadian time point across all days within each of the three categories. The cumulative total EA was then detrended, e.g. normalised (deEA), to reveal potential underlying patterns and across the three categories described above. Before the time shift, we observed a peak in detrended EA at the end of the dark phase, corresponding to the period of preferred seizure occurrence observed in a 12-hour light-dark cycling paradigm. During the adaptation period, detrended EA did not show any peak. After the adaptation period, we observed a shifted peak in detrended EA (Sup. Fig. 7b)

4.4 Circadian seizure cycle and sleep homeostasis

We used a semi-supervised automated approach based on NNMF (Fig. 2,8-9, Sup. Fig. 2) to automatically annotate vigilance states across our dataset. The time spend in a given vigilance state was the same for epileptic and non-epileptic mice. Across conditions mice spend approximately 55% in NREM sleep, 38% in wakefulness and 7% in REM sleep (Sup. Fig. 8). As expected, both epileptic and control mice spend more time in NREM sleep (ANOVA: p_{KA}=0.02, p_{NaCl}=0.01) and less time in wake (ANOVA: p_{KA}=0.04, p_{NaCl}=0.01) in a LL, compared to LD (Sup. Fig. 8). This may be attributed to the fact that in mice, which are nocturnal, the presence of light typically signifies the resting phase. Therefore, when subjected to LL, these mice may experience a heightened inclination to sleep. We did not observe an significant increase in wakefulness during DD. Epileptic mice generally exhibit a higher occurrence of seizures during NREM sleep compared to wakefulness, with the lowest seizure duration observed during REM sleep across all chronobiological conditions(Sup. Fig. 9).

To experimentally assess the effect of sleep homeostasis on seizure occurrence, we performed GSD either at the beginning (7am-11am, n= 10x KA, 6x NaCl) or at the end of the resting phase (3pm-7pm, n=7x KA, 4x NaCl) in LD (Fig. 15 a, b respectively f, g). GSD at the beginning of the resting phase captured a period when endogenous sleep pressure is already high, while GSD at the end of the resting phase captured a period when endogenous sleep pressure is low. Furthermore, we performed GSD at different phases of the physiological circadian cycle during in LL (8am-12am., n=10xKa, 6x NaCl, Fig. 15 k, l) capturing periods with various endogenous sleep pressure depending on the phase of the physiological cycle. A total of four sessions of GSD were performed every second or third day. The day before GSD was considered as baseline and the period immediately following GSD was considered as recovery. To assess the effect of GSD we compared the increase in

SWA and changes in EA during the day of acute GSD to the baseline. SWA was extracted from NREM bouts longer than 1 minute and vigilance state annotation was performed automatically using the semi-supervised approach based on NNMF described above (Fig. 9, Fig. 10). For GSD at the beginning of the resting phase we observed an increase in SWA within the first 3-4 hours after sleep deprivation (Fig. 14c). Since GSD at the beginning of the resting phase aligned closely to the period with the peak in seizure occurrence observed in LD paradigm (~3am) we sought to disentangle the circadian effect from the effect of GSD. We therefore detrended, e.g. normalised, the cumulative epileptiform activity (deEA) of days with GSD by the cumulative epileptiform activity during BL. By detrending the signal in such way, we were able to remove the expected circadian changes, emphasizing only the potential effects of GSD. We observed a mild increase in epileptiform activity at the onset of GSD which plateaued thereafter (Fig. 15e). One mouse experienced status epilepticus after acute GSD and was not included in this analysis. When performing GSD at the end of the resting phase we observed only a minimal increase in SWA after GSD and no change in deEA (Fig. 15h,j). When performing GSD at various phases of the underlying physiological cycle we could observe a mild increase of EA during and acutely after GSD (Fig. 15m,o). This set of results, suggest that increased sleep pressure increases the likelihood of seizures.

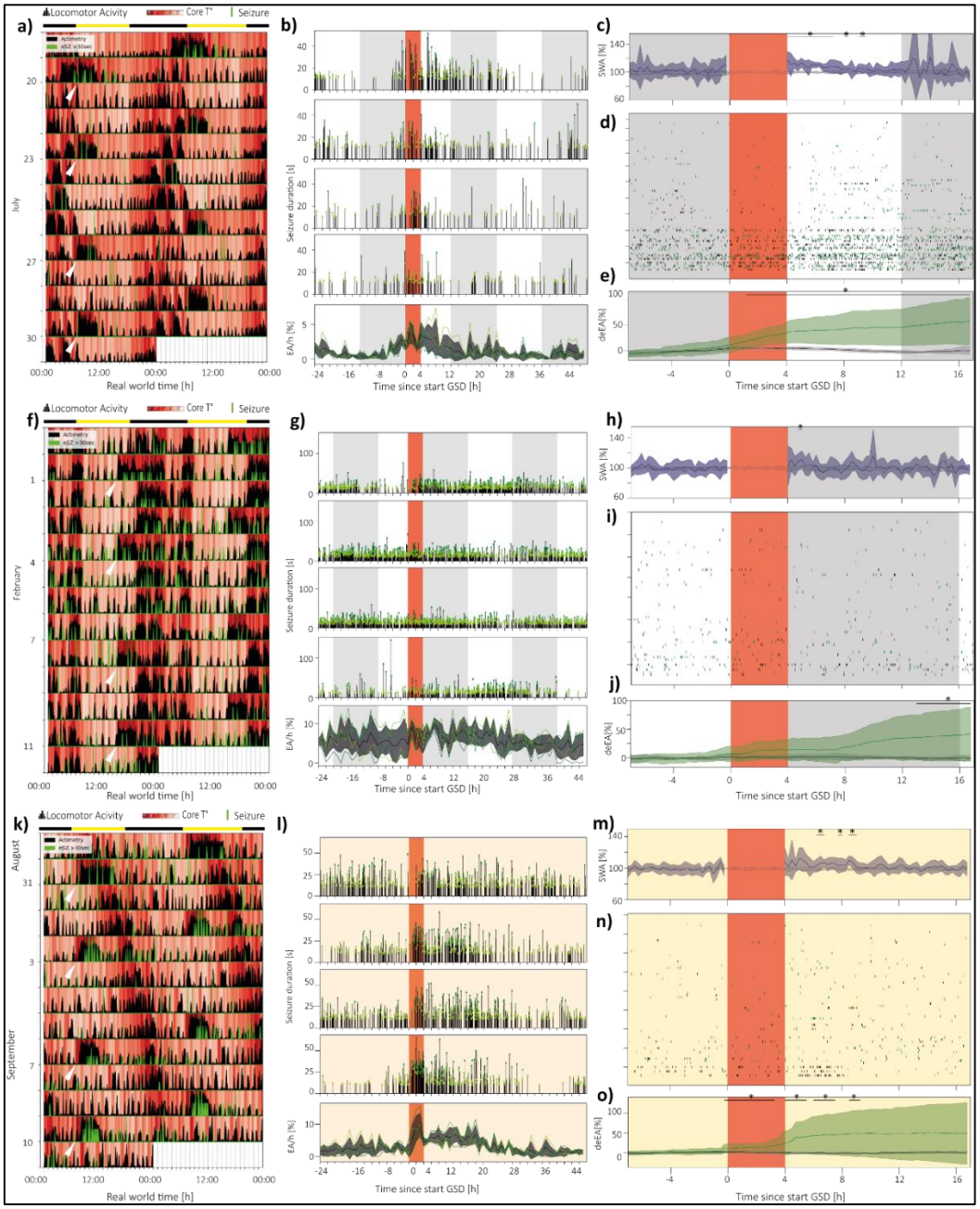

Figure 15 Effect of Gentle sleep deprivation on seizure timing

a) Double-plotted actimetry, core temperature, and seizures in one epileptic mouse over two weeks with GSD every third or fourth day at the onset of the light phase in LD (white arrow). **b)** Top: Stem plots showing the time of occurrence (x-axis) and duration (y-axis) of electrographic seizures in one epileptic mouse 24h before onset of individual GSD until 48 hours after onset of GSD. Note that different coloured dots show seizure duration while density of the vertical lines shows seizure frequency. Shading indicates lighting condition respectively period of acute GSD (dark orange). Bottom: deEA per hour before, during and after acute GSD. (Green lines indicate deEA of single days, Black line indicates average ± SD **c)** Average (± SD, shading) SWA during BL and GSD normalised to the corresponding circadian time, binned in 15-minute intervals. Shading indicates lighting condition respectively period of acute GSD (dark orange). Note the rebound in SWA within the first hours after GSD. (*=p<0.05 Wilcoxon rank-sum test) **d)** Rasterplot showing individual seizures over 24 hours for all mice during day before (black) and during acute GSD (green). Ticks on y axis indicate sets of GSD of an individual mouse **e)** detrended EA (deEA) for days before (grey) and during acute GSD (green). Values are normalized to the total epileptiform activity over 24h for days before GSD. Note the increase in deEA during acute GSD followed by plateauing (*=p<0.05 Wilcoxon rank-sum test). **f) -j)** Same as a) – f) but for GSD at the offset of the light phase in LD (3pm-7pm). **k) -o)** Same as a) – f) conducted at the same real world time (8am-12am) but which corresponded to different phases of the free-running physiological circadian cycle in LL.

Other results obtained during my PhD thesis are listed in the supplementary data including:

- My contributions in the development of an “on demand” optogenetic seizure model
- Quantification of the developed algorithm for the automated detection of vigilance states
- An overview of the mouse cohort used in this thesis and their use in different chronobiological paradigms
- A characterisation of the model under cycling (12h light/ 12h dark and 10h light/ 10h dark) and constant environment
- The artificially generated multidian rhythm obtained in the T20 paradigm
- Effect of the jetlag paradigm
- Characterisation of vigilance states and seizure occurrence during different in this model.
- Circadian timing of seizures and circadian modulation of seizure duration in accordance to the extracted core T° cycle

5 Discussion

In this study, we made several significant findings. In the LD paradigm, we observed a mild to moderate circadian clustering of seizures, which typically occurred between the peak and falling phases of the physiological circadian cycle, specifically during the late active phase (Fig. 12). In the DD paradigm, we noted the preserved strength of both the physiological circadian cycle and the circadian seizure cycle (Fig 13). However, in the LL paradigm, we observed a weakening of the circadian seizure cycle in proportion to the weakening of the physiological circadian cycle (Fig 13). Subsequently, we aimed to decouple the active rest cycle from the core T° cycle through three distinct paradigms. In the T20 paradigm, we observed the interaction of the core T° cycle, which was following mostly a circadian rhythm and the active-rest cycle which was influenced by both the circadian cycle and the externally imposed light- dark schedule, resulting in periods when both cycles were aligned respectively misaligned. We observed that the strength of the circadian seizure cycle was dependent on the alignment of these two cycles (Fig. 14). Finally, in the GSD paradigm, we found an increase in seizure rate that coincided with an increase in SWA (Fig.15).

Our model has value for translation. The preferred timing of seizures is reminiscent of the circadian pattern observed in human epilepsy, specifically the evening chronotype where seizures tend to occur in the late afternoon and evening. It is noteworthy that in the context of existing literature, all other models have demonstrated a circadian peak during the resting phase (in rats) and at the transition from the resting to the active phase (in mice). Expression of genes with circadian rhythmicity varies across brain regions[143], and different brain regions are differentially involved in sleep[23,212] and are uniquely impacted by sleep deprivation[213]. It is therefore plausible that seizures arising from various aetiologies and

brain regions across models may be modulated to varying degrees by both process S and process C. Overall, given that various human epilepsy types are most accurately represented by distinct models, it is probable that each human seizure chronotype will necessitate the use of distinct animal model as well.

In accordance with Quigg et al.[142], we show that seizure timing is preserved in DD (Fig 13) confirming that the circadian timing of seizures is endogenously generated and independent of exogenous Zeitgeber. This indicates that the endogenous physiological circadian rhythm in these mice is sufficient to govern circadian seizure timing. Since seizures can sometimes be photosensitive (i.e. under direct influence by light inputs) this is a non- trivial finding in our model, where the peak in the circadian seizure cycle occurs at the end of the active phase, close to the time when the light is turned on.

We took a step further by exposing mice also to a LL paradigm known to weaken the physiological circadian cycle and drive it to a longer periodicity (Fig 13). Although we observed a weakening of the physiological circadian cycle and a proportional weakening of the circadian seizure cycle. Importantly, the preferred phase of seizure occurrence was preserved also in LL. These findings suggest that the physiological circadian cycle is not only sufficient but also necessary for the maintenance of the circadian seizure cycle and its strength could potentially also influence seizure rates. By demonstrating both sufficiency and necessity, we emphasize the essential role of a physiological circadian cycle in the maintenance of a circadian seizure cycle.

In a physiological 12-hour light-12-hour dark cycling environment, as well as in constant environments (DD and LL), both process S and process C oscillate in synchrony, collectively influencing the circadian timing of seizures. These paradigms allow us to draw conclusions about the overall impact of the physiological circadian cycle on the circadian

seizure cycle but not on their individual role on governing seizure timing. To dissect the individual roles of process S and process C, it is necessary to manipulate and assess the effect on the circadian seizure cycle individually. Behaviourally, the most straightforward approach involves manipulating ambient light conditions (as light is the strongest Zeitgeber) by imposing an artificial light-dark cycle that falls outside the entrainment range of process C. This artificial cycle still entrains process S by promoting sleep during the light phase, but since it is outside of the entrainment range of process C, process C will follow its endogenously generated rhythm with an about 24h periodicity. It is important to note that the interactions[214] between process S and process C are not eliminated under these conditions, but rather create an interference pattern between a imposed 20h rhythm (active rest cycle) and a endogenously generated ~24h rhythm (core T° cycle), allowing to distinguish periods with and without synchrony between process S and process C. Our findings demonstrate the dependence of the circadian seizure cycle on this synchrony with circadian seizure clustering being stronger when both, the active rest cycle and the core T° cycle were aligned. A separate study[199] involving wild-type mice subjected to a T20 protocol showed an increase in SWA during aligned periods. Furthermore they showed that NREM sleep showed only a weak circadian modulation and was strongly influenced by the artificial light- dark cycle. It can be hypothesized that seizures tend to cluster when process S reaches its maximal amplitude, facilitated by process C (i.e., longer periods of wakefulness), rather than being organized around a shorter period characterized by more frequent sleep (and shorter periods of wakefulness).

To further characterize the extent to which process S is influencing the circadian seizure cycle we compared the effect of extended wakefulness (GSD) at times with high (dawn) or low (dusk) endogenous sleep-pressure (Fig. 15). GSD during periods with high endogenous sleep pressure led to a moderate increase in SWA after GSD and a stepwise decrease of

SWA in the hours after GSD (sleep rebound). In alignment with this, we observed an increase in EA during periods when SWA was elevated compared to baseline levels. Conversely GSD during periods with low endogenous sleep pressure did not lead to a significant increase in SWA or EA. This indicates that sleep pressure, reflected by SWA, proportionally influences seizure risk. In the context of the relation between seizure risk and sleep deprivation, recent literature has begun to consider various factors beyond the mere amount of sleep leading up to a seizure and delve deeper into the concept of sleep pressure itself. Experiments in drosophila have shown that artificially increasing sleep pressure by activating sleep networks was sufficient to increase seizure risk, independent on the amount of sleep before[194]. Furthermore, the notion of sleep pressure is intricately tied to the amount of SWA during sleep. Importantly, sleep SWA is not solely determined by the preceding duration of wakefulness but is also influenced by the 'intensity' of wakefulness. In other words, previous behaviour during wakefulness modulates sleep pressure afterwards[215].

Another interesting side-finding, considering epilepsy as a multiscale cyclical disorder, is the emergence of an artificial multidian cycle, created by the interference of process S and process C due to their misalignment in a T20 paradigm (Sup. Fig. 6). The precise mechanisms underlying multidian cycles in epilepsy, remains elusive but it is plausible that multidian rhythms are the result of interactions between multiple physiological oscillators on a shorter timescale, similar to what we observed in the T20 paradigms. These oscillators may encompass oscillators on the circadian scale like processes S and C but also oscillators on the ultradian scale like the sleep cycle, each oscillating at different periodicities. Each of these physiological oscillators likely has its own phases associated to heightened and diminished seizure risk. It is plausible that seizures occur when the phases of increased seizure risk associated with these different physiological oscillators align[54].

In summary, in our study on circadian timing of limbic seizures in epileptic mice, we explored circadian seizure timing and its underlying chronobiological mechanisms. We observed a moderate circadian increase in seizures at the end of the active period, akin to the evening chronotype observed in human epilepsy. We underscored the importance of a physiological circadian cycle for the maintenance of a circadian seizure cycle by showing its sufficiency and necessity. Additionally, our experiments shed light on the possible individual roles of process S and process C for the circadian seizure cycle: seizures tend to follow the Core T° cycle (Process C), while the active-rest cycle (Process S) creates a seizure-permissive window, presumably in the form of elevated sleep pressure. .

These findings hold important clinical implications. Aligning with the evolving paradigm of personalized medicine the understanding of the circadian seizure cycle can be leveraged in chronotherapy, where dosage of antiseizure medication is tailored to periods with high or low seizure risk. Further insights in the mechanisms behind circadian seizure cycles may also spark the exploration of novel targets for antiseizure medications, such as targeting the mTOR[216–218] pathway. Additionally, despite the relatively modest impact of process S in our model, it reinforces the fundamental importance of maintaining optimal sleep hygiene among individuals with epilepsy. Furthermore, multidian cycles have demonstrated utility in forecasting seizures, and our findings provide some first insights into potential mechanisms.

5.1 Strengths

We consider our study to have several strengths. First, we implanted depth electrodes in different nodes of the limbic circuit which allowed for a localized perspective and enabled us to detect seizures which might remain undetected using a more limited approach (e. g. using only surface EEG). Additionally, we harnessed the power of machine learning by using NNMF to automatically annotate vigilance states in our large dataset. This semi-

automated approach was necessary as manual scoring of vigilance states, while considered being the gold standard, can be time and labour intensive and only limited applicable in months-long datasets like ours. We have developed an approach which is generalizable across mice and works despite ictal and interictal activity in the EEG, a non-trivial task as ictal and interictal activity can introduce complexity when employing any visual or automated approach.

Furthermore, our study design represents a notable strength as it offers a first mechanistic approach to investigating the influences of both process S and process C on the circadian seizure cycle. In previous literature they were commonly treated as two different fields when studying their impact on seizures, with little consideration for their potential interactions. Furthermore we involved sufficiently large number of mice and conducted prolonged recordings of minimum three weeks in each paradigm. By adopting a longitudinal approach we were able compare the effects of different chronobiological paradigms to baseline condition (LD) within mouse. This allows for more robust insights, which are not achievable when using group-wise comparisons. In our investigation of the impact of gentle sleep deprivation (GSD) on seizure occurrence, we executed GSD at various time points, considering periods of both high and low endogenous sleep pressure, while keeping the same methodological approach. This design allowed us to disentangle the effects of GSD from those of the physiological circadian cycle on seizure occurrence. Lastly, our manipulation of the physiological circadian cycle through behavioural means, without genetic knockouts or other invasive methods, ensures that the effects we observed are attributable to an intact circadian machinery. This approach eliminated potential confounding factors associated with more invasive manipulations, such as core clock gene knockouts or invasive manipulations of the hormonal system, which could produce

unknown systemic or molecular-level effects that obscure the true underlying mechanisms of interest.

5.2 Limitations

We have chosen the intrahippocampal KA model of MTLE in mice to study the circadian seizure cycle. This model has several advantages including its ability to reproduce key aspects of MTLE in humans including hippocampal sclerosis and the occurrence of spontaneous recurrent seizures. This model has been well established and due to the localised injection of KA, this model allows for high reproducibility across mice. However, as any model also our model shows several limitations. First of all, our model only replicates human MTLE. Results of our model need to be taken with caution, when extrapolating to other forms of epilepsies (e.g. different localisation of the seizure focus or different aetiologies). An important characteristic of our model is the very high number of seizures in some mice, making separation between ictal and interictal events particularly challenging. We have addressed these limitations by defining seizures electrophysiological based on the count of spikes and categorizing seizure based on their duration, revealing the circadian modulation of seizure duration. Additional to analysing seizure duration we recognize the importance of also investigating seizure propagation networks, which are known to exhibit circadian modulation[89], although we did not explore this aspect in our study. It is plausible that, alongside the observed circadian modulation of seizure occurrence and seizure duration we could also observe a circadian modulation of seizure propagation. Furthermore, it would be interesting to explore the effects of GSD on seizure propagation.

The aim of our study was to dissect the individual effects of process S and process C on the circadian seizure cycle. While core T° is a well-established marker for the process C, since it is directly influenced by the central clock in the SCN, the active rest cycle can only be

seen as an approximation of process S. To directly link seizure occurrence to process S it would require modelling process S based on the changes of SWA during NREM sleep[219]. Furthermore, although we have observed a weakening of the physiological circadian cycle in LL across mice, we never observed true arhythmicity. To further underpin the necessity of a physiological circadian cycle for the maintenance of the circadian seizure cycle it is essential to knock out the physiological circadian cycle by making the mice arrhythmic using invasive approaches e.g. knock- out of the circadian machinery. Furthermore, to dissect the individual roles or process S and process C their separation is essential. We attempted to address this challenge by performing GSD with the same methodology during different phases of process C.

5.3 Outlook

Our findings highlight the essential role of the physiological circadian cycle in maintaining the circadian seizure cycle within our model, with Process C appearing to significantly influence seizure timing, while Process S contributes by creating a seizure-permissive window. Future investigations should involve assessing circadian seizure timing in the absence of the circadian clock machinery. Transgenic mouse models with knock-out of core clock genes have previously been shown to lose rhythmicity in constant environments[220], and a similar study involving the disruption of circadian cardiac rhythms through clock gene knockouts has been published[221]. A similar approach could be taken where the presence of an circadian seizure cycle is assessed in arrhythmic mice with knock out of core clock genes. Additionally, our study demonstrates the adaptability and diversity of NNMF, as we successfully employed it for the automated annotation of vigilance states in large datasets from epileptic mice, a non-trivial task. Similar approaches could be explored to leverage NNMF for characterizing seizure propagation across different nodes of the

limbic circuit, enabling not only the quantification of seizures as discrete events with specific durations but also their categorization based on propagation patterns.

6 References

1. Scheffer, I. E. *et al.* ILAE POSITION PAPER ILAE classification of the epilepsies : Position paper of the ILAE Commission for Classification and Terminology. 512–521 (2017) doi:10.1111/epi.13709.
2. Shneker, B. F., Fountain, N. B. & Orlowski, J. M. Epilepsy. *Disease-a-Month* **49**, 426–478 (2003).
3. Trinka, E. *et al.* A definition and classification of status epilepticus - Report of the ILAE Task Force on Classification of Status Epilepticus. *Epilepsia* **56**, 1515–1523 (2015).
4. Ruggiero, S. M., Xian, J. & Helbig, I. The current landscape of epilepsy genetics: where are we, and where are we going? *Curr. Opin. Neurol.* **36**, 86–94 (2023).
5. Whelan, C. D. *et al.* Structural brain abnormalities in the common epilepsies assessed in a worldwide ENIGMA study. *Brain* **141**, 391–408 (2018).
6. Vezzani, A., Lang, B. & Aronica, E. Immunity and inflammation in epilepsy. *Cold Spring Harb. Perspect. Med.* **6**, 1–21 (2016).
7. Fei, Y., Shi, R., Song, Z. & Wu, J. Metabolic Control of Epilepsy: A Promising Therapeutic Target for Epilepsy. *Front. Neurol.* **11**, 1–16 (2020).
8. Tatum, W. O. Mesial temporal lobe epilepsy. *J. Clin. Neurophysiol.* **29**, 356–365 (2012).
9. Engel, J. Surgery for Seizures. *N. Engl. J. Med.* **334**, 647–653 (1996).
10. Curia, G. *et al.* Pathophysiogenesis of Mesial Temporal Lobe Epilepsy: Is Prevention of Damage Antiepileptogenic? *Curr. Med. Chem.* **21**, 663–688 (2014).
11. Blümcke, I. *et al.* International consensus classification of hippocampal sclerosis in temporal lobe epilepsy: a Task Force report from the ILAE Commission on Diagnostic Methods. *Epilepsia* **54**, 1315–29 (2013).
12. Prayson, R. A. Pathology of Epilepsy. in *Practical Surgical Neuropathology: A Diagnostic Approach* (eds. Perry, A. & Brat, D. J. .) vol. 50 617–632 (Elsevier, 2018).
13. Thom, M. Hippocampal sclerosis in epilepsy: a neuropathology review. *Neuropathol. Appl. Neurobiol.* **40**, 520–543 (2014).
14. Houser, C. R. Granule cell dispersion in the dentate gyrus of humans with temporal lobe epilepsy. *Brain Res.* **535**, 195–204 (1990).
15. Von Campe, G., Spencer, D. D. & De Lanerolle, N. C. Morphology of dentate granule cells in the human epileptogenic hippocampus. *Hippocampus* **7**, 472–488 (1997).
16. Buckmaster, P. S., Zhang, G. F. & Yamawaki, R. Axon sprouting in a model of

temporal lobe epilepsy creates a predominantly excitatory feedback circuit. *J. Neurosci.* **22**, 6650–6658 (2002).

17. Pierce, J. P., Melton, J., Punsoni, M., McCloskey, D. P. & Scharfman, H. E. Mossy fibers are the primary source of afferent input to ectopic granule cells that are born after pilocarpine-induced seizures. *Exp. Neurol.* **196**, 316–31 (2005).

18. Tóth, K. *et al.* Loss and reorganization of calretinin-containing interneurons in the epileptic human hippocampus. *Brain* **133**, 2763–77 (2010).

19. Arellano, J. I., Muñoz, A., Ballesteros-Yáñez, I., Sola, R. G. & DeFelipe, J. Histopathology and reorganization of chandelier cells in the human epileptic sclerotic hippocampus. *Brain* **127**, 45–64 (2004).

20. Sutula, T., Cascino, G., Cavazos, J., Parada, I. & Ramirez, L. Mossy fiber synaptic reorganization in the epileptic human temporal lobe. *Ann. Neurol.* **26**, 321–330 (1989).

21. Becker, A. J. *et al.* Correlated stage- and subfield-associated hippocampal gene expression patterns in experimental and human temporal lobe epilepsy. *Eur. J. Neurosci.* **18**, 2792–2802 (2003).

22. Baulac, M. MTLE with hippocampal sclerosis in adult as a syndrome. *Rev. Neurol. (Paris).* **171**, 259–266 (2015).

23. Adamantidis, A. R., Gutierrez Herrera, C. & Gent, T. C. Oscillating circuitries in the sleeping brain. *Nat. Rev. Neurosci.* **20**, 746–762 (2019).

24. Britton, J. W. *et al. Electroencephalography - An Introductory Text and Atlas of Normal and Abnormal Findings in Adults, Children, and Infants*. (American Epilepsy Society, 2016).

25. Wenzel, M., Huberfeld, G., Grayden, D. B., de Curtis, M. & Trevelyan, A. J. A debate on the neuronal origin of focal seizures. *Epilepsia* 1–12 (2023) doi:10.1111/epi.17650.

26. Gnatkovsky, V., Librizzi, L., Trombin, F. & De Curtis, M. Fast activity at seizure onset is mediated by inhibitory circuits in the entorhinal cortex in vitro. *Ann. Neurol.* **64**, 674–686 (2008).

27. Truccolo, W. *et al.* Single-neuron dynamics in human focal epilepsy. *Nat. Neurosci.* **14**, 635–643 (2011).

28. Jiruska, P. *et al.* Synchronization and desynchronization in epilepsy: Controversies and hypotheses. *J. Physiol.* **591**, 787–797 (2013).

29. Englot, D. J. *et al.* Impaired consciousness in temporal lobe seizures: role of cortical slow activity. *Brain* **133**, 3764–3777 (2010).

30. Staley, K. J. & Dudek, F. E. Interictal Spikes and Epileptogenesis. *Epilepsy Curr.* **6**, 199–202 (2006).

31. Fisher, R. S., Scharfman, H. E. & DeCurtis, M. How can we identify ictal and interictal abnormal activity? *Adv. Exp. Med. Biol.* **813**, 3–23 (2014).

32. Pail, M. *et al.* High frequency oscillations in epileptic and non-epileptic human hippocampus during a cognitive task. *Sci. Rep.* **10**, 1–12 (2020).

33. Lepeu, G. *et al.* Probing cortical excitability under GABAergic modulation. *bioRxiv* 2021.02.18.431873 (2021) doi:https://doi.org/10.1101/2021.02.18.431873.

34. Lisanby, S. H. Update on magnetic seizure therapy: A novel form of convulsive therapy. *J. ECT* **18**, 182–188 (2002).

35. Munkholm, K., Jørgensen, K. J. & Paludan-Müller, A. S. Electroconvulsive therapy for depression. *Cochrane Database Syst. Rev.* **2021**, 1939–1945 (2021).

36. Chang, W. C. *et al.* Loss of neuronal network resilience precedes seizures and determines the ictogenic nature of interictal synaptic perturbations. *Nat. Neurosci.* **21**, 1742–1752 (2018).

37. Wilson, C. L. *et al.* Paired pulsed suppression and facilitation in human epileptogenic hippocampal formation. *Epilepsy Res.* **31**, 211–230 (1998).

38. Valentín, A. *et al.* Responses to single pulse electrical stimulation identify epileptogenesis in the human brain in vivo. *Brain* **125**, 1709–1718 (2002).

39. Mouthaan, B. E. *et al.* Single Pulse Electrical Stimulation to identify epileptogenic cortex: Clinical information obtained from early evoked responses. *Clin. Neurophysiol.* **127**, 1088–1098 (2016).

40. Baud, M. O., Proix, T., Rao, V. R. & Schindler, K. Chance and risk in epilepsy. *Curr. Opin. Neurol.* **33**, 163–172 (2020).

41. Barker-Haliski, M. & Steve White, H. Glutamatergic mechanisms associated with seizures and epilepsy. *Cold Spring Harb. Perspect. Med.* **5**, 1–15 (2015).

42. Galanopoulou, A. GABAA Receptors in Normal Development and Seizures: Friends or Foes? *Curr. Neuropharmacol.* **6**, 1–20 (2008).

43. Khoshkhoo, S., Vogt, D. & Sohal, V. S. Dynamic, Cell-Type-Specific Roles for GABAergic Interneurons in a Mouse Model of Optogenetically Inducible Seizures. *Neuron* **93**, 291–298 (2017).

44. Wang, Y. *et al.* Pharmaco-genetic therapeutics targeting parvalbumin neurons attenuate temporal lobe epilepsy. *Neurobiol. Dis.* **117**, 149–160 (2018).

45. Krook-Magnuson, E., Armstrong, C., Oijala, M. & Soltesz, I. On-demand optogenetic control of spontaneous seizures in temporal lobe epilepsy. *Nat. Commun.* **4**, 1376–1378 (2013).

46. Wang, Y. *et al.* Depolarized GABAergic Signaling in Subicular Microcircuits Mediates Generalized Seizure in Temporal Lobe Epilepsy. *Neuron* **95**, 92-105.e5 (2017).

47. Keller, C. J. *et al.* Induction and quantification of excitability changes in human cortical networks. *J. Neurosci.* **38**, 5384–5398 (2018).

48. Matzen, J., Buchheim, K. & Holtkamp, M. Circadian dentate gyrus excitability in a rat model of temporal lobe epilepsy. *Exp. Neurol.* **234**, 105–111 (2012).

49. Huber, R. *et al.* Human Cortical Excitability Increases with Time Awake. *Cereb. Cortex* 332–338 (2013) doi:10.1093/cercor/bhs014.

50. Ly, J. Q. M. *et al.* Circadian regulation of human cortical excitability. (2016)

doi:10.1038/ncomms11828.

51. Ziemann, U., Lönnecker, S., Steinhoff, B. J. & Paulus, W. The effect of lorazepam on the motor cortical excitability in man. *Exp. Brain Res.* **109**, 127–135 (1996).

52. Hallett, M. Transcranial Magnetic Stimulation: A Primer. *Neuron* **55**, 187–199 (2007).

53. Klorig, D. C., Alberto, G. E., Smith, T. & Godwin, D. W. Optogenetically-Induced Population Discharge Threshold as a Sensitive Measure of Network Excitability. *eneuro* **6**, ENEURO.0229-18.2019 (2019).

54. Baud, M. O. *et al.* Multi-day rhythms modulate seizure risk in epilepsy. *Nat. Commun.* **9**, 88 (2018).

55. Leguia, M. G. *et al.* Learning to generalize seizure forecasts. *Epilepsia* **64**, 99–113 (2023).

56. Karoly, P. J. *et al.* Cycles in epilepsy. *Nat. Rev. Neurol.* **17**, 267–284 (2021).

57. Foster, R. G. & Roenneberg, T. Human Responses to the Geophysical Daily, Annual and Lunar Cycles. *Curr. Biol.* **18**, 784–794 (2008).

58. Chen, J., Okimura, K. & Yoshimura, T. Light and Hormones in Seasonal Regulation of Reproduction and Mood. *Endocrinol. (United States)* **161**, 1–8 (2020).

59. Magnusson, A. An overview of epidemiological studies on seasonal affective disorder. *Acta Psychiatr. Scand.* **101**, 176–184 (2000).

60. Spitzer, N. C. Neurotransmitter Switching in the Developing and Adult Brain. *Annu. Rev. Neurosci.* **40**, 1–19 (2017).

61. Meyer, C. *et al.* Seasonality in human cognitive brain responses. *Proc. Natl. Acad. Sci. U. S. A.* **113**, 3066–3071 (2016).

62. Lim, A. S. P. *et al.* Seasonal plasticity of cognition and related biological measures in adults with and without Alzheimer disease: Analysis of multiple cohorts. *PLOS Med.* **15**, e1002647 (2018).

63. Tendler, A. *et al.* Hormone seasonality in medical records suggests circannual endocrine circuits. *Proc. Natl. Acad. Sci. U. S. A.* **118**, 1–8 (2021).

64. Leguia, M. G. *et al.* Seizure Cycles in Focal Epilepsy. *JAMA Neurol.* **78**, 454–463 (2021).

65. Motta, E., Gołba, A., Bal, A., Kazibutowska, Z. & Strzała-Orzeł, M. Seizure frequency and bioelectric brain activity in epileptic patients in stable and unstable atmospheric pressure and temperature in different seasons of the year - a preliminary report. *Neurol. Neurochir. Pol.* **45**, 561–566 (2011).

66. Rakers, F. *et al.* Weather as a risk factor for epileptic seizures: A case-crossover study. *Epilepsia* **58**, 1287–1295 (2017).

67. Baxendale, S. Seeing the light? Seizures and sunlight. *Epilepsy Res.* **84**, 72–76 (2009).

68. Rao, V. R., G. Leguia, M., Tcheng, T. K. & Baud, M. O. Cues for seizure timing.

Epilepsia **62**, S15–S31 (2020).

69. Griffiths, G. M. & Fox, J. T. Rhythm in Epilepsy. *Lancet* **232**, 409–416 (1938).

70. Karoly, P. J. *et al.* Interictal spikes and epileptic seizures: Their relationship and underlying rhythmicity. *Brain* **139**, 1066–1078 (2016).

71. Baud, M. O. *et al.* European trends in epilepsy surgery. *Neurology* **91**, e96–e106 (2018).

72. Maturana, M. I. *et al.* Critical slowing down as a biomarker for seizure susceptibility. *Nat. Commun.* **11**, 2172 (2020).

73. Herzog, A. G., Klein, P. & Rand, B. J. Three Patterns of Catamenial Epilepsy. *Epilepsia* **38**, 1082–1088 (1997).

74. Gregg, N. M. *et al.* Circadian and multiday seizure periodicities, and seizure clusters in canine epilepsy. *Brain Commun.* **2**, 1–13 (2020).

75. Baud, M. O., Ghestem, A., Benoliel, J. J., Becker, C. & Bernard, C. Endogenous multidien rhythm of epilepsy in rats. *Exp. Neurol.* **315**, 82–87 (2019).

76. Benedetti, F. Infradian mood fluctuations during a Major Depressive episode. *J. Affect. Disord.* **41**, 81–87 (1996).

77. Wehr, T. A. Bipolar mood cycles and lunar tidal cycles. *Mol. Psychiatry* **23**, 923–931 (2018).

78. Coventry, B. J. *et al.* CRP identifies homeostatic immune oscillations in cancer patients: a potential treatment targeting tool? *J. Transl. Med.* **7**, 102 (2009).

79. Zoghi, M. *et al.* Circadian and infradian rhythms of vasovagal syncope in young and middle-aged subjects. *PACE - Pacing Clin. Electrophysiol.* **31**, 1581–1584 (2008).

80. Gowers, W. R. *Epilepsy and other chronic convulsive disorders: their causes, symptoms, and treatment*. (Churchill, 1881).

81. Langdon-Down, M. & Russell Brain, W. Time of Day in Relation To Convulsions in Epilepsy. *Lancet* **213**, 1029–1032 (1929).

82. Reynolds, E. H. Epilepsy: Its Symptoms, Treatment, and Relation to Other Chronic Convulsive Diseases. *Br. foreign medico-chirurgical Rev.* **30**, 309–312 (1861).

83. Karoly, P. J. *et al.* Circadian and circaseptan rhythms in human epilepsy: a retrospective cohort study. *Lancet Neurol.* **17**, 977–985 (2018).

84. Quigg, M. & Straume, M. Dual epileptic foci in a single patient express distinct temporal patterns dependent on limbic versus nonlimbic brain location. *Ann. Neurol.* **48**, 117–120 (2000).

85. Loddenkemper, T. *et al.* Circadian patterns of pediatric seizures. *Neurology* **76**, 145–153 (2011).

86. Sánchez Fernández, I. *et al.* Clinical evolution of seizures: Distribution across time of day and sleep/wakefulness cycle. *J. Neurol.* **260**, 549–557 (2013).

87. Goldenholz, D. M. *et al.* Different as night and day: Patterns of isolated seizures,

clusters, and status epilepticus. *Epilepsia* **59**, e73–e77 (2018).

88. Ung, H. *et al.* Temporal behavior of seizures and interictal bursts in prolonged intracranial recordings from epileptic canines. *Epilepsia* **57**, 1949–1957 (2016).

89. Schroeder, G. M. *et al.* Seizure pathways change on circadian and slower timescales in individual patients with focal epilepsy. *Proc. Natl. Acad. Sci. U. S. A.* **117**, 11048–11058 (2020).

90. Hofstra, W. A., Grootemarsink, B. E., Dieker, R., Van Der Palen, J. & De Weerd, A. W. Temporal distribution of clinical seizures over the 24-h day: A retrospective observational study in a tertiary epilepsy clinic. *Epilepsia* **50**, 2019–2026 (2009).

91. Malow, B. A., Selwa, L. M., Ross, D. & Aldrich, M. S. Lateralizing value of interictal spikes on overnight sleep-EEG studies in temporal lobe epilepsy. *Epilepsia* **40**, 1587–1592 (1999).

92. Lambert, I. *et al.* Brain regions and epileptogenicity influence epileptic interictal spike production and propagation during NREM sleep in comparison with wakefulness. *Epilepsia* **59**, 235–243 (2018).

93. Tinuper, P. *et al.* Definition and diagnostic criteria of sleep-related hypermotor epilepsy. *Neurology* **86**, 1834–1842 (2016).

94. Schmitt, B. Sleep and epilepsy syndromes. *Neuropediatrics* **46**, 171–179 (2015).

95. Ng, M. & Pavlova, M. Why Are Seizures Rare in Rapid Eye Movement Sleep ? Review of the Frequency of Seizures in Different Sleep Stages. *Epilepsy Res. Treat.* **2013**, 10 (2013).

96. Drinkenburg, W. H. I. M., Coenen, A. M. L., Vossen, J. M. H. & Van Luijtelaar, E. L. J. M. Sleep deprivation and spike-wave discharges in epileptic rats. *Sleep* **18**, 252–256 (1995).

97. Kumar, P. & Raju, T. R. Seizure susceptibility decreases with enhancement of rapid eye movement sleep. *Brain Res.* **922**, 299–304 (2001).

98. Shouse, M. N., Siegel, J. M., Wu, M. F., Szymusiak, R. & Morrison, A. R. Mechanisms of seizure suppression during rapid-eye-movement (REM) sleep in cats. *Brain Res.* **505**, 271–282 (1989).

99. Miller, J. W., Turner, G. M. & Gray, B. C. Anticonvulsant effects of the experimental induction of hippocampal theta activity. *Epilepsy Res.* **18**, 195–204 (1994).

100. Rocamora, R., Andrzejak, R. G., Jiménez-Conde, J. & Elger, C. E. Sleep modulation of epileptic activity in mesial and neocortical temporal lobe epilepsy: A study with depth and subdural electrodes. *Epilepsy Behav.* **28**, 185–190 (2013).

101. Campana, C. *et al.* Suppression of interictal spikes during phasic rapid eye movement sleep: a quantitative stereo-electroencephalography study. *J. Sleep Res.* **26**, 606–613 (2017).

102. Fouad, A. *et al.* Interictal epileptiform discharges show distinct spatiotemporal and morphological patterns across wake and sleep. *Brain Commun.* **4**, 1–15 (2022).

103. Frauscher, B. *et al.* Facilitation of epileptic activity during sleep is mediated by

high amplitude slow waves. *Brain* **138**, 1629–1641 (2015).

104. Frauscher, B. & Gotman, J. Sleep, oscillations, interictal discharges, and seizures in human focal epilepsy. *Neurobiol. Dis.* **127**, 545–553 (2019).

105. Pavlova, M. K., Shea, S. A., Scheer, F. A. J. L. & Bromfield, E. B. Is there a circadian variation of epileptiform abnormalities in idiopathic generalized epilepsy? *Epilepsy Behav.* **16**, 461–467 (2009).

106. Saper, C. B., Scammell, T. E. & Lu, J. Hypothalamic regulation of sleep and circadian rhythms. *Nature* **437**, 1257–1263 (2005).

107. Steriade, M. Sleep, epilepsy and thalamic reticular inhibitory neurons. *Trends Neurosci.* **28**, 317–324 (2005).

108. Borbely, A. A. A Two Process Model of Sleep Regulation. *Hum. Neurobiol.* 195–204 (1982).

109. Daan, S., Beersma, D. G. M. & Borbely, A. A. Timing of human sleep: recovery process gated by a circadian pacemaker. *Am. J. Physiol. Integr. Comp. Physiol.* **246**, R161–R183 (1984).

110. Dubé, C. *et al.* Temporal lobe epilepsy after experimental prolonged febrile seizures: prospective analysis. *Brain* **129**, 911–922 (2006).

111. Gorter, J. A., van Vliet, E. A. & Lopes da Silva, F. H. Which insights have we gained from the kindling and post-status epilepticus models? *J. Neurosci. Methods* **260**, 96–108 (2016).

112. Cavalheiro, E. A., Riche, D. A. & Le Gal La Salle, G. Long-term effects of intrahippocampal kainic acid injection in rats: a method for inducing spontaneous recurrent seizures. *Electroencephalogr. Clin. Neurophysiol.* **53**, 581–589 (1982).

113. Lévesque, M. & Avoli, M. The kainic acid model of temporal lobe epilepsy. *Neurosci. Biobehav. Rev.* **37**, 2887–2899 (2013).

114. Curia, G., Longo, D., Biagini, G., Jones, R. S. G. & Avoli, M. The pilocarpine model of temporal lobe epilepsy. *J. Neurosci. Methods* **172**, 143–157 (2008).

115. Lothman, E. W., Bertram, E. H., Bekenstein, J. W. & Perlin, J. B. Self-sustaining limbic status epilepticus induced by 'continuous' hippocampal stimulation: electrographic and behavioral characteristics. *Epilepsy Res.* **3**, 107–119 (1989).

116. Nissinen, J., Halonen, T., Koivisto, E. & Pitkänen, A. A new model of chronic temporal lobe epilepsy induced by electrical stimulation of the amygdala in rat. *Epilepsy Res.* **38**, 177–205 (2000).

117. Turski, W. A. *et al.* Limbic seizures produced by pilocarpine in rats: Behavioural, electroencephalographic and neuropathological study. *Behav. Brain Res.* **9**, 315–335 (1983).

118. Schwob, J. E., Fuller, T., Price, J. L. & Olney, J. W. Widespread patterns of neuronal damage following systemic or intracerebral injections of kainic acid: A histological study. *Neuroscience* **5**, 991–1014 (1980).

119. Sperk, G. *et al.* Kainic acid induced seizures: Neurochemical and histopathological changes. *Neuroscience* **10**, 1301–1315 (1983).

120. Fonnum, F. & Walaas, I. The Effect of Intrahippocampal Kainic Acid Injections and Surgical Lesions on Neurotransmitters in Hippocampus and Septum. *J. Neurochem.* **31**, 1173–1181 (1978).

121. Mello, L. E. A. M. *et al.* Circuit Mechanisms of Seizures in the Pilocarpine Model of Chronic Epilepsy: Cell Loss and Mossy Fiber Sprouting. *Epilepsia* **34**, 985–995 (1993).

122. Mathern, G. W., Cifuentes, F., Leite, J. P., Pretorius, J. K. & Babb, T. L. Hippocampal EEG excitability and chronic spontaneous seizures are associated with aberrant synaptic reorganization in the rat intrahippocampal kainate model. *Electroencephalogr. Clin. Neurophysiol.* **87**, 326–339 (1993).

123. Gorter, J. A., Van Vliet, E. A., Aronica, E. & Da Silva, F. H. L. Progression of spontaneous seizures after status epilepticus is associated with mossy fibre sprouting and extensive bilateral loss of hilar parvalbumin and somatostatin-immunoreactive neurons. *Eur. J. Neurosci.* **13**, 657–669 (2001).

124. Leite, J. P. *et al.* Neuron loss, mossy fiber sprouting, and interictal spikes after intrahippocampal kainate in developing rats. *Epilepsy Res.* **26**, 219–231 (1996).

125. French, E. D., Aldinio, C. & Schwarcz, R. Intrahippocampal kainic acid, seizures and local neuronal degeneration: Relationships assessed in unanesthetized rats. *Neuroscience* **7**, 2525–2536 (1982).

126. Sharma, S., Puttachary, S., Thippeswamy, A., Kanthasamy, A. G. & Thippeswamy, T. Status Epilepticus: Behavioral and Electroencephalography Seizure Correlates in Kainate Experimental Models. *Front. Neurol.* **9**, 1–8 (2018).

127. Gröticke, I., Hoffmann, K. & Löscher, W. Behavioral alterations in a mouse model of temporal lobe epilepsy induced by intrahippocampal injection of kainate. *Exp. Neurol.* **213**, 71–83 (2008).

128. Shinoda, S. *et al.* Development of a Model of Seizure-Induced Hippocampal Injury with Features of Programmed Cell Death in the BALB/c Mouse. *J. Neurosci. Res.* **76**, 121–128 (2004).

129. Gouder, N., Fritschy, J. M. & Boison, D. Seizure suppression by adenosine A1 receptor activation in a mouse model of pharmacoresistant epilepsy. *Epilepsia* **44**, 877–885 (2003).

130. Riban, V. *et al.* Evolution of hippocampal epileptic activity during the development of hippocampal sclerosis in a mouse model of temporal lobe epilepsy. *Neuroscience* **112**, 101–111 (2002).

131. Lisgaras, C. P. & Scharfman, H. E. Robust chronic convulsive seizures, high frequency oscillations, and human seizure onset patterns in an intrahippocampal kainic acid model in mice. *Neurobiol. Dis.* **166**, 1–49 (2022).

132. Rusina, E., Bernard, C. & Williamson, A. The kainic acid models of temporal lobe epilepsy. *eNeuro* **8**, (2021).

133. Hellier, J. L. & Dudek, F. E. Spontaneous motor seizures of rats with kainate-induced epilepsy: effect of time of day and activity state. *Epilepsy Res.* **35**, 47–57 (1999).

134. Tchekalarova, J. *et al.* Diurnal rhythms of spontaneous recurrent seizures and behavioral alterations of Wistar and spontaneously hypertensive rats in the kainate model of epilepsy. *Epilepsy Behav.* **17**, 23–32 (2010).

135. Quigg, M., Straume, M., Menaker, M. & Bertram, E. H. Temporal distribution of partial seizures: Comparison of an animal model with human partial epilepsy. *Ann. Neurol.* **43**, 748–755 (1998).

136. Pitsch, J. *et al.* Circadian clustering of spontaneous epileptic seizures emerges after pilocarpine-induced status epilepticus. *Epilepsia* **58**, 1159–1171 (2017).

137. Schreiber, R. A. & Schlesinger, K. Circadian rhythms and seizure susceptibility: Relation to 5-hydroxytryptamine and norepinephrine in brain. *Physiol. Behav.* **6**, 635–640 (1971).

138. Fenoglio-Simeone, K. A. *et al.* Ketogenic diet treatment abolishes seizure periodicity and improves diurnal rhythmicity in epileptic Kcna1-null mice. *Epilepsia* **50**, 2027–2034 (2009).

139. Wright, S., Wallace, E., Hwang, Y. & Maganti, R. Seizure phenotypes, periodicity, and sleep-wake pattern of seizures in Kcna-1 null mice. *Epilepsy Behav.* **55**, 24–29 (2016).

140. Li, P. *et al.* Loss of CLOCK Results in Dysfunction of Brain Circuits Underlying Focal Epilepsy. *Neuron* **96**, 387-401.e6 (2017).

141. Purnell, B. S., Petrucci, A. N., Li, R. & Buchanan, G. F. The effect of time-of-day and circadian phase on vulnerability to seizure-induced death in two mouse models. *J. Physiol.* **0**, 1–15 (2021).

142. Quigg, M., Clayburn, H., Straume, M., Menaker, M. & Bertram, E. H. Effects of circadian regulation and rest-activity state on spontaneous seizures in a rat model of limbic epilepsy. *Epilepsia* **41**, 502–509 (2000).

143. Mure, L. S. *et al.* Diurnal transcriptome atlas of a primate across major neural and peripheral tissues. *Science (80-.).* **359**, 1–16 (2018).

144. Borbély, A. A., Daan, S., Wirz-Justice, A. & Deboer, T. The two-process model of sleep regulation: A reappraisal. *J. Sleep Res.* **25**, 131–143 (2016).

145. Franken, P., Tober, I. & Borby, A. A. Short light-dark cycles influence sleep stages and EEG power spectra in the rat. *Behav. Brain Res.* **43**, 125–131 (1991).

146. Huber, R., Deboer, T. & Tobler, I. Effects of sleep deprivation on sleep and sleep EEG in three mouse strains: Empirical data and simulations. *Brain Res.* **857**, 8–19 (2000).

147. Jan, M. *et al.* Model integration of circadian and sleep-wake driven contributions to rhythmic gene expression reveals novel regulatory principles. *bioRxiv* (2023) doi:;https://doi.org/10.1101/2023.08.10.552614.

148. Dibner, C., Schibler, U. & Albrecht, U. The Mammalian Circadian Timing System: Organization and Coordination of Central and Peripheral Clocks. *Annu. Rev. Physiol.* **72**, 517–549 (2010).

149. Huang, N. *et al.* Crystal structure of the heterodimeric CLOCK:BMAL1

transcriptional activator complex. *Science (80-.).* **337**, 189–194 (2012).

150. Patke, A., Young, M. W. & Axelrod, S. Molecular mechanisms and physiological importance of circadian rhythms. *Nat. Rev. Mol. Cell Biol.* **21**, 67–84 (2020).

151. Takahashi, J. S. Transcriptional architecture of the mammalian circadian clock. *Nat. Rev. Genet.* **18**, 164–179 (2017).

152. Lee, Y. Roles of circadian clocks in cancer pathogenesis and treatment. *Exp. Mol. Med.* **53**, 1529–1538 (2021).

153. Jud, C., Schmutz, I., Hampp, G., Oster, H. & Albrecht, U. A guideline for analyzing circadian wheel-running behavior in rodents under different lighting conditions. *Biol. Proced. Online* **7**, 101–116 (2005).

154. Refinetti, R. Comparison of light, food, and temperature as environmental synchronizers of the circadian rhythm of activity in mice. *J. Physiol. Sci.* **65**, 359–366 (2015).

155. Mure, L. S. Intrinsically Photosensitive Retinal Ganglion Cells of the Human Retina. *Front. Neurol.* **12**, 1–10 (2021).

156. Shigeyoshi, Y. *et al.* Light-induced resetting of a mammalian circadian clock is associated with rapid induction of the mPer1 transcript. *Cell* **91**, 1043–1053 (1997).

157. Albrecht, U., Sun, Z. S., Eichele, G. & Lee, C. C. A Differential Response of Two Putative Mammalian Circadian Regulators, mper1and mper2, to Light. *Cell* **91**, 1055–1064 (1997).

158. Todd, W. D. *et al.* Suprachiasmatic VIP neurons are required for normal circadian rhythmicity and comprised of molecularly distinct subpopulations. *Nat. Commun.* **11**, 1–20 (2020).

159. Paul, S. *et al.* Output from VIP cells of the mammalian central clock regulates daily physiological rhythms. *Nat. Commun.* **11**, 1453 (2020).

160. Kalsbeek, A. *et al.* SCN Outputs and the Hypothalamic Balance of Life. *J. Biol. Rhythms* **21**, 458–469 (2006).

161. Noya, S. B. *et al.* The forebrain synaptic transcriptome is organized by clocks but its proteome is driven by sleep. *Science (80-.).* **366**, (2019).

162. Brüning, F. *et al.* Sleep-wake cycles drive daily dynamics of synaptic phosphorylation. *Science (80-.).* **366**, (2019).

163. Yue, J. *et al.* Decreased expression of Rev-Erbα in the epileptic foci of temporal lobe epilepsy and activation of Rev-Erbα have anti-inflammatory and neuroprotective effects in the pilocarpine model. *J. Neuroinflammation* **17**, 1–15 (2020).

164. Zhang, T. *et al.* Dysregulation of REV-ERBα impairs GABAergic function and promotes epileptic seizures in preclinical models. *Nat. Commun.* **12**, (2021).

165. Kim, S. H. *et al.* Electroconvulsive Seizure Alters the Expression and Daily Oscillation of Circadian Genes in the Rat Frontal Cortex. *Psychiatry Investig.* **15**, 717–726 (2018).

166. Matos, H. de C. *et al.* Rhythms of core clock genes and spontaneous locomotor activity in post-status Epilepticus model of mesial temporal lobe epilepsy. *Front. Neurol.* **9**, 1–13 (2018).

167. Rambousek, L. *et al.* Aberrant expression of PAR bZIP transcription factors is associated with epileptogenesis, focus on hepatic leukemia factor. *Sci. Rep.* **10**, 1–16 (2020).

168. Wallace, E. *et al.* Altered circadian rhythms and oscillation of clock genes and sirtuin 1 in a model of sudden unexpected death in epilepsy. *Epilepsia* **59**, 1527–1539 (2018).

169. Debski, K. J. *et al.* The circadian dynamics of the hippocampal transcriptome and proteome is altered in experimental temporal lobe epilepsy. *Sci. Adv.* **6**, 1–16 (2020).

170. Gerstner, J. R. *et al.* BMAL1 controls the diurnal rhythm and set point for electrical seizure threshold in mice. *Front. Syst. Neurosci.* **8**, 1–7 (2014).

171. Gachon, F. *et al.* The loss of circadian PAR bZip transcription factors results in epilepsy. *Genes Dev.* **18**, 1397–1412 (2004).

172. Zhang, E. E. *et al.* A Genome-wide RNAi Screen for Modifiers of the Circadian Clock in Human Cells. *Cell* **139**, 199–210 (2009).

173. Lipton, J. O. & Sahin, M. The Neurology of mTOR. *Neuron* **84**, 275–291 (2014).

174. Lipton, J. O. *et al.* The Circadian Protein BMAL1 Regulates Translation in Response to S6K1-Mediated Phosphorylation. *Cell* **161**, 1138–1151 (2015).

175. Brown, R. E., Basheer, R., McKenna, J. T., Strecker, R. E. & McCarley, R. W. Control of Sleep and Wakefulness. *Physiol. Rev.* **92**, 1087–1187 (2012).

176. Bergmann, M. *et al.* Sleep quality and daytime sleepiness in epilepsy: Systematic review and meta-analysis of 25 studies including 8,196 individuals. *Sleep Med. Rev.* **57**, (2021).

177. Latreille, V., St. Louis, E. K. & Pavlova, M. Co-morbid sleep disorders and epilepsy: A narrative review and case examples. *Epilepsy Res.* **145**, 185–197 (2018).

178. Bernard, C., Frauscher, B., Gelinas, J. & Timofeev, I. Sleep, oscillations, and epilepsy. *Epilepsia* 1–10 (2023) doi:10.1111/epi.17664.

179. Rossi, K. C., Joe, J., Makhija, M. & Goldenholz, D. M. Insufficient Sleep, Electroencephalogram Activation, and Seizure Risk: Re-Evaluating the Evidence. *Ann. Neurol.* 1–9 (2020) doi:10.1002/ana.25710.

180. Giorgi, F. S. *et al.* Usefulness of a simple sleep-deprived EEG protocol for epilepsy diagnosis in de novo subjects. *Clin. Neurophysiol.* **124**, 2101–2107 (2013).

181. Haut, S. R., Hall, C. B., Masur, J. & Lipton, R. B. Seizure occurrence: Precipitants and prediction. *Neurology* **69**, 1905–1910 (2007).

182. Rajna, P. & Veres, J. Correlations Between Night Sleep Duration and Seizure Frequency in Temporal Lobe Epilepsy. *Epilepsia* **34**, 574–579 (1993).

183. Samsonsen, C., Sand, T., Bråthen, G., Helde, G. & Brodtkorb, E. The impact of sleep loss on the facilitation of seizures: A prospective case-crossover study. *Epilepsy Res.* **127**, 260–266 (2016).

184. Malow, B. A., Passaro, E., Milling, C., Minecan, D. N. & Levy, K. Sleep deprivation does not affect seizure frequency during inpatient video-EEG monitoring. *Neurology* **59**, 1371–1374 (2002).

185. Cobabe, M. M. *et al.* Impact of sleep duration on seizure frequency in adults with epilepsy: A sleep diary study. *Epilepsy Behav.* **43**, 143–148 (2015).

186. Stirling, R. E. *et al.* Sleep and seizure risk in epilepsy: bed and wake times are more important than sleep duration. *Brain* **146**, 2803–2813 (2023).

187. Dell, K. L. *et al.* Seizure likelihood varies with day-to-day variations in sleep duration in patients with refractory focal epilepsy: A longitudinal electroencephalography investigation. *eClinicalMedicine* **37**, 100934 (2021).

188. Shouse, M. N. Sleep Deprivation Increases Susceptibility to Kindled and Penicillin Seizure Events during All Waking and Sleep States in Cats. *Sleep* **11**, 162–171 (1988).

189. Cohen, H. B. & Dement, W. C. Prolonged tonic convulsions in REM deprived mice. *Brain Res.* **22**, 421–422 (1970).

190. Cohen, H., Thomas, J. & Dement, W. C. Sleep stages, REM deprivation and electroconvulsive threshold in the cat. *Brain Res.* **19**, 317–321 (1970).

191. Cohen, H. B. & Dement, W. C. Sleep: Changes in Threshold to Electroconvulsive Shock in Rats after Deprivation of 'Paradoxical' Phase. *Science (80-.).* **150**, 1318–1319 (1965).

192. Konduru, S. S. *et al.* Sleep Deprivation Exacerbates Seizures and Diminishes GABAergic Tonic Inhibition. *Ann. Neurol.* **90**, 840–844 (2021).

193. Iyer, S. H., Matthews, S. A., Simeone, T. A., Maganti, R. & Simeone, K. A. Accumulation of rest deficiency precedes sudden death of epileptic Kv1.1 knockout mice, a model of sudden unexpected death in epilepsy. *Epilepsia* **59**, 92–105 (2018).

194. Cuddapah, V. A. *et al.* Sleepiness, not total sleep amount, increases seizure risk. *bioRxiv* 2023.09.30.560325 (2023) doi:10.1101/2023.09.30.560325.

195. Brown, L. A., Fisk, A. S., Pothecary, C. A. & Peirson, S. N. Telling the time with a broken clock: Quantifying circadian disruption in animal models. *Biology (Basel).* **8**, (2019).

196. Richardson, G. S., Moore-Ede, M. C., Czeisler, C. A. & Dement, W. C. Circadian rhythms of sleep and wakefulness in mice: Analysis using long-term automated recording of sleep. *Am. J. Physiol. - Regul. Integr. Comp. Physiol.* **17**, (1985).

197. Ketelauri, P., Scharov, K., von Gall, C. & Johann, S. Acute Circadian Disruption Due to Constant Light Promotes Caspase 1 Activation in the Mouse Hippocampus. *Cells* **12**, 1836 (2023).

198. Campuzano, A., Vilaplana, J., Cambras, T. & Díez-Noguera, A. Dissociation of the

rat motor activity rhythm under T cycles shorter than 24 hours. *Physiol. Behav.* **63**, 171–176 (1998).

199. Hasan, S., Foster, R. G., Vyazovskiy, V. V. & Peirson, S. N. Effects of circadian misalignment on sleep in mice. *Sci. Rep.* **8**, 1–13 (2018).

200. Baud, M. O. *et al.* Unsupervised learning of spatiotemporal interictal discharges in focal epilepsy. *Clin. Neurosurg.* **83**, 683–691 (2018).

201. Paatero, P. & Tapper, U. Positive matrix factorization: A non-negative factor model with optimal utilization of error estimates of data values. *Environmetrics* **5**, 111–126 (1994).

202. Lee, D. D. & Seung, H. S. Learning the parts of objects by non-negative matrix factorization. *Nature* **401**, 788–791 (1999).

203. Wang, Y.-X. & Zhang, Y.-J. Nonnegative Matrix Factorization: A Comprehensive Review. *IEEE Trans. Knowl. Data Eng.* **25**, 1336–1353 (2013).

204. Fogel, P., Geissler, C., Morizet, N. & Luta, G. On Rank Selection in Non-Negative Matrix Factorization Using Concordance. *Mathematics* **11**, 4611 (2023).

205. Brunet, J.-P., Tamayo, P., Golub, T. R. & Mesirov, J. P. Metagenes and molecular pattern discovery using matrix factorization. *Proc. Natl. Acad. Sci.* **101**, 4164–4169 (2004).

206. Wu, S. *et al.* Stability-driven nonnegative matrix factorization to interpret Spatial gene expression and build local gene networks. *Proc. Natl. Acad. Sci. U. S. A.* **113**, 4290–4295 (2016).

207. Esteller, R., Echauz, J. & Tcheng, T. Comparison of line length feature before and after brain electrical stimulation in epileptic patients. *Annu. Int. Conf. IEEE Eng. Med. Biol. - Proc.* **26 VII**, 4710–4713 (2004).

208. Pedersen, M., Omidvarnia, A., Zalesky, A. & Jackson, G. D. On the relationship between instantaneous phase synchrony and correlation-based sliding windows for time-resolved fMRI connectivity analysis. *Neuroimage* **181**, 85–94 (2018).

209. Lachaux, J. P., Rodriguez, E., Martinerie, J. & Varela, F. J. Measuring phase synchrony in brain signals. *Hum. Brain Mapp.* **8**, 194–208 (1999).

210. Leguia, M. G., Rao, V. R., Kleen, J. K. & Baud, M. O. Measuring synchrony in bio-medical timeseries. *Chaos* **31**, (2021).

211. Cambras, T. *et al.* Circadian desynchronization of core body temperature and sleep stages in the rat. *Proc. Natl. Acad. Sci. U. S. A.* **104**, 7634–7639 (2007).

212. Sulaman, B. A., Wang, S., Tyan, J. & Eban-Rothschild, A. Neuro-orchestration of sleep and wakefulness. *Nat. Neurosci.* **26**, 196–212 (2023).

213. Krause, A. J. *et al.* The sleep-deprived human brain. *Nat. Rev. Neurosci.* **18**, 404–418 (2017).

214. Deboer, T. Sleep homeostasis and the circadian clock: Do the circadian pacemaker and the sleep homeostat influence each other's functioning? *Neurobiol. Sleep Circadian Rhythm.* **5**, 68–77 (2018).

215. Milinski, L. *et al.* Waking experience modulates sleep need in mice. *BMC Biol.* **19**, 65 (2021).

216. Buckmaster, P. S., Ingram, E. A. & Wen, X. Inhibition of the Mammalian Target of Rapamycin Signaling Pathway Suppresses Dentate Granule Cell Axon Sprouting in a Rodent Model of Temporal Lobe Epilepsy. *J. Neurosci.* **29**, 8259–8269 (2009).

217. Zeng, L.-H., Rensing, N. R. & Wong, M. The mammalian target of rapamycin signaling pathway mediates epileptogenesis in a model of temporal lobe epilepsy. *J. Neurosci.* **29**, 6964–72 (2009).

218. Moloney, P. B., Cavalleri, G. L. & Delanty, N. Epilepsy in the mTORopathies: opportunities for precision medicine. *Brain Commun.* **3**, (2021).

219. Franken, P., Tobler, I. & Borbély, A. A. Sleep homeostasis in the rat: Simulation of the time course of EEG slow-wave activity. *Neurosci. Lett.* **130**, 141–144 (1991).

220. Haque, S. N., Booreddy, S. R. & Welsh, D. K. Effects of BMAL1 manipulation on the Brain's master circadian clock and behavior. *Yale J. Biol. Med.* **92**, 251–258 (2019).

221. Hayter, E. A. *et al.* Distinct circadian mechanisms govern cardiac rhythms and susceptibility to arrhythmia. *Nat. Commun.* **12**, 1–13 (2021).

222. Weitz, A. J. *et al.* Optogenetic fMRI reveals distinct, frequency-dependent networks recruited by dorsal and intermediate hippocampus stimulations. *Neuroimage* **107**, 229–241 (2015).

223. Berglind, F., Andersson, M. & Kokaia, M. Dynamic interaction of local and transhemispheric networks is necessary for progressive intensification of hippocampal seizures. *Sci. Rep.* **8**, 1–15 (2018).

224. Osawa, S. I. *et al.* Optogenetically Induced Seizure and the Longitudinal Hippocampal Network Dynamics. *PLoS One* **8**, (2013).

7 Supplementary

List of supplementary figures

List of supplementary tables

7.1 Development of an “seizure on-demand” model

During the first year of my PhD, I was involved in establishing an optogenetic "seizures on demand" model in non-epileptic animals, with a specific focus on the limbic circuit, particularly the Entorhinal cortex (Ent) and the hippocampus, both known to be involved in seizure activity[222–224]. I was further involved in developing electrophysiological measurements to assess cortical excitability in this model. This work was then continued by a former PhD student in our lab Dr. Gregory Lepeu and a first version of the paper was published on bioarxiv[33]. The current version of the paper, on which I am a co-author is now under review.

I was particularly involved in confirming the specificity of our viral approach, which targeted the principal cells of the temporoammonic pathway. We utilized two viral preparations—one targeting all cells projecting from the Entorhinal to the hippocampal CA1 subfield and the other specifically targeting the principal cells of the temporoammonic pathway.

Additionally, I contributed to the development of electrophysiological measurements to assess cortical excitability within the limbic circuit. Seizures were induced in the Entorhinal and hippocampus using optogenetic pulses, and we introduced the concept of "time to seizure" (TTSZ) to quantify the stimulations required to induce a seizure, which later became a variable in characterizing cortical excitability in the publication of Dr. Lepeu. I also explored another variable, the paired pulse ratio, which assessed the perturbation of the brain by paired optogenetic pulses, i.e. two optogenetic pulses were delivered in the entorhinal of hippocampus with a varying inter- pulse interval. A paired pulse ratio (amplitude of the second pulse as function of the first one) greater than 1 indicated facilitation, while a ratio less than 1 indicated suppression of the second pulse. I investigated the modulation of cortical excitability using diazepam, a GABAergic enhancer

known to decrease cortical excitability. Diazepam administration resulted in an increased time to seizure and stronger suppression visible in the paired pulse ratio, both indicative of a higher seizure threshold.

Furthermore, I conducted research to characterize the electrophysiological properties of the targeted circuit. This involved tracking cortico-cortical evoked potentials evoked by paired optogenetic pulses in the Entorhinal and CA1 across different nodes of the network bidirectional. We calculated the onset delay, which increased proportionally to the path length (i.e., the number of synapses) to the stimulation site.

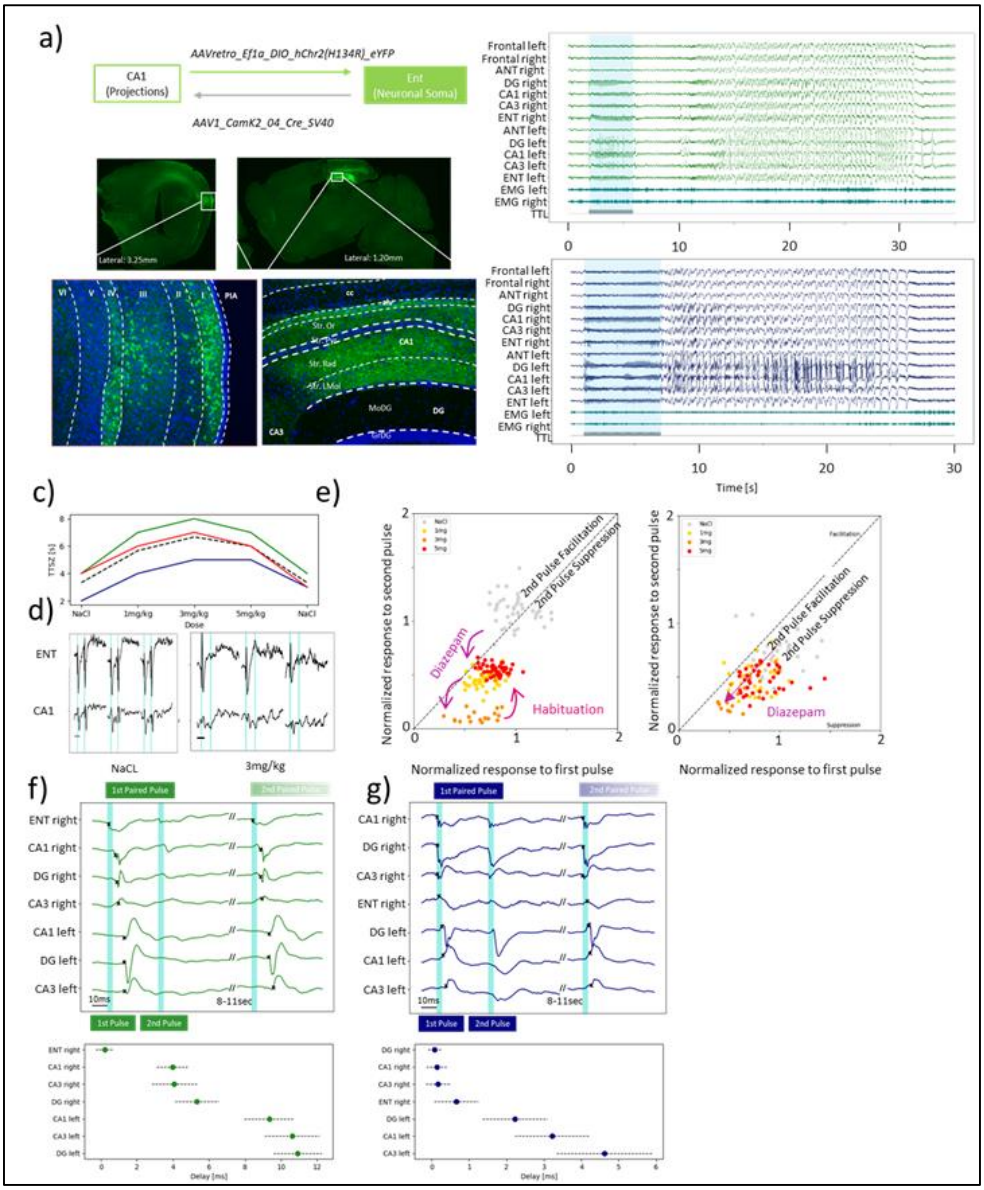

Supplementary Figure 1. Development of an "seizure on-demand" model

a) Top: Schematic showing viral preparation used. Bottom: Histology showing the expression of Channel Rhodopsin 2 (ChR2) (green) in Ent and CA1. Note the presence of labelled cell soma in the Layer II/III of the Ent and the absence of it in CA1 pyramidal layer (Str. Pyr.). **b)** Examples of seizures elicited by stimulating either the neuronal some in Ent (top) or the axonal projections in CA1 (bottom). **c)** TTSZ with different doses of Diazepam. Each animal is represented by a different colour. Dotted line represents mean TTSZ of all animals (n=3). Note the highest TTSZ in all animals with 3mg/kg). d) Representative examples of paired pulse stimulations with 30ms inter pulse interval without Diazepam (NaCl) and 3mg/kg Diazepam. Turquoise bars indicate light pulse of 3ms. Note the clear response to the second pulse without Diazepam in Ent and CA1, compared to the suppressed response with 3mg/kg Diazepam in Ent and CA1. **e)** Scatterplot of the normalized response to the first and the second pulse with an inter pulse interval of 30ms and for different doses of Diazepam in Ent (left) and downstream in CA1 (right). Each dot represents one pair of pulses (n=30). Please note the oblique (Ent) and downward (Ent and hippocampus) shifts towards the lower left corner with increasing doses of diazepam. In Ent we can observe a shift from partial facilitation (dots above diagonal) towards a complete suppression for all paired pulse (below diagonal), while in CA1 we can observe a similar decrease of the response to the first and for the second pulse. Note the similar location of the pulses for 1mg/kg and 5mg/kg indicating a habituation of the animal to the effect of Diazepam. Responses were normalized to the mean of the first pulse in control session with NaCl. **f)** Top: Schematic showing two cortico-cortical evoked potentials in different channels after stimulation in Ent. Signal is propagated across all channels. Onset of the response is indicated by crosses. Turquoise bar indicates light pulse (3ms). The onset delay was calculated as the time difference between the light stimulus and the onset of the response in the investigated channel. Bottom: Quantification of the corresponding examples described on top after stimulations in Ent. **g)** same as f) but for optogenetic stimulation in downstream CA1

7.2 Circadian timing of limbic seizures in the epileptic mouse

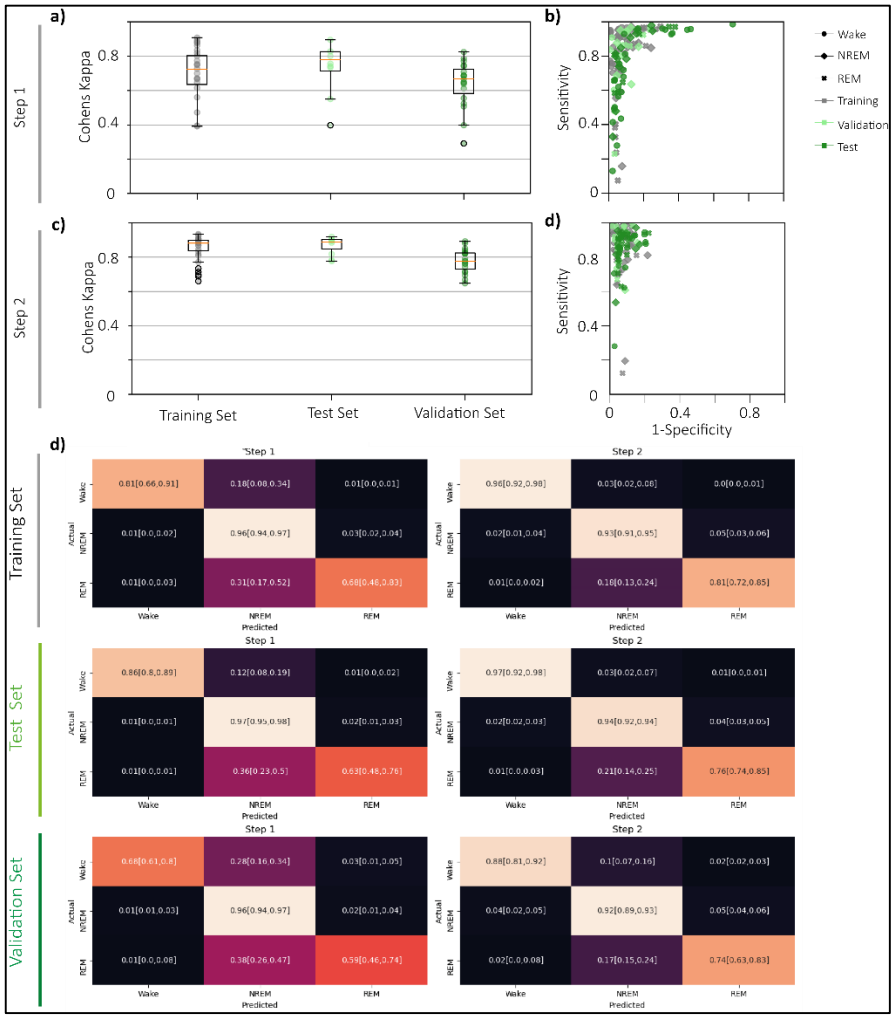

Supplementary Figure 2. Evaluation of semi- supervised automated annotation algorithm

a) &c) *Cohens Kappa scores for the training (grey), test (light green), and validation (dark green) datasets at the first (a) and second (b) step of the automated annotation of vigilance states.* ***b)& d)*** *Sensitivity and Specificity analysis for the automated annotation of different vigilance states (dot = wake, square = NREM, and cross = REM) at the first (b) and second (d) step of the automated annotation of vigilance states. Results are presented for the training (grey), test (light green), and validation (dark green) datasets.* ***d)*** *Confusion matrices for the training (top, grey), test (middle, light green), and validation (bottom, dark green) datasets at the first (first column) and second (second column) step of the automated annotation of vigilance states. Numbers indicate median and [IQR]*

We evaluated the performance of our algorithm in two different datasets against visual expert labelling. The test dataset encompassed two days (one with undisturbed sleep and one with GSD) taken from the mice that contributed data to construct the universal BF. Importantly the days in the validation dataset were not used in the construction of the universal BF. The test dataset comprised data from a set of mice (n=4 mice) with 10 days

of undisturbed sleep and 10 days of gentle sleep deprivation. This data has been manually labelled beforehand and has not been previously seen by the algorithm. To evaluate the performance of our algorithm we calculated the Cohens Kappa score together with sensitivity and specificity for each state.

We observed that the standalone implementation of Step 1 (solely using universal BF for the annotation of wake, NREM and REM) yielded lower Cohens Kappa scores (Cohens Kappa $_{Training}$: 0.72 [IQR:0.63,0.8], Cohens Kappa$_{Validation}$: 0.78 [IQR:0.71,0.83], Cohens Kappa$_{Test}$: 0.67 [IQR:0.58,0.73], Sup. Fig. 2a) than the combined approach of Step 1 and Step 2 (using first universal BF and then use individual BF derived on 24h file) across all datasets, with the latter displaying a more clustered Cohen's Kappa score distribution. (Cohens Kappa$_{Training}$: 0.88 [IQR:0.84,0.9], Cohens Kappa$_{Validation}$: 0.89 [IQR:0.85,0.9], Cohens Kappa$_{Test}$: 0.78 [IQR:0.73,0.82], Sup. Fig. 2c). Across all datasets we observed a high performance for the Training and the validation dataset and a slight drop in performance in the Test dataset. When comparing the performance for the different vigilance states, our algorithm showed high sensitivity and specificity for wakefulness and NREM, which was improved when refining the detection in Step2. (Step 1: Sensitivity$_{Wake}$: 0.92 [IQR:0.63,0.8], Sensitivity$_{Wake}$: 0.72 [IQR:0.63,0.8], Sensitivity$_{Wake}$: 0.72 [IQR:0.63,0.8], Sensitivity$_{Wake}$: 0.72 [IQR:0.63,0.8], Step 2: Sensitivity$_{Wake}$: 0.72 [IQR:0.63,0.8], Sensitivity$_{Wake}$: 0.72 [IQR:0.63,0.8], Sensitivity$_{Wake}$: 0.72 [IQR:0.63,0.8], Sensitivity$_{Wake}$: 0.72 [IQR:0.63,0.8], Sup. Fig. 2b and 2d). In the case of REM, solely applying Step 1 showed high levels of specificity but very low sensitivity (Sensitivity$_{Wake}$: 0.72 [IQR:0.63,0.8], Sensitivity$_{Wake}$: 0.72 [IQR:0.63,0.8], Sup. Fig. 2b). Refinement of the state detection using individual BF in Step 2 mitigated this issue leading to an improved sensitivity for REM sleep (Sensitivity$_{Wake}$: 0.72 [IQR:0.63,0.8], Sensitivity$_{Wake}$: 0.72 [IQR:0.63,0.8], Sup. Fig. 2d).

Animal	Injection	Experimental group	Recorded data	Chronobiological manipulation [days]					GSD [# Sessions]			Died during recording	Total days recorded& analyzed
				LD	Jetlag	DD	LL	T20	LD morning	LD afternoon	LL		
KA_Hpc_CamK2_chron_03	KA	Epileptic	16chEEG, EMG, LMA	93	x	x	x	x	4	4	x	No	93
KA_Hpc_CamK2_chron_04	KA	Epileptic	16chEEG, EMG, LMA	4	x	x	x	x	x	x	x	Yes (SUDEP)	4
KA_Hpc_chron_01*	KA	Epileptic	16chEEG, EMG, LMA	93	x	x	x	x	4	4	x	No	93
KA_Hpc_chron_02	KA	Epileptic	16chEEG, EMG, LMA	70	x	x	x	x	4	0	x	Yes (Sickness)	70
KA_Hpc_chron_03	KA	Epileptic	16chEEG, EMG, LMA	51	x	x	x	x	4	0	x	Yes (Sickness)	51
KA_Hpc_chron_22	KA	Epileptic	16chEEG, EMG, LMA	45	x	30	32	x	4	0	4	No	107
KA_Hpc_chron_26	KA	Epileptic	16chEEG, EMG, LMA	26	x	17	x	x	4	0	x	Yes (Sickness)	43
KA_Hpc_chron_27	KA	Epileptic	16chEEG, EMG, LMA	49	x	35	36	x	4	0	4	No	120
KA_Hpc_chron_33	KA	Epileptic	16chEEG, EMG, LMA Core T°	5	x	x	x	x	x	x	x	SUDEP	5
KA_Hpc_chron_35	KA	Epileptic	16chEEG, EMG, LMA Core T°	42	x	x	49	45	4	x	x	No	136
KA_Hpc_chron_37	KA	Epileptic	16chEEG, EMG, LMA Core T°	34	x	x	49	45	2	x	x	No	128
KA_Hpc_chron_310	KA	Epileptic	16chEEG, EMG, LMA Core T°	46	x	x	49	45	4	x	x	No	140
KA_Hpc_chron_311	KA	Epileptic	16chEEG, EMG, LMA Core T°	42	x	x	49	26	2	x	x	No	117
KA_Hpc_chron_312	KA	Epileptic	16chEEG, EMG, LMA Core T°	3	x	x	x	x	x	x	x	SUDEP	3
KA_Hpc_chron_41	KA	Epileptic	16chEEG, EMG, LMA Core T°	41	12	18	48	37	x	4	4	NA	156
KA_Hpc_chron_42	KA	Epileptic	16chEEG, EMG, LMA Core T°	5	x	x	x	x	x	x	x	SUDEP	5
KA_Hpc_chron_43	KA	Epileptic	16chEEG, EMG, LMA Core T°	52	12	18	48	37	x	4	4	NA	167
KA_Hpc_chron_47	KA	Epileptic	16chEEG, EMG, LMA Core T°	24	12	x	x	x	x	4	x	SUDEP	36
KA_Hpc_chron_49	KA	Epileptic	16chEEG, EMG, LMA Core T°	36	12	16	48	37	x	4	4	NA	149
KA_Hpc_chron_410	KA	Epileptic	16chEEG, EMG, LMA Core T°	44	12	18	x	x	x	4	x	NA	74
KA_Hpc_chron_412	KA	Epileptic	16chEEG, EMG, LMA Core T°	36	x	x	x	x	x	3	x	Yes (Sickness)	36
KA_Hpc_chron_414	KA	Epileptic	16chEEG, EMG, LMA Core T°	46	12	18	48	37	x	4	4	NA	161
KA_Hpc_chron_415	KA	Epileptic	16chEEG, EMG, LMA Core T°	41	12	18	48	23	x	x	4	NA	142
KA_Hpc_chron_417	KA	Epileptic	16chEEG, EMG, LMA Core T°	12	x	x	x	x	x	x	x	SUDEP	12
NaCl_Hpc_chron_02	NaCl	Control	16chEEG, EMG, LMA	93	x	x	x	x	4	4	4	No	93
NaCl_Hpc_chron_03	NaCl	Control	16chEEG, EMG, LMA	93	x	x	x	x	4	4	4	No	93
NaCl_Hpc_chron_21	NaCl	Control	16chEEG, EMG, LMA	49	x	35	36	x	4	x	4	No	120
NaCl_Hpc_chron_23	NaCl	Control	16chEEG, EMG, LMA	49	x	35	36	x	4	x	4	No	120
NaCl_Hpc_chron_32	NaCl	Control	16chEEG, EMG, LMA Core T°	43	x	x	49	44	4	x	4	No	136
NaCl_Hpc_chron_33	NaCl	Control	16chEEG, EMG, LMA Core T°	46	x	x	49	44	4	x	4	No	139
NaCl_Hpc_chron_41	NaCl	Control	16chEEG, EMG, LMA Core T°	17	x	18	48	NA	X	4	4	NA	83
NaCl_Hpc_chron_42	NaCl	Control	16chEEG, EMG, LMA Core T°	57	12	17	48	37	X	0	4	NA	171
Mean ± STD KA				39.2 ± 23.6	12 ± 0	20.9 ± 6.3	45.8 ± 5.7	36.9 ± 7.5					85.3 ± 55.8
Mean ± STD NaCL				51.4 ± 23.1	12 ± 0	22.6 ± 10.1	40.2 ± 16.2	35.2 ± 16.2					110.5 ± 37.3

Supplementary Table 1: Mouse cohort.

*All animals were either injected with KA or NaCl in the right CA1. All animals injected with KA showed ictal activity in their chronic EEG recordings (no acute EEG recordings). Animals injected with NaCl served as a control group. The numbers indicate the recorded days for each chronobiological paradigm that an animal was exposed to. For the days with gentle sleep deprivation (GSD) followed by two to three days of recovery, the number of sessions is indicated. "X" indicates that the animal was not recorded under this specific chronobiological paradigm. NA= not applicable (animal was sacrificed at the end of the recording). * indicates mouse that experienced SE. after GSD*

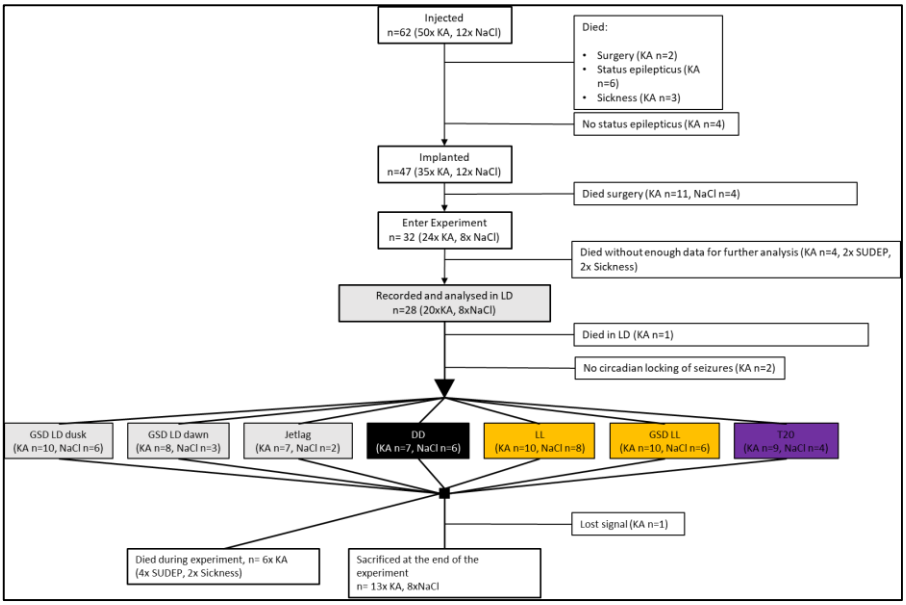

Supplementary Figure 3 Flowchart: Mice used at each step

Note that one animal can be recorded during different chronobiological paradigms.

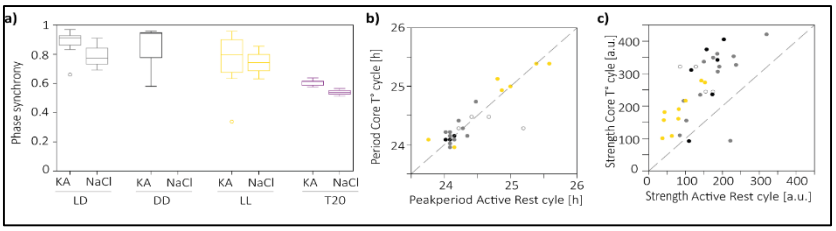

Supplementary Figure 4 Characterisation of the model in cycling and constant environment

a) *Phase synchrony between the extracted active rest cycle and Core T° cycle (a),* ***b-c)*** *Relationship between period (b) and strength (c) of the active rest cycle and core T° cycle across all chronobiological paradigms. Empty dots indicate NaCl animals. (active rest cycle: n=20x KA, 8x NaCl, core T° cycle n= 13x KA, 4x NaCl).*

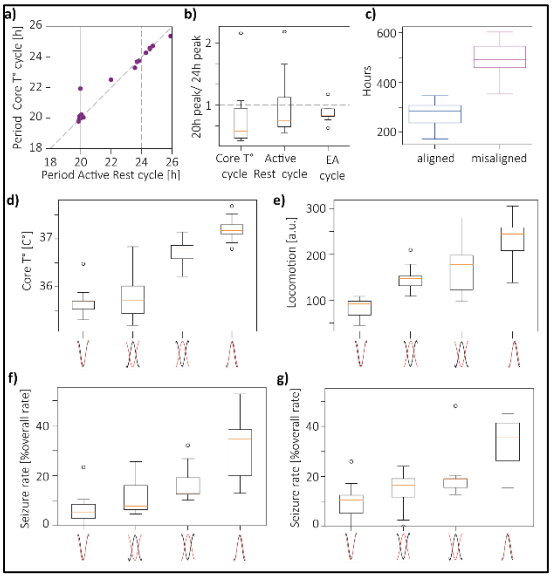

Supplementary Figure 5 Characterisation of the model in T20 environment

a) *Extracted dual periodicities for the active rest cycle and core T° cycle.* ***b)*** *Relative strength of the extracted 20h cycle as a function of strength of the extracted ~24h cycle for active rest, core T° and EA cycle.* ***c)*** *Time spent in aligned periods (when the active rest cycle and core T° cycle are oscillating in synchrony) and misaligned periods (i.e. the two rhythms are out of synchrony).* ***d)*** *Core T° during the peak and the through of core T° cycle with different levels of activity indicating that core T° is following an endogenous ~24h cycle with minor additive effect of locomotion. Schematic at the bottom indicates the phase relationship between both cycles (red= core T° cycle, black= active rest cycle).* ***e)*** *Same as d) but for a stepwise increase of locomotor activity indicating a true diurnal regulation of the behaviour.* ***f)- g)*** *same as d) and e) but for seizure rate at different phases of the underlying core T° (f) and active rest cycle (g) when the ~20h active rest cycle and ~24h core T° cycle are oscillating in synchrony respectively out of synchrony.*

To confirm whether the observed peak in core T° cycle at 24h represents a genuine circadian modulation of core T°, independent of mouse behaviour, we evaluated the mean core T° during both the peak (high core T°) and trough (low core T°) of the approximately 24-hour core T° cycle. Initially, we computed the mean core T° during periods when the 24h core T° cycle synchronized with the imposed 20h active-rest cycle. As expected, core T° was higher during the peak compared to the trough. Subsequently, we examined core T° values during the peak and trough of the core T° cycle but for periods when the ~24h core T° cycle was out of phase with the active-rest cycle. Given that both cycles were in opposite phases, core T° was anticipated to be high when locomotor activity was low and vice versa. Our observations showed that during periods when both cycles were out of phase, core T° remained elevated during the core T° cycle's peak, even when locomotor activity was low, and decreased during the trough when locomotion was high. This consistent activity-

independent increase in core T° during the core T° cycle's peak supports the interpretation of a true circadian modulation of the core T° cycle. We applied the same approach to analyse mean locomotor activity and observed a gradual increase in locomotion, indicating a strong influence of the imposed 10-hour light/10-hour dark cycle with a weaker circadian modulation[211].

		EA cycle			**Core T° cycle**		
		20h component	24h component	Both components	20h component	24h component	Both components
Active rest cycle	20h component	1	0	1	1	0	1
	24h component	0	0	0	0	1	0
	Both components	0	3	4	0	2	4
Core T° cycle	20h component	1	0	0			
	24h component	0	2	1			
	Both components	0	1	4			

***Supplementary Table 2** Dual periodicities in active-rest, core T° and EA cycle.*

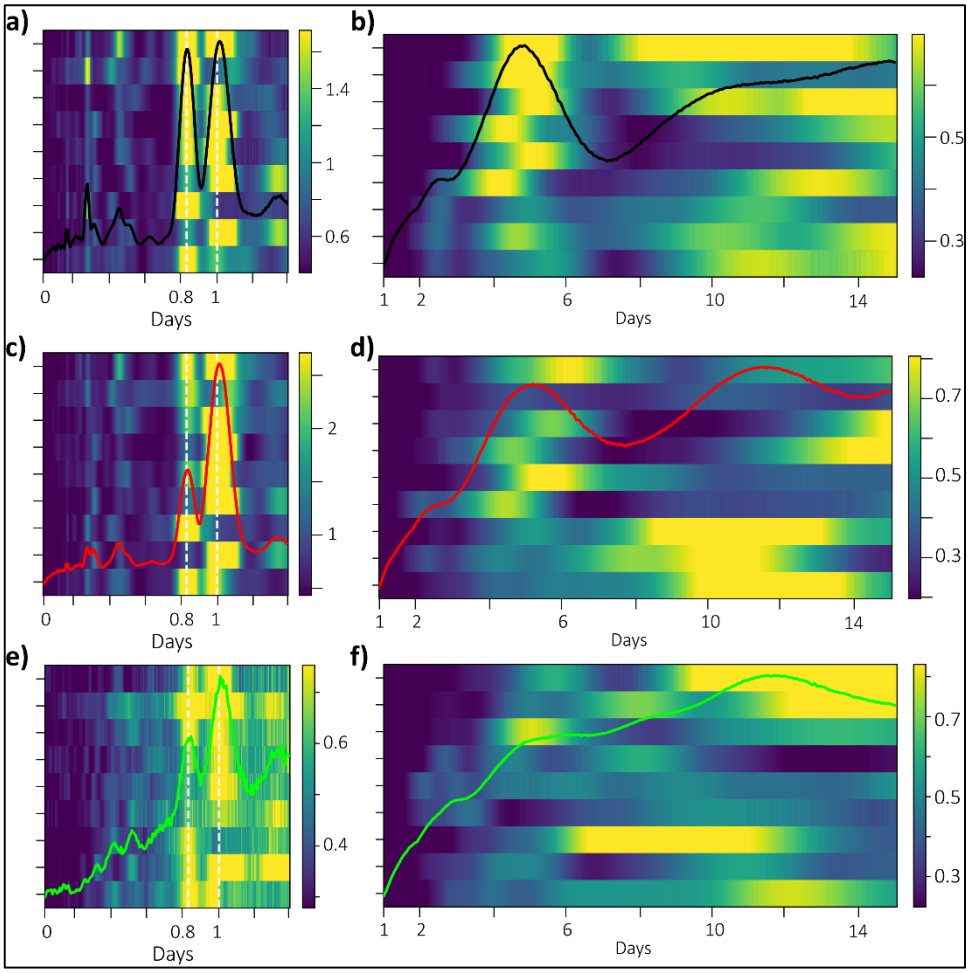

Supplementary Figure 6 Artificially generated multidian rhythm T20 environment.

a) *Black line: Mean extracted periodogram for the active rest cycle on a circadian scale across all mice submitted to a T20 environment. Heat map: Heat map showing power on the circadian scale across mice. Each row represents an individual mouse.* ***b)*** *Same as a but for multi day periods.* ***c)*** *&* ***d)*** *same as a) and b) but for Core T° cycle.* ***e)*** *&* ***f)*** *same as a) & b) but for EA cycle.*

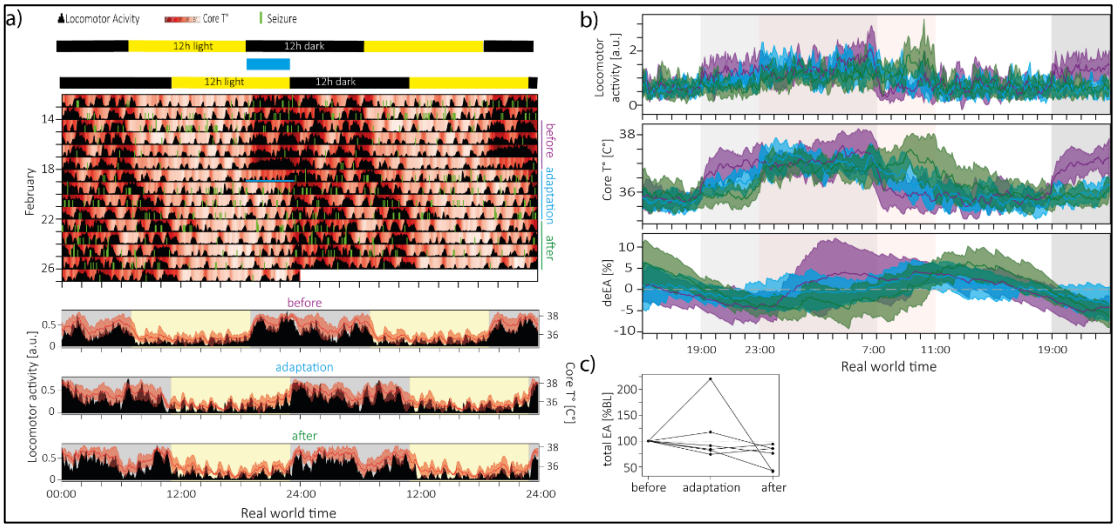

Supplementary Figure 7 Seizure occurrence after 4h time shift.

a) *Top: Double-plotted actimetry, core temperature, and seizures in one epileptic mouse over several days with 4h forward time shift (indicated by blue line). Bars on top indicate lighting conditions. Upper bar represents lighting condition before 4h time shift. Blue bar indicates time shift and lower bar indicates lighting condition after 4h time shift. Days preceding and following the time shift were categorized as follows: "Before", representing the four days immediately before the time shift; "Adaptation", which included the day of the induced time shift and the following three consecutive days; and "after", encompassing the four days following the "adaptation" period. Bottom: Mean locomotor activity (black trace) and core abdominal temperature (red trace) over the days shown on top, categorized into "before," "adaptation," and "after" the time shift.* ***b)*** *Average (± SD, shading) locomotor activity (top), Core T° (middle) and deEA expressed as a percentage of the total EA for the example shown in a) Average was taken across marked days for each condition. Background shading represents lighting conditions before (grey) and after (red) time shift. Note the increase in deEA during the dark period before the time shift (grey shading), which diminishes during and after the time shift. c) Total EA is presented in the bar graph, normalized to the total EA during the period before the time shift, for "before," "adaptation," and "after" the time shift.*

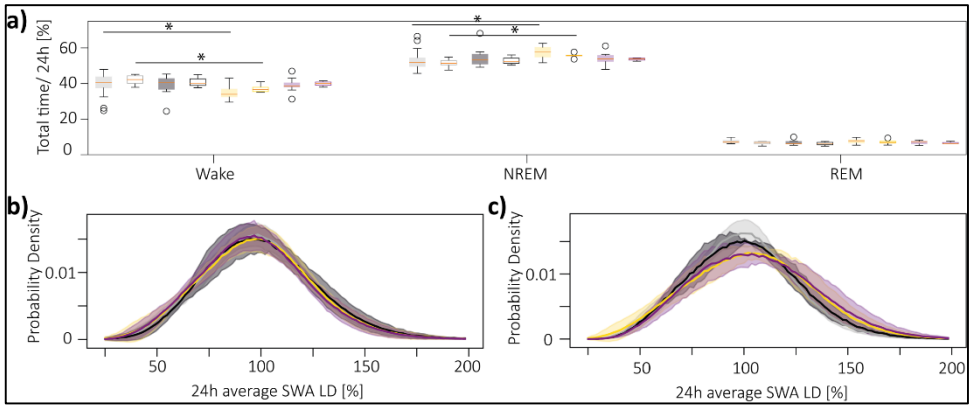

Supplementary Figure 8 Characterisation of sleep across different environments.

a) Time spend in given vigilance state expressed as percentage of 24h for KA (full) and NaCl animals (empty). Different colours represent different environments (grey= LD, black= DD, yellow= LL, purple= T20). ***b)*** *Probability density function for SWA in epileptic mice across different environments. SWA across different chronobiological paradigms was normalized to the average SWA across 24h in a LD (same colour code as in a).* ***c)*** *same as b) but for mice injected with NaCl.*

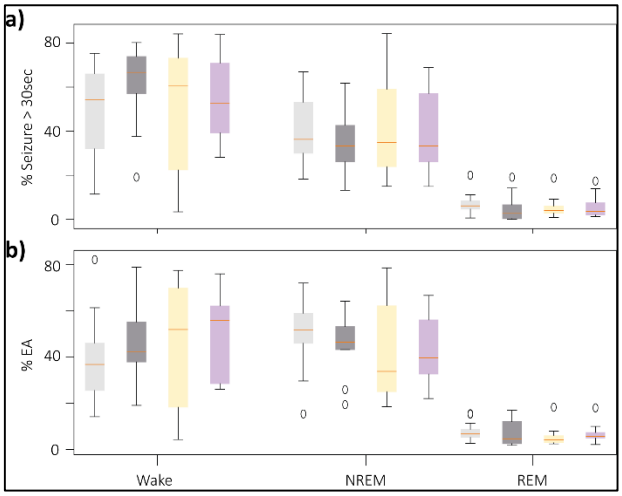

Supplementary Figure 9 Distribution of seizures across vigilance states.

a) *Percentage of total electrographic seizures longer than 30sec across all environments emerging from different vigilance states. Different colours show different environments (grey= LD, black= DD, yellow= LL, purple= T20).* ***b)*** *Same as a) but for total EA.*

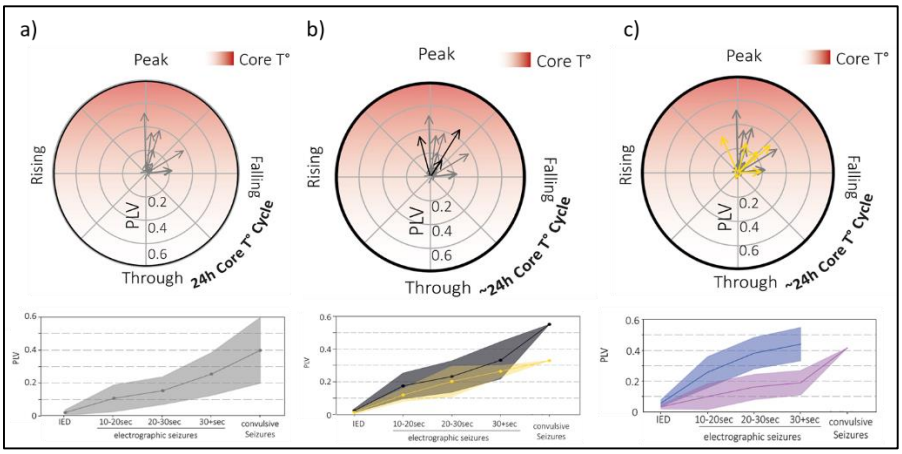

Supplementary Figure 10 Circadian seizure clustering according to core T° cycle

a) *Top: Circadian clustering of seizures longer than 30sec within peak and falling phase of the underlying 24h core T° cycle shown as individual mean resultant vectors for each mouse recorded with significant seizure clustering in LD (Please note that core T° was only recorded in a subset of animals). The angle of the vector corresponds to the preferential hour of seizure timing, and the length corresponds to the strength of seizure clustering (PLV). Bottom: Strength of seizure clustering as a function of the duration of the epileptiform discharge.* ***b)*** *same as a but for circadian clustering of seizures in DD. Grey arrows show circadian clustering of seizures in LD.* ***c)*** *same as b) but for circadian clustering of seizures in LL*

8 Acknowledgments

Embarking on my Ph.D. journey, I encountered the saying, "A Ph.D. is not a sprint, but a marathon." Having now completed both a literal marathon and a metaphorical one in the form of my Ph.D., I can say that there is some truth to this saying.

Both, the act of signing up for a marathon, much like committing to a Ph.D. program, marks the beginning of a long and challenging journey. Both require long term commitment and perseverance. Throughout this journey, I faced numerous mental challenges demanding resilience and the need to understand my own capabilities transforming this journey into a period of personal growth.

However, the most critical similarity lies in the necessity of a robust support system. Completing a marathon, and even more so a Ph.D., is a feat that one cannot accomplished on its own.

I am profoundly grateful to my supervisor, Prof. Dr. Maxime Baud, for his continuous support, guidance, and coaching throughout this race.

My gratitude also extends to my co-supervisor, Prof. Dr. Reto Huber, and my mentor, Prof. Dr. Tobias Nef, for their willingness to engage in my scientific journey and development.

And specifically I would like to thank my external co-referee, Prof. Dr. Christophe Bernard for his readiness to evaluate my thesis and for the fruitful discussions at various occasions.

Running a marathon race means being surrounded by fellow runners each facing their own set of challenges. I therefore extend my warmest thanks to all current and former members of the eLab and the ZEN. The friendship and shared moments of frustration, madness, joy and excitement made this race less daunting.

Finally, every marathon is energized by the cheers of spectators. In a similar vein, I owe a debt of gratitude to my family and friends, whose unwavering support and encouragement have been a great support throughout the years of my PhD. A special mention goes to my mother, who has ignited the initial spark to pursue a scientific career and tackling the challenge of completing a PhD.

In every marathon, there's a critical point where one "hits the wall." For me, that critical point lies between kilometre 35 and 37, and I believe it aligns with the final months of each PhD journey. Now, as I have passed this critical point and approach the finish line, I carry with me not just the scientific knowledge I've gained throughout these years but also the experiences and relationships that have shaped this extraordinary marathon.

9 List of publications

- Lepeu, G.,Van Maren E., **Slabeva K**., Fuchs M., Anso J., Z'Graggen W.J., Pollo C., Schindler K.A., Adamantidis A., Baud M.O. 2021. Probing cortical excitability under GABAergic modulation. BioRxiv (preprint)

10 Curriculum Vitae

Personal Data:

Name:	Slabeva Kristina
Address:	Funkerstrasse 25, 3013 Bern
Phone Number:	+41 79 429 86 92
Email:	kslabeva@gmail.com
Date of birth:	24.04.1995

Working Experience:

04/2019 - today	PhD in the eLab, a research group in the "Zentrum für experimentelle Neurologie" at the Inselspital Bern **PhD Thesis**: Circadian timing of limbic seizures in the epileptic mouse Supervisor: Prof. Maxime Baud
02/2011 – today	Student assistant at a hourly rate at the Institute for Media and Communication Management at the University of St. Gallen
18.07.2017 – 28.07.2017	Internship in the research group of Prof. Dr. Jean-Pierre Bresciani at the University of Fribourg
27.06.2016 – 08.07.2016	Internship in the laboratory of Prof. Dr. Thomas Kaufmann at the pharmacological institute at the University of Bern

Education:

09/2017 – 03.2019	Master in biomedical sciences at the University of Bern with the Latin honors *insigni cum laude*. Thesis: "Viral tracing and characterization of ictal activity in a mouse model of temporal lobe epilepsy"
09/2014 – 09/2017	Bachelor in biomedical sciences at the University of Fribourg
08/2007 – 07/2014	Lower school and upper school (Gymnasium) at «Kantonsschule am Burggraben» in St. Gallen, Focus fold biology and chemistry

Languages:

German	Mother tongue
English	Proficient
French	Good
Macedonian	Mother tongue

Research skills:

Advanced data analysis (Python, Matlab), rodent electrophysiology (EEG,LFP) using custom made electrodes, stereotaxic brain surgery and virus injection in mice, epilepsy rodent model (Kainic acid), optogenetics, mouse handling, management of genetically modified mouse line

Hobbies:

Science, running, literature

Publication and Presentation List

Publications:

18.02.2018	Probing cortical excitability under GABAergic modulation Grégory Lepeu, Ellen Van Maren, Kristina Slabeva, Markus Fuchs, Juan Anso, Werner J. Z'Graggen, Claudio Pollo, Kaspar A. Schindler, Antoine Adamantidis, Maxime O. Baud BioRxiv 2021.02.18.431873; doi : https://doi.org/10.1101/2021.02.18.431873

Presentations at international conferences:

03.07.2023	IES 2023 Dublin; "Circadian timing of limbic seizures in the epileptic mouse", *Talk*
10.07.2022	FENS 2022 Paris; "Circadian timing of limbic seizures in the epileptic mouse"; *Poster*
05.07.2022	Ictals 2022 Bern; "Circadian timing of limbic seizures in the epileptic mouse"; *Talk*

Presentations at national conferences:

14.07.2023	DBMR Day of Biomedical Research; "Circadian timing of limbic seizures in the epileptic mouse"; *Poster*
29.06.2023	GCB Symposium; "Circadian timing of limbic seizures in the epileptic mouse"; *Flash Talk and Poster*
20.01.2023	BENEFRI Bern; "Circadian timing of limbic seizures in the epileptic mouse"; *Poster*
11.06.2022	SSN Annual Meeting Fribourg; "Circadian timing of limbic seizures in the epileptic mouse"; *Poster*

28.01.2021	GCB Symposium Bern (online); Network propagation of circadian seizures"; *Poster Flash*
23.10.2020	CNB Bern; A circuit model of limbic seizures"; *Poster*
27.10.2020	GCB Symposium Bern; A circuit model of limbic seizures"; *Poster*
17.06.2020	CNB Bern; "Characterisation of neuronal networks in a mouse model of temporal lobe epilepsy", *Poster*
31.01.2019	ERS Bern; A circuit model of limbic seizures", *Poster*

Declaration of Originality

Last name, first name: Slabeva, Kristina

Matriculation number: 14-213-276

I hereby declare that this thesis represents my original work and that I have used no other sources except as noted by citations.

All data, tables, figures and text citations which have been reproduced from any other source, including the internet, have been explicitly acknowledged as such.

I am aware that in case of non-compliance, the Senate is entitled to withdraw the doctorate degree awarded to me on the basis of the present thesis, in accordance with the "Statut der Universität Bern (Universitätsstatut; UniSt)", Art. 69, of 7 June 2011.

Place, date

Bern, 29.12.2023

Signature